

# DATA-DRIVEN LIFE PREDICTION MODEL FOR BEARING FAILURE

by

Anthony Silva Reyes

A thesis submitted in partial fulfillment of the requirements for the degree of

MASTER OF SCIENCE  
in  
MECHANICAL ENGINEERING

UNIVERSITY OF PUERTO RICO  
MAYAGÜEZ CAMPUS  
2009

Approved by:

---

Yi Jia, Ph.D.  
Member, Graduate Committee

---

Date

---

Ricky Valentín, Ph.D.  
Member, Graduate Committee

---

Date

---

Vijay K. Goyal, Ph.D.  
Chair, Graduate Committee

---

Date

---

Lev Steinberg, Ph.D.  
Representative of Graduate Studies

---

Date

---

Gustavo Gutierrez, Ph.D.  
Chairperson of the Department

---

Date

# ABSTRACT

Throughout this work, a prognostic tool for the prediction of the remaining useful life of bearings using experimental data based on vibration data analysis is developed using MATLAB®. The experimental data used us that from NASA Prognostics Repository, where three run-to-failure tests we performed under normal load conditions and data was measured using accelerometers. Our tool is tested using experimental data from the second test in order to confirm a failure on the outer race and perform a remaining useful life prediction. The life prediction is achieved by monitoring the energy level of frequency domain features known as Bearing Fault Frequencies and trending several condition indicators such as Kurtosis, *RMS* and Power of the interested frequency. Since the damage occurred in the outer race, the Ball Pass Outer Raceway Frequency is selected to perform the life prediction. A set of MATLAB® algorithms are developed to calculate the bearing fault frequencies, trend key condition indicators and perform a life prediction. The remaining useful life prediction is based on the evolution of a selected degradation signal. The selected degradation signal is the *RMS* vibration level over time. In this approach, instead of calculate the *RMS* vibration across the entire spectrum; it is calculated around the interested frequency and its first five harmonics using a window of  $\pm 15\%$  BPOF. Then the average of these *RMS* values is calculated and becomes the degradation signal trended over time. Bearing remaining life prediction is achieved based on a predefined failure threshold. Based on the available data, there is an 8.6% error between the actual and predicted bearing failure time.

## RESUMEN

A través de este trabajo, una herramienta para la predicción de vida útil de cajas de bolas usando data experimental y basado en análisis vibracional es desarrollada usando MATLAB®. La data experimental usada en este trabajo es obtenida a través del Repositorio de Pronósticos de la NASA, donde tres pruebas fueron realizadas bajo condiciones normales de carga. La data fue extraída usando acelerómetros. La herramienta es probada usando data experimental de la segunda prueba para confirmar una falla en el riel exterior de una caja de bola y realizar la predicción de vida útil de la misma. La predicción de vida útil es llevada a cabo mediante el monitoreo del nivel de energía de unos parámetros importantes conocidos como Frecuencias de Falla y el análisis de las tendencias de varios indicadores de condición tales como Kurtosis, Raíz Promedio de Cuadrados y la energía asociada a la frecuencia de falla de interés. Debido a que la falla ocurrió en el riel exterior, la Frecuencia Rotacional de Pasaje del Riel Exterior es seleccionada para realizar la predicción de vida útil. Un conjunto de algoritmos en MATLAB® son desarrollados para calcular las frecuencias de falla, analizar las tendencias de indicadores de condición y realizar la predicción de vida útil. La predicción de vida útil es basada en la evolución de una señal de degradación pre-seleccionada. En este método se calcula la raíz promedio de cuadrados alrededor de la frecuencia de interés y alrededor de sus primeras cinco armónicas usando una ventana de  $\pm 15\%$ . Luego, el promedio de los valores de la raíz promedio de cuadrados se convierte en la señal de degradación que es monitoreada como función del tiempo. La predicción de vida útil es basada en un límite de falla predefinido. Basado en la data disponible, el error entre el tiempo actual y el predicho es de un 8.6%.

## **DEDICATION**

*To my Lord Jesus, my lovely parents and in memory of my grandma Irma and Carol Agosto*

# ACKNOWLEDGEMENTS

---

---

First, the most important acknowledgement goes to God for be my main support, guide and the light during my college career. Without Him I never could reach anything of what I have been proposed in my life. All my achieved goals during my life are thanks to Him. Thanks to my parents Manuel and Priscila and my sister Priscila Dennise for bring me their unique special love and support.

During the past year many people were related to me in the professional and personal aspect and contributed in a great manner to this achievement. I would like express my sincere acknowledgment to my advisor, Dr. Vijay K. Goyal, for providing me the necessary support and supervision to make possible this big step of obtain a master's degree. More than an advisor, Dr. Goyal has been a great friend by giving me encouragement and support throughout my studies. Thanks to Dr. Ricky Valentín for make great contributions to this work and for share his valuable knowledge in several key areas. I would like to express my gratitude to Mr. David S. Bodden, Lockheed Martin Senior Fellow, and Dr. Scott Clements LM Systems Engineer for their advice and support during the course of this work.

Thanks to Yolanda Pérez for her friendly support, to Evangeline Jiménez for her friendship and significant encouragement and to Jessamine Hernández for her advice. I would like to thank Emmanuel Irizarry and Juan J. Reinés for all the support regarding Computer Aided Design using NX-6. Very special thanks and appreciation to my college friends Pablo J. Rosado, Mayra S. Artiles, Christian Escudero, Luis A. Martínez, and Zolliam A. Pérez for their continuous support and for the unforgettable moments we spent together. I love you all!

# TABLE OF CONTENTS

---

---

<b>ABSTRACT</b>	<b>II</b>
<b>RESUMEN</b>	<b>III</b>
<b>LIST OF TABLES</b>	<b>VIII</b>
<b>LIST OF FIGURES</b>	<b>IX</b>
<b>CHAPTER 1. PRELIMINARY REMARKS</b>	<b>1</b>
<b>1.1 BACKGROUND</b>	<b>1</b>
<b>1.2 PROBLEM DESCRIPTION</b>	<b>2</b>
1.2.1 Lockheed Martin Co. Specifications	2
1.2.2 Bearing Experimental Data from NASA	4
<b>1.3 GOALS</b>	<b>6</b>
1.3.1 Overall Goals	6
1.3.2 Intellectual Merit	6
1.3.3 Broader Impacts	7
<b>1.4 APPROACH</b>	<b>7</b>
<b>CHAPTER 2. BEARING PROGNOSTICS</b>	<b>13</b>
<b>2.1 HEALTH MONITORING METHODS</b>	<b>13</b>
2.1.1 Life Consumption Monitoring (LCM)	14
2.1.2 Condition Monitoring (CM)	15
<b>2.2 BEARING PROGNOSTICS</b>	<b>17</b>
2.2.1 Physics-Based Prognostics Models	17
2.2.2 Data-Driven Prognostics Models	19
<b>2.3 BEARING FAILURE MECHANISMS AND FAULT DETECTION</b>	<b>19</b>
<b>CHAPTER 3. VIBRATION DATA ANALYSIS USING EXPERIMENTAL DATA</b>	<b>22</b>

<b>3.1</b>	<b>DATA ANALYSIS METHODS</b>	<b>23</b>
3.1.1	Statistical Analysis	23
3.1.2	FFT and Spectral Analysis	23
<b>3.2</b>	<b>BEARING TYPES</b>	<b>26</b>
<b>3.3</b>	<b>BEARING FAULT FREQUENCIES</b>	<b>27</b>
<b>3.4</b>	<b>CONDITION INDICATORS</b>	<b>38</b>
3.4.1	Kurtosis	38
3.4.2	Root Mean Square Value ( <i>RMS</i> )	41
<b>3.5</b>	<b>THE FAST FOURIER TRANSFORM (FFT) PROCEDURE</b>	<b>43</b>
<b>3.6</b>	<b>BASELINES</b>	<b>44</b>
<b>3.7</b>	<b>ANALYSIS ON TEST 2</b>	<b>44</b>
3.7.1	Creation of Frequency Data Windows	47
3.7.2	PSD Plots Comparison	48
3.7.3	Kurtosis of BPOF	51
3.7.4	<i>RMS</i> of BPOF	54
3.7.5	Trending the Power of BPOF	55
<b>3.8</b>	<b>DEGRADATION SIGNAL SELECTION</b>	<b>59</b>
<b>3.9</b>	<b>REMAINING USEFUL LIFE PREDICTION ON TEST 2</b>	<b>61</b>
3.9.1	Vector Scaling	63
3.9.2	Development of a Moving Window Algorithm	64
<b>3.10</b>	<b>BEARINGS PROGNOSTIC TOOL</b>	<b>72</b>
<b>CHAPTER 4. CONCLUDING REMARKS</b>		<b>80</b>
<b>4.1</b>	<b>CONCLUSIONS</b>	<b>80</b>
<b>4.2</b>	<b>RECOMMENDED FUTURE WORK</b>	<b>81</b>
<b>REFERENCES</b>		<b>83</b>
<b>A.</b>	<b>DATA ACQUISITION</b>	<b>87</b>
<b>B.</b>	<b>CODE FLOWCHARTS</b>	<b>92</b>
<b>C.</b>	<b>MATLAB BUILT-IN FUNCTIONS</b>	<b>100</b>

# LIST OF TABLES

---

---

Table 1.1: Actuator Characteristics.....	3
Table 1.2: Actuator Gearing Ratios. ....	4
Table 1.3: Gear/Bearing Information.....	4
Table 3.1: Bearing characteristics.....	26
Table 3.2: Vibration frequency characteristics. ....	36
Table 3.3: Fault frequencies based on bearing dimensions. ....	45
Table 3.4: Signal limits added into the tool. ....	66
Table 3.5: Capabilities and limitations of the bearings prognostic tool .....	79

# LIST OF FIGURES

---

---

Figure 1.1: Actuator Power Train. ....	3
Figure 1.2: Bearing test rig and sensor placement (Qiu et al 2006). ....	5
Figure 1.3: Proposed approach for health monitoring. ....	8
Figure 1.4: Data Simplification Process. ....	9
Figure 1.5: Detailed flowchart of the proposed approach.....	10
Figure 2.1: Health monitoring methods.....	14
Figure 2.2: Methods for predicting bearing failures.....	18
Figure 3.1: Components of a data acquisition system.....	22
Figure 3.2: Bearing dynamics.....	28
Figure 3.3: Bearing geometry.....	28
Figure 3.4: Frequencies in a bearing.....	35
Figure 3.5: Kurtosis value for bearing 1 in X-direction.....	40
Figure 3.6: <i>RMS</i> value for bearing 1 in X-direction.....	42
Figure 3.7: Vibration signal recorded on 02/12/2004.....	46
Figure 3.8: Vibration signal recorded on 02/18/2004.....	46
Figure 3.9: Ideal bandpass filter.....	48
Figure 3.10: PSD plot for the file #3.....	49
Figure 3.11: PSD plot of file #3 for the selected frequency range ( $200.94 < f < 271.86$ Hz). ....	50
Figure 3.12: PSD plot for the file #350.....	50
Figure 3.13: PSD plot of file #350 for the selected frequency range ( $200.94 < f < 271.86$ Hz). .	51
Figure 3.14: Kurtosis of time-domain data for Bearing 1 in X-direction.....	52
Figure 3.15: Kurtosis of time-domain data for Bearing 1 in Y-direction.....	53
Figure 3.16: <i>RMS</i> of time-domain data for Bearing 1 in X-direction.....	54
Figure 3.17: <i>RMS</i> of time-domain data for Bearing 1 in Y-direction. ....	55
Figure 3.18: BPOF power trend for bearing 1 in both X and Y directions.....	56
Figure 3.19: BPIF power trend for bearing 1 in both X and Y directions. ....	57
Figure 3.20: FB power trend for bearing 1 in both X and Y directions.....	58
Figure 3.21: FCF power trend for bearing 1 in both X and Y directions. ....	59
Figure 3.22: Example of the proposed approach to calculate bearing's remaining useful life. ....	60
Figure 3.23: Average <i>RMS</i> for bearing 1 in both X and Y directions using a window of $\pm 15\%$ . ....	61
Figure 3.24: Average <i>RMS</i> for bearing 1 in X-direction.....	62
Figure 3.25: Average <i>RMS</i> /Failure Threshold (%) for bearing 1 in both X and Y directions ....	63
Figure 3.26: Average <i>RMS</i> /Failure Threshold (%) in X-direction.....	65
Figure 3.27: General approach used into the algorithm.....	67
Figure 3.28: Exponential fit with 95% confidence bounds for X-direction.....	70
Figure 3.29: Exponential fit with 95% confidence bounds for Y-direction.....	71
Figure 3.30: Structure of the code.....	72
Figure 3.31: General view of the bearing prognostic tool for bearings.....	73
Figure 3.32: Features within bearings prognostic tool.....	74

Figure 3.33: Bearings prognostic tool showing the Kurtosis plot. ....	75
Figure 3.34: Bearings prognostic tool showing the power of selected frequency. ....	76
Figure 3.35: Prognostic tool showing the Average <i>RMS</i> / Failure Threshold (%) as a function of elapsed time. ....	77
Figure 3.36: Predicted TTF's and exponential fit with 95% confidence bounds plot. ....	78
Figure 4.1: Arbitrary speed cycle. ....	82
Figure A.1: Sensor data acquisition. ....	87
Figure A.2: Accelerometers mounting ....	88
Figure A.3: PCB 353B33 High Sensitivity Quartz ICP Accelerometer ....	89
Figure A.4: National Instruments data acquisition card ....	89
Figure A.5: Sampling of a continuous time record. ....	90
Figure B.1: Subroutine: Calculate critical frequencies ....	92
Figure B.2: Subroutine: Create data windows ....	93
Figure B.3: Subroutine: Calculate initial mean and slope ....	94
Figure B.4: Subroutine: RMS defective frequency and 5 harmonics ....	95
Figure B.5: Function: RMS, continued on next page ....	96
Figure B.6: Function: RMS, continued from previous page. ....	97
Figure B.7: Subroutine: Analysis, continued on next page ....	98
Figure B.8: Subroutine: Analysis, continued from previous page. ....	99
Figure C.1: MATLAB output of Kurtosis value. ....	101
Figure C.2: Accelerometer data. ....	102
Figure C.3: Comparison of the FFT calculation using both the definition and MATLAB built-in function. ....	102
Figure C.4: MATLAB results using the function find. ....	103

# CHAPTER 1. PRELIMINARY REMARKS

---

---

The focus of this project is to develop an effective life prediction model able to accurately characterize bearings condition in order to provide sufficient time to asses an optimum maintenance before an imminent failure occurs. Different modules will be developed during the different stages of the research in order to asses a prognostic for bearings.

## 1.1 BACKGROUND

Predicting the remaining life of bearing systems is an essential role in health monitoring of mechanical devices. As we know, bearings are fundamental components of many mechanical systems used in the aerospace industry. The reliability of many components such as gearboxes, rotor systems and electromechanical actuators depend significantly on the well operation bearings. Therefore, in order to reduce the risk, aerospace companies want to be able to perform a continuous monitoring of these components to predict if there is a possible failure.

Existing aircraft monitoring systems focus on diagnostics, which is the ability to non-invasively sense the actual condition of critical components and determine which component broke and how or why it broke. Although diagnostics are relatively well developed, an accurate prediction of remaining useful life once an incipient fault has been detected is more difficult. To achieve the full economic and operational benefits of predictive maintenance, newer platforms such as the Joint Strike Fighter (JSF) are moving toward prognostics. Prognostics include the ability to predict future component condition based on anticipated usage , diagnostic history, and a model of the fault-to-failure progression of the component.

Developing a way to prognosticate the condition of gearboxes has been a research imperative for a considerable time. Turbine engine bearing failures are the leading cause of class-A mechanical failures which include loss of aircraft (Wade 2005). Even one aircraft saved would

pay for development of prognostics. However, the fault-to-failure progression models required to enable the predictive aspects of prognosis do not yet exist for most component types.

## **1.2 PROBLEM DESCRIPTION**

In this project we will develop effective life prediction model for the prognostic of bearings. The project combines the use of sensors technology and vibration data analysis based on experimental data. Sensors are used as a complement to capture the condition of the system. After capture the condition of the system, data simplification is essential to extract the interested features. Vibration data analysis enables us to trend key condition indicators, predict the remaining useful life of the bearing in order to have sufficient time before failure and asses a proper and effective maintenance to the machinery.

### **1.2.1 Lockheed Martin Co. Specifications**

The original effort of this work is to develop life prediction models for gears and bearings that can be utilized in an electro-mechanical actuator (EMA). The EMA to be used as a reference for this work is illustrated in **Figure 1.1**. This actuator is 1/2 HP and was developed by Parker Aerospace. It is a simple actuator design powered by a 28V brushless DC Motor. The actuator physical characteristics are identified in **Table 1.1**. Power transfer from the brushless DC motor to the Output Ram is achieved as follows.

A pinion gear is fixed to the end of the motor rotor shaft. The pinion gear drives a cluster gear which drives the output gear. The output gear is connected to the ball screw shaft. The ball screw nut, which rides on the ball screw shaft via ball bearings, is fixed to the output rod. As the ball screw shaft turns due to the torque of the output gear, power is transferred to the output rod via the ball screw bearings and ball screw nut. Gearing ratios between the various components are identified in **Table 1.2**. From this information it can be calculated that 46.875 turns of the pinion gear, i.e. 46.875 turns of the motor shaft, produces 1 inch of output rod movement. For the output rod to move at 3.7 in/sec, the motor would have to operate at approximately 10,500 rpm.

It is desired to be able to monitor the health of the cluster gear, output gear, and pinion gear. In addition, it is desired to be able to monitor the health of the thrust bearings, output gear bearing, cluster gear bearings, and motor bearing. Characteristics of the gear and bearings are shown in **Table 1.3**. The EMA has the following sensor information and/or state information available:

1. Output rod position
2. Motor position
3. Motor current and voltage

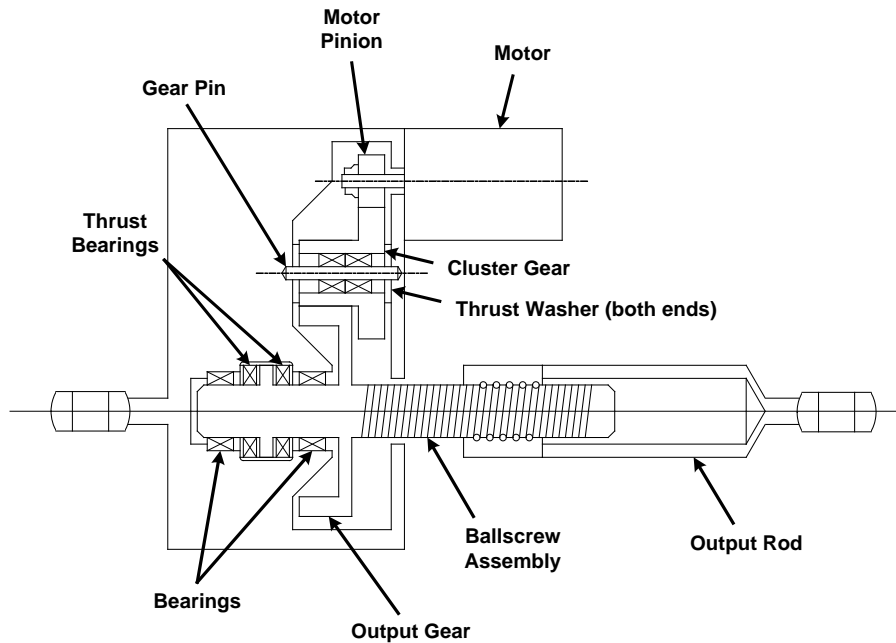


**Figure 1.1:** Actuator Power Train.

**Table 1.1:** Actuator Characteristics.

Actuator Centerline Distance	12.000 inches
Actuator Stroke	$\pm 0.875$ inches
Actuator Performance	2.0 in/sec @ 1620 lbs. Load 3.7 in/sec @ 214 lbs. Load
Bandwidth	6 Hz @ -90 Deg
Stall Load	2400 lbs. @ 65 A Current limit

**Table 1.2:** Actuator Gearing Ratios.

Pinion to Cluster Gear	3 to 1
Cluster Gear to Output Gear	3.125 to 1
Ballscrew to Ram (rev/in)	5 to 1

**Table 1.3:** Gear/Bearing Information.

Component	No. Bearings	No. Gear Teeth	Comments
<i>Bearings</i>			
Motor	11	-	Ball Bearing
Cluster Gear	8	-	Needle Bearing
Ballscrew Support	29	-	Needle Bearing
Thrust	28	-	Needle Bearing
<i>Gears</i>			
Motor Pinion	-	16	Attached to Motor Shaft
Cluster - Large	-	48	Driven by Motor Pinion
Cluster - Small	-	16	Drives Output Gear
Output	-	50	Fixed to Ballscrew Shaft
<i>Ballscrew</i>	-	-	5 Turns/Inch Displacement

### 1.2.2 Bearing Experimental Data from NASA

The purpose of using experimental data is to develop life prediction models to be used as part of a prognostic solution for assessment of wear and prediction of failure for bearings. The objective is to perform a frequency analysis of a bearing experimental data. Using this data several algorithms can be developed in order to analyze frequency components of the bearings. This data was recorded by Qiu et al (2006) in their research of “Wavelet filter-based weak signature detection method and its application on rolling element bearing prognostics”. They used four Rexnord ZA-2115 double row bearings installed on one shaft as shown in **Figure 1.2**. The

rotation speed was kept constant at 2000 rpm and a radial load of 6000 lbs is added to the shaft and bearing by a spring mechanism. Two PCB 353B33 High Sensitivity Quartz ICP Accelerometers were installed on each bearing for a total of 8 accelerometers (one on the horizontal  $X$ -direction and one on the vertical  $Y$ -direction). Vibration data was collected using a National Instruments DAQCard-6062E data acquisition card. They performed three run-to-failure tests under normal load conditions. The bearing data was downloaded from the NASA Prognostics Repository<sup>1</sup>.

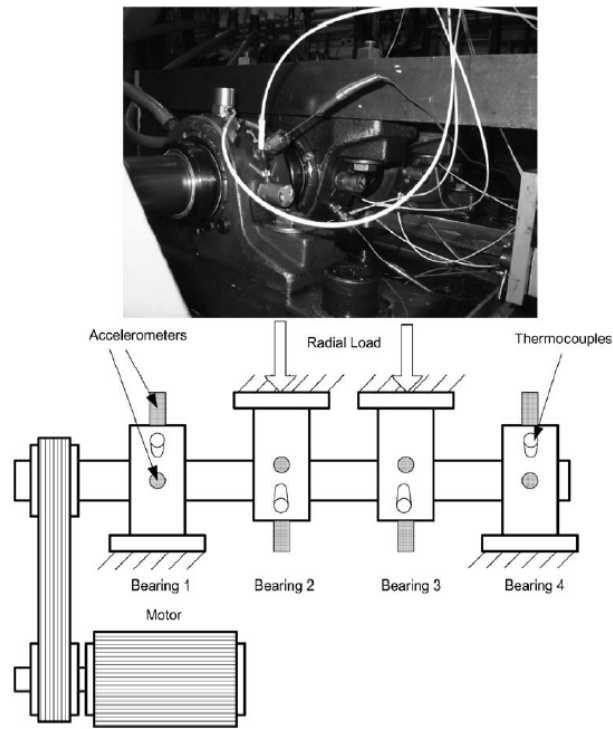


**Figure 1.2:** Bearing test rig and sensor placement (Qiu et al 2006).

This work describes the development and demonstration of a practical methodology for condition monitoring. The various steps involved in the methodology will be clearly documented. Algorithms for data simplification, vibration data analysis including key features

---

<sup>1</sup> <http://ti.arc.nasa.gov/project/prognostic-data-repository>

trending and remaining useful life prediction will be developed and documented. Procedures for characterizing real-time environmental data (vibration) will be documented.

This case study aims to demonstrate the application of the condition monitoring methodology in a real-time environment, which involves the following steps:

1. Placing a bearing model assembly in a simulated load environment.
2. Determining the damage caused to the model system by monitoring its real-time environment and performing a vibration data analysis for life prediction assessment.

## **1.3 GOALS**

### **1.3.1 Overall Goals**

The goals presented in this section are applicable for all of the bearings and can be summarize as follows:

1. Identify required data sampling characteristics such as rate, number of samples, data reduction techniques, key condition indicators, etc., necessary for the prognostics solution based on constant shaft speed scenario.
2. Trending of condition indicators to identify bearing's degradation phases such as damage initiation and damage progression up to failure.
3. Develop a MATLAB® based set of algorithms to perform prognostic feature extraction from vibration data associated with bearings for determination of remaining useful life; integrate these algorithms using a Graphical User Interface (GUI) within MATLAB®.
4. Document the details of the technical approach utilized for the prognostic solution.

### **1.3.2 Intellectual Merit**

The research objective of this project is to develop methods for improving the prognostic ball bearings. Ball bearings are inherently subject to faults, and information on abnormal behavior and processes can be obtained through measured signals. The aim of this research is to exploit

the information provided by sensor signals to create a unified framework for the systematic design of prognostic algorithms and for the prediction of bearing aging. Today, there are few, if any, general results concerning system prognostic and aging; the research, if successful, will result in methods that are general enough to be applied to ball bearings. Deliverables for this project include software for the design and analysis of prognostic algorithms, experimental data, and educational materials for engineering professionals.

### **1.3.3 Broader Impacts**

The potential outcomes of this project should broadly impact science and technology in structures and their interactions. A better understanding of vibration data will allow us to identify the noise and thus remove it successfully and therefore make a better judgment of diagnosis and prognostics. This project is conducted in close collaboration with a major aeronautic manufacturer, Lockheed Martin, and aims to apply the new methodology to the diagnosis of aeronautic mechanical systems and to the life prediction of actuators. Bearings are critical components of actuators. Therefore, the remaining useful life prediction of bearings will have a positive impact on the development of maintenance standards for actuators. If successful, the research will result in significantly greater reliability of future mechanical systems. This may eventually result in reduced maintenance costs and increased customer satisfaction, with the potential of touching millions of LM product owners around the world. The research may also have a positive impact on accelerating the introduction of advanced mechanical prognostic systems in future aeronautic products by increasing their reliability and serviceability. Further, the educational outcomes of the project will affect undergraduate and graduate engineering students at a major Hispanic serving institution as well as practicing engineers in the aeronautic industry through future distance education programs.

## **1.4 APPROACH**

The proposed approach is shown in **Figure 1.3**. It consists in a combination of a sensor technology and vibration data analysis in order to predict the remaining life of bearings in a rotating machine. A sensor's network is responsible of obtain the vibration behavior of the system during its operation. Simplification of the measured data using selected techniques is also

required during the process. **Figure 1.4** shows a flowchart of the data simplification process. Vibration data analysis will help us to capture the behavior of critical frequencies, trend key condition indicators (e.g., Kurtosis, RMS, etc.) in order to perform a prediction of remaining useful life. **Figure 1.5** shows a more detailed flowchart of the proposed approach.

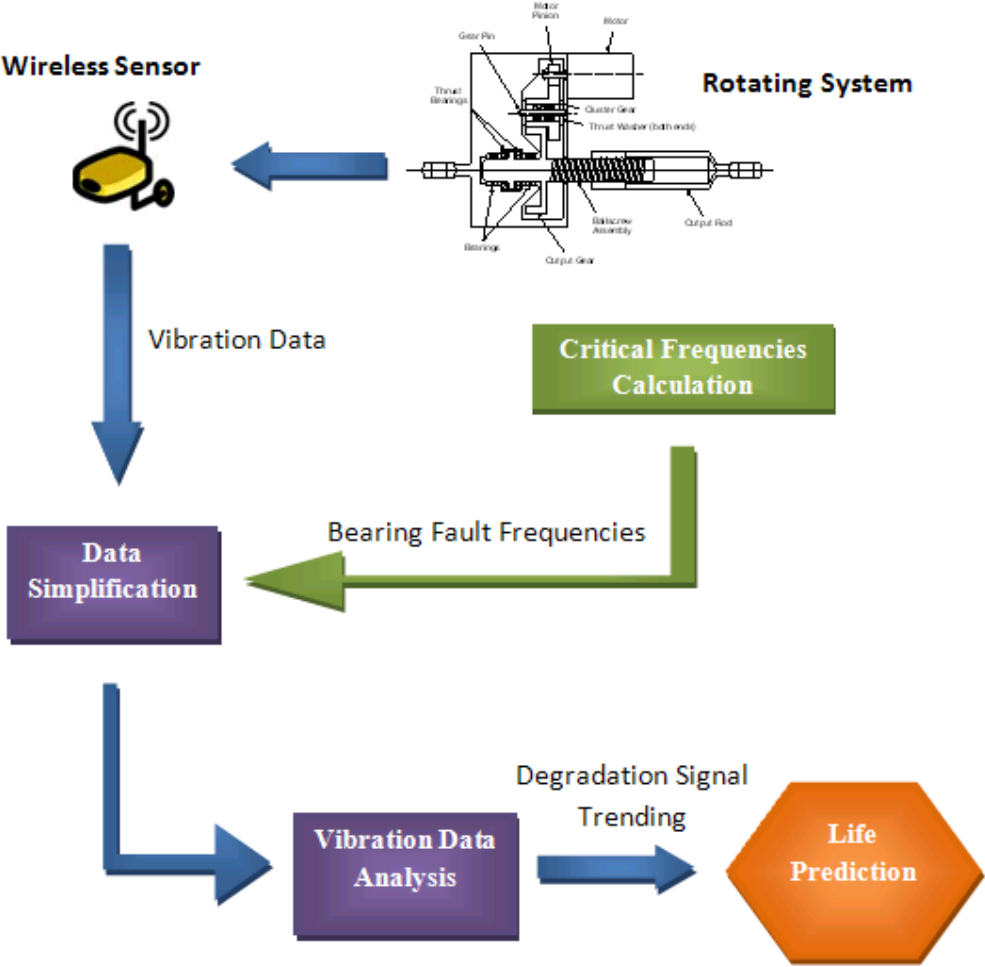


**Figure 1.3:** Proposed approach for health monitoring.

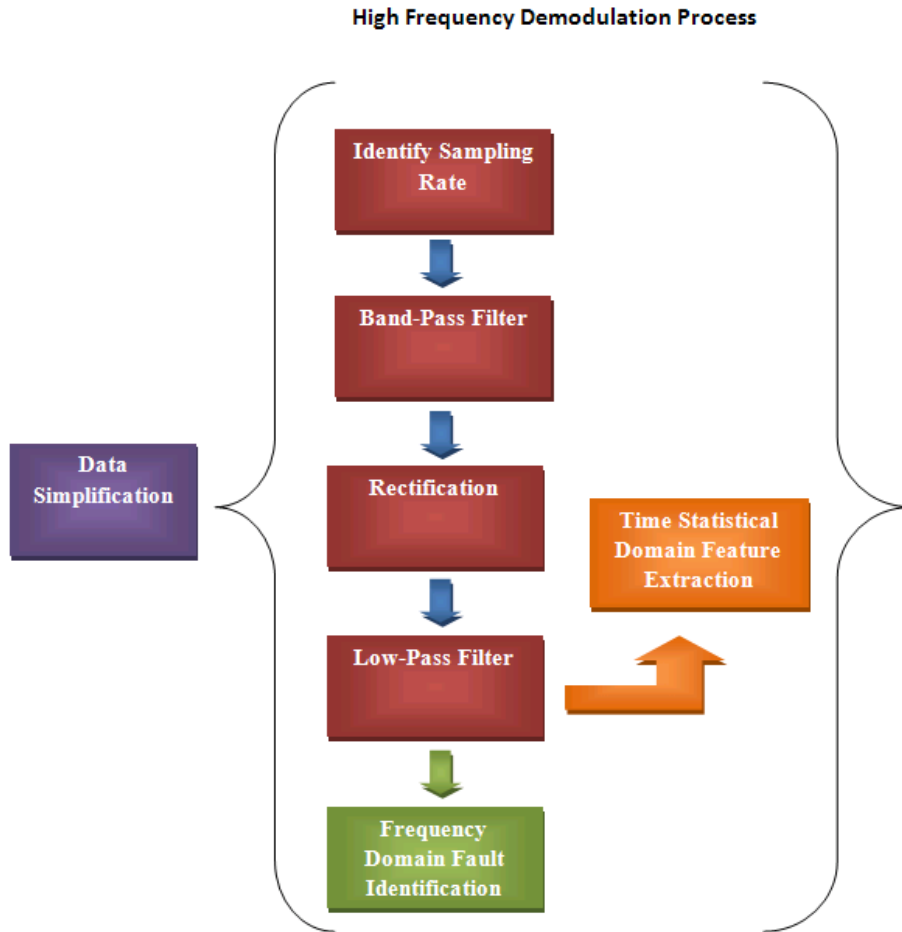


**Figure 1.4:** Data Simplification Process.

The purpose of divide the approach in two modules (Data Acquisition and Vibration Data Analysis) is to monitor the behavior of the components, identify the damage initiation phase and incorporate models in order to perform an accurate estimation of remaining useful life when that failure mechanism occurs. The advantage of this approach is that is applicable for all the bearings in a rotating machine.

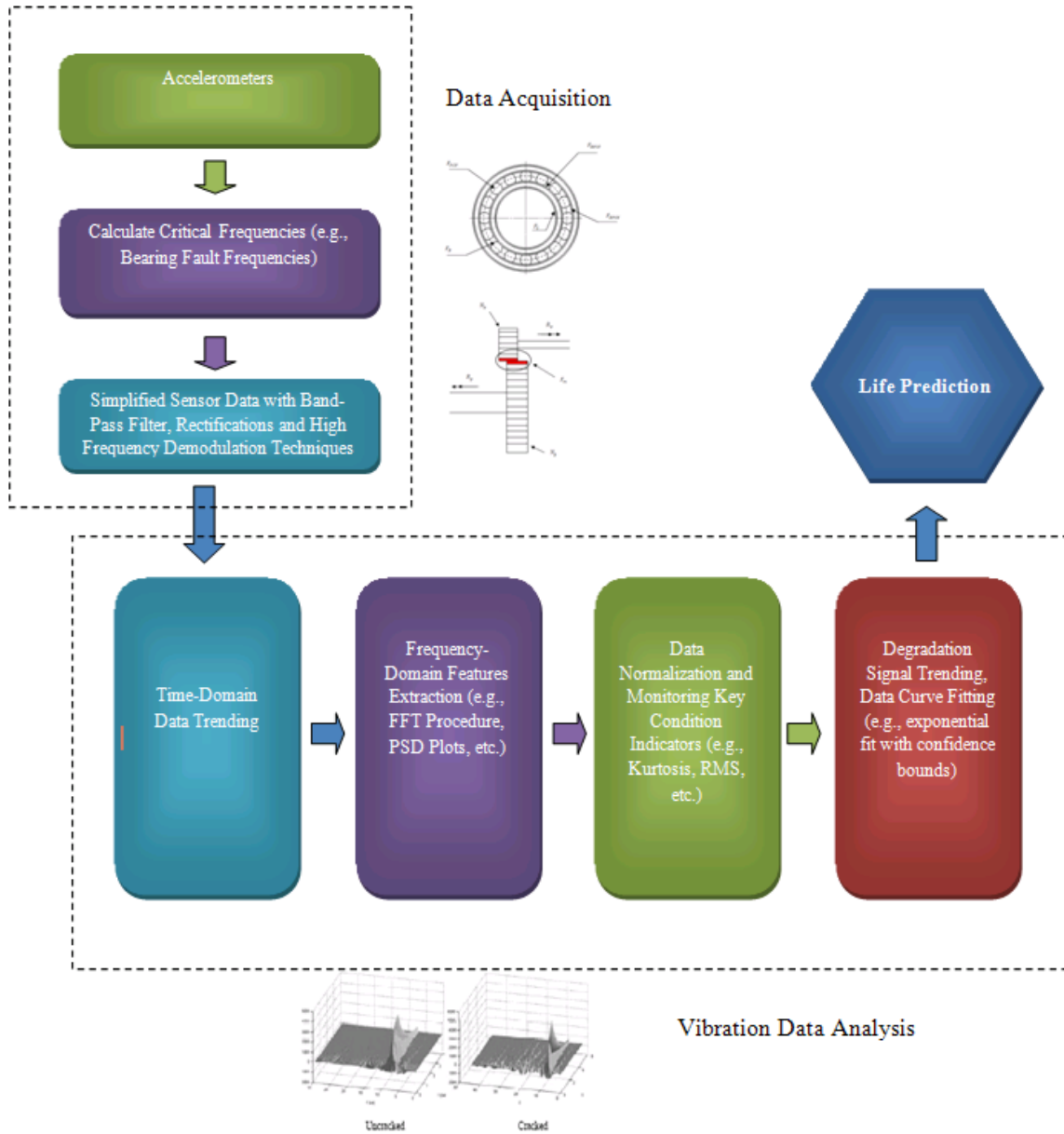


**Figure 1.5:** Detailed flowchart of the proposed approach.

The two modules mentioned before are the following:

1. **Data Acquisition:** In most of the existing life prediction systems, the selected sensor technology plays an important role during the development of a prognostic approach. That is because in a prognostic approach the measurements of critical parameters have to be accurate in order to compare them with numerical results. In this phase we incorporate sensor technology that measures vibration responses. Our selected sensors need to be capable of measure vibration changes in order to start identifying damage. It is for that reason that accelerometers will be use to monitor the vibration behavior of the system. One of the most important factors is the mounting and location of the sensor. Sensors situated in locations that are relatively inaccessible may have wireless connectivity to the processing location. Bearing fault frequencies are calculated using our MATLAB algorithms. In bearings, each one of the fault frequencies is associated with a particular bearing component. After gathering all the desired data we need to simplify it with some kind of tool such as band-pass filter, rectifications and high frequency demodulation technique. Gears and bearings generate a noise between them and that may cause problems at the time of the interpretation of the signal. The objective is to separate gears frequencies from bearings ones which is one of the principal concerns in health monitoring of bearings.
2. **Vibration Data Analysis:** In this phase we perform a frequency analysis to bearing measured data. The purpose of this analysis is to analyze the bearing fault frequencies in order to detect an abnormal change in those features. A Fast Fourier Transform algorithm is applied to the measured data in order to convert it to the frequency-domain. This is a fundamental step because converting the data to the frequency-domain enables us to obtain the Power Spectral Density (PSD) plots. The purpose of the PSD plots is to compare the frequency spectrum when no damage is present against the resulting spectrum when damage initiation begins. Statistical parameters such as Kurtosis and RMS are applied to the data in order to trend the variation in the vibration characteristics of the critical frequencies. The Kurtosis value helps us to determine the "peakedness" of a data distribution. When damage is present, the

vibration signal contains sharp peaks resulting in an increase in the Kurtosis value. On the other hand, the RMS is used to monitor the vibration level of the interested critical frequency. In order to achieve the remaining useful life prediction, a signal that captures the evolution of bearing's degradation is selected. This type of signal is called a *degradation signal*. By trending this degradation signal, the life prediction can be achieved when the signal exceeds the permissible limits which are integrated into the MATLAB algorithms. An interface is developed to incorporate all the developed MATLAB programs in order to perform a life prediction. Chapter 3 will include full details of the development of this module and discussion of the results.

## **CHAPTER 2. BEARING PROGNOSTICS**

---

We can define bearing prognostics as the ability to predict the bearing's remaining useful operational life based on the available condition monitoring data. By knowing about impending failure, based on actual application conditions, procedures can be designed to mitigate, manage or maintain the product (Kelkar et al 1997). In other words, if a specific problem can be identified before a catastrophic failure occurs, a cost-effective maintenance can be scheduled. Further, since bearing prognostics involves determination of actual application conditions, it also offers a novel approach for designing systems for the loads they are expected to encounter.

There is a continuing need to reduce design costs of new systems and maintenance costs of in-service systems in today's industry. Due to uncertainties regarding the actual life cycle loads for a system, the common practice of design has been to provide a safety margin, i.e., designing for a high stress and recommending operation at a lower value. If the actual life cycle loads are different from the designed ones, this design practice can lead to costly overdesign or hazardous under-design, and consequently, increased investment (Beder 1993). If the actual life cycle environment for an in-service system can be obtained, the uncertainty in the life cycle loads basically can be eliminated and systems can be designed for future expected loads, leading to more practical designs that may help lower material cost and design.

### **2.1 HEALTH MONITORING METHODS**

Health monitoring is a method for evaluating the extent of a product's degradation with time. In bearing prognostics, the ability to monitor the structural health is becoming important because damage detection depends on how well the bearing structure is monitored. Health monitoring represents one of the most promising developments in the evolution of industrial maintenance practices. The health monitoring program has been recognized as the most cost-effective maintenance program (Mitchell 1993). In health monitoring, the specific problem can be identified before failure, allowing the correct repair parts, tools, and labor skills to be made available to correct the problem before it occurs. By knowing whether and, more significantly,

when failure will occur, production or operation schedules can be made more streamlined and maintenance cost can be designed to reflect actual requirements instead of statistical ones. With organizations being increasingly faced with demands to lower design and maintenance costs, increase product reliability, and accelerate organizational responsiveness, health monitoring has emerged as a viable alternative to traditional scheduled maintenance, run-to-failure operation, and the various maintenance approaches between the two extremes. A system's health is the extent of its degradation or deviation from its normal operating state. A system's degradation can be determined in two ways, namely *life consumption monitoring* and *condition monitoring* (Pecht et al 2001; Kelkar et al 1997). **Figure 2.1** shows different methods of health monitoring.

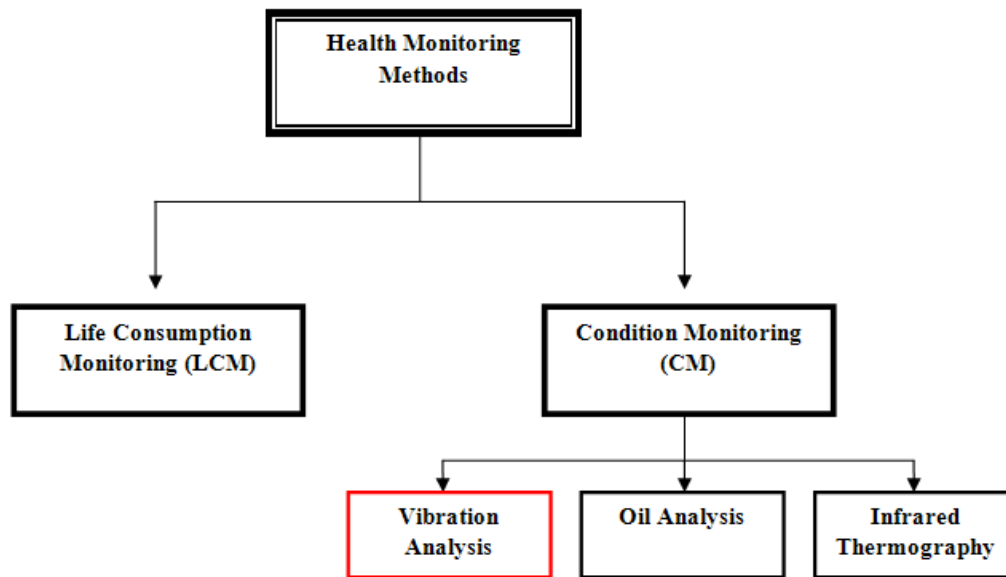


**Figure 2.1:** Health monitoring methods

### 2.1.1 Life Consumption Monitoring (LCM)

Life consumption monitoring (LCM) is a method of quantifying a system's degradation by monitoring parameters related to the system's life cycle environment and converting the measured data into life consumption. Life consumption monitoring is defined as the technical activity that involves the periodic or continuous measurement, sensing, recording and interpretation of physical parameters associated with a system's life cycle environment with the purpose of quantifying the amount of system degradation, and hence to support decisions related

to the operation and maintenance of the system. If the actual life cycle environment for an in-service system can be obtained, systems can be designed for the loads they are expected to encounter and in-service systems can be monitored for degradation during their operation and maintained only when necessary.

### **2.1.2 Condition Monitoring (CM)**

Condition monitoring is the process of monitoring a condition parameter for the purpose of track a significant change that would result in a failure. CM is a method of evaluating a system's degradation in terms of 1) physical degradation, such as lengths of cracks, increase in resistance, increase in threshold voltage, and amount of deflection, or 2) performance degradation, such as deviation of the system's operating parameters (e.g., mechanical, acoustic or electrical) from expected values. The use of CM allows maintenance to be scheduled to avoid the consequences of failure before it occurs. Equipment can be monitored using sophisticated instrumentation such as vibration analysis equipment or the human senses. By using the right condition monitoring equipment, any changes in critical parameters such as vibration, temperature and speed can be identified. An effective CM system pays for itself within a significant short time. Some condition monitoring techniques include:

#### **1. Vibration Analysis**

Vibration analysis is the most commonly used condition monitoring technique. The frequencies of the vibrations can also be tracked since certain frequencies will only be present when conditions that indicate an incipient fault are present. Comparison of the vibration spectra of a healthy component versus a damaged one will provide the information required to make a decision when a maintenance action is required. In this work, vibration analysis (as shown in **Figure 2.1**, in red color) will be used to monitor the bearing response in order to identify the damage initiation phase.

#### **2. Infrared Thermography (Thermal Imaging)**

Condition monitoring using infrared thermography provides a safe and fast way of detecting abnormal behaviors in many different scenarios. Modern infrared

cameras have been used to detect increases in temperature that could result in potential problems. Since this technique does not require any direct contact with the machinery, it can be carried out safely while equipment is running.

### 3. Oil Analysis

The objective of oil analysis is to detect a presence of contamination in oil. This contamination can be caused by many things such as water and particles of other mineral. By analyzing oil samples during the operation of a particular machine, trends can be established in order to schedule a proper maintenance action. Oil analysis is used in the study of wear in machinery and has been used by tribologists. Many researchers have used oil debris sensors in order to quantify the amount of bearing material that has been lost during run-to-failure tests.

Condition monitoring systems use the following two methods to the variable of interest, as for an example, acceleration (Carr 1993):

1. **Direct Monitoring:** Direct monitoring is a measurement of the parameter itself, without the need for interpretation or calculation. An example of a direct-monitoring system is a force sensor that directly measures the applied force and a bourdon gage that directly measures pressure. Since any measurement involves disturbing the system, an ideal direct-sensing device should have the following requirements:

- ✓ Compatible with the development of existing electronics so that it has minimal impact on the performance and reliability of the monitored product.
- ✓ Accurate and self-correcting in operation.
- ✓ Fast in operation.
- ✓ Self-powered (e.g., battery or solar) or consuming system-independent or as little power from the parent system as possible.
- ✓ Lightweight so that it does not affect the weight and build of the monitored system.
- ✓ Easy to install and remove from the system for data acquisition, service and maintenance.

✓ Robust so that it does not get damaged during handling, shipping or operation.

2. **Indirect Monitoring:** Indirect monitoring involves determining the value of the desired parameter through the measurement of a related parameter (Choy et al 2003). The methods can be classified into time domain analysis, frequency domain analysis, joint time-frequency domain analysis and chaotic methods.

## 2.2 BEARING PROGNOSTICS

The prediction of remaining useful life of bearings has become of great importance because rotating machinery is one of the most common classes of machines. During the past years, a considerable amount of publications have emerged resulting in a development of valuable prognostic approaches in bearings. Bearings are critical components of many mechanical systems found in different applications in aerospace industry. Therefore, fault diagnosis and prognostics are frequently employed as a maintenance requirement in rotating machinery applications. Heng et al (2009) presented a review of different rotating machinery methods and identified the challenges and opportunities for future research. **Figure 2.2** shows the different methods in bearing prognostics. The existing methods are the following:

1. **Traditional reliability approaches**
2. **Prognostics approaches**
  - a. Physics-based prognostics models
  - b. Data-driven prognostics models
3. **Integrated approaches**

### 2.2.1 Physics-Based Prognostics Models

Typically, physics-based models are based on mathematical models that describe the physics of the system and failure modes, such as spall growth and crack propagation. The objective of these models is to combine the mechanics of the system, defect grow equations and CM in order to give a prognostic output. Qiu et al (2002) considered a bearing system as a single-degree of freedom and combined the acceleration response at the natural frequency with damage mechanics

principles in order to calculate the failure lifetime. Marble and Morton (2006) developed a software called Contact Analysis for Bearing Prognostics (CABPro) that uses a physics-based model to compute the spall growth trajectory and time to failure based on operating conditions.

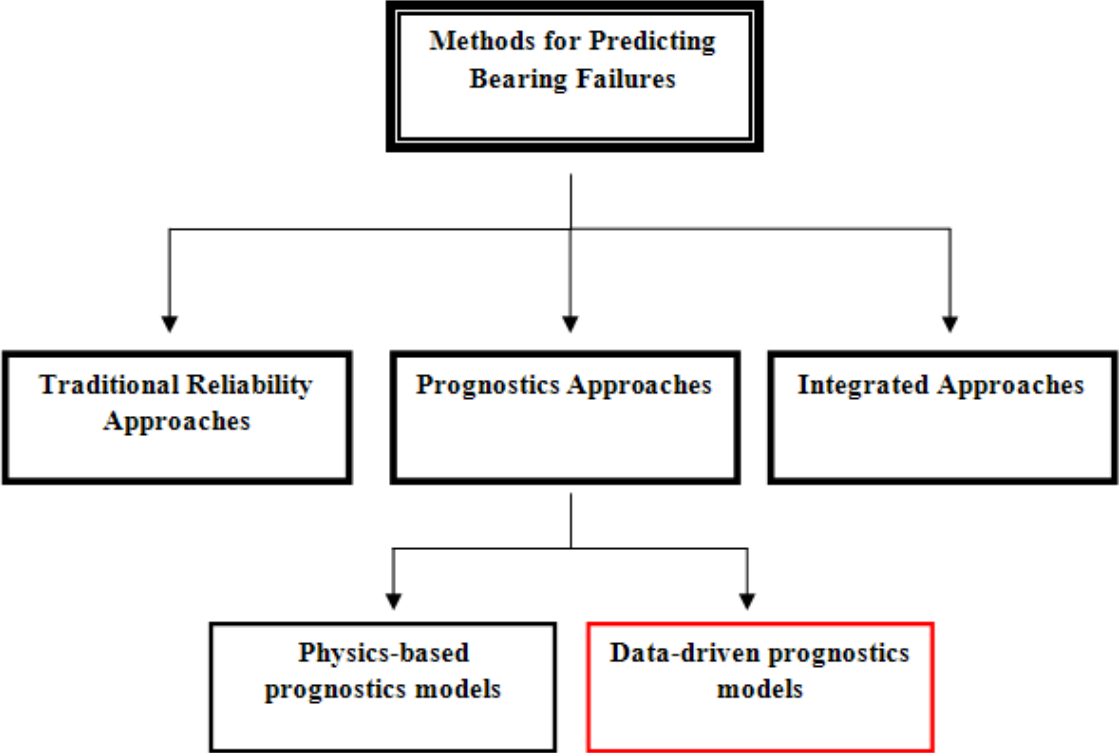


**Figure 2.2:** Methods for predicting bearing failures

### **2.2.2 Data-Driven Prognostics Models**

This work focuses on the data-driven approach (as shown in **Figure 2.2** in red color) to predict the bearing remaining useful life utilizing the current and past observations. Vibration signals will be used to characterize the behavior of the bearing in order to determine the life prediction. The objective of data-driven approaches is to derive models directly from regularly measured CM data instead of building models based on system physics and human knowledge. Some of data-driven models include simple projection methods, artificial neural networks (ANNs), particle filtering, high-order regression functions and Hidden Markov models (HMMs).

## **2.3 BEARING FAILURE MECHANISMS AND FAULT DETECTION**

As we know a bearing does not have infinite life. Sooner or later, the material fatigue will occur due to the operating conditions resulting in the failure of the component. The root cause of a bearing failure can occur during normal operation, installation, or transportation of the bearings. Often, a bearing may operate for a significant length of time after the initial cause of the failure, but fail well short of its estimated life span. The estimated life span is based on statistical laboratory studies and fatigue models. A premature bearing failure can be caused by any of several failure mechanisms, including (but not limited to) misalignment, electrical fluting, ingestion of contaminants or particles into the lubrication, improper fit, brinelling, corrosion, loss of lubrication, excessive temperature, manufacturing defects, material inconsistencies, and mechanical damage (Braun and Datner 1979; Afshari 1996). In most of these instances, the initial cause of the failure serves to reduce the fatigue life of the bearing by damaging the bearing surfaces and increasing the localized stresses on and below the bearing surfaces. By the time the bearing fails catastrophically, if the failure has not been detected sooner, the initial cause of the bearing failure may be masked by the massive damage that can accumulate (Harris 1991).

Fatigue is the result of cyclic shear stresses appearing on the surface. After a period of time, these stresses cause cracks which progressively extend up to the surface. In bearings, fatigue cracks form under high compressive stress. The spall formation is a result of a continuous initiation of thousands of small cracks. It is important to empathize that the spall initiation develops randomly which means that do not occurs in all bearings. The spalling progressively

increases until the bearing become unserviceable. The presence of spall produces an increase in noise and vibration levels in the bearing. The bearing life has two phases. The first phase is called bearing initial life and is defined as the portion of useful life prior spall initiation. Then, the next phase is the propagation life and this is the life from spall initiation to failure. Marble and Morton (2006) performed a comprehensive experimental study of bearing spall progression and developed a physics-based model for bearing prognosis. The model computes the spall growth trajectory and time to failure based on operating conditions and uses diagnostic feedback to self-adjust and reduce prediction uncertainty.

In order to analyze the spall of the bearing we need some type of indicators. Vibro-acoustic data provides reliable quantitative indicators. Using sensors that collect high frequency vibration data from bearings we can develop diagnostics algorithms to effectively track the bearing condition. It has been demonstrated that early failure symptoms are detectable at higher frequencies. Therefore, it's essential to perform waveform analysis and demodulation at these frequencies in order to incorporate time/frequency domain processing. Since the bearings generate an impulse every time that the defect rolls over the race, the demodulation process can be used to detect these impulse events. Either faults on the outer race or faults on the inner race generate response pulses. Bearing fault frequencies are clearly identifiable in the vibro-acoustic region of 1 through 100 kHz (Byington et al 2006). They developed a vibration monitoring system called ImpactEnergy® and it was used to detect spall defects on rolling elements bearings located on aircraft engines. After conducting a test contained three stages of operation at different speed and loads levels to simulate military accelerated mission tests, the results revealed that the areas of high energy were between 10 kHz and 30 kHz and between 40 kHz and 60 kHz. They used accelerometers to measure the vibration signals. Therefore, so far it is recommended to use sensors capable of read data within these frequency ranges. A critical problem in detecting faults in bearings is that their signals are masked by gear signals (Randall 2004). In other words, the gear signals affect the bearing signals by the introduction of noise which is a problem at the time of the interpretation of the signal. A classical approach to clean a noisy signal is to pass it through a filter to remove the unwanted noise (Khemili and Chouchane 2005).

In general, bearing elements are preloaded against one another by some desired amount during installation in order to yield the desired stiffness, load bearing and life characteristics during operation. This preload is achieved by press fitting the bearing onto the shaft, causing the inner raceway to expand, the initial clearances in the bearing to close, and a small amount of residual initial interference and corresponding preload to exist between the rolling elements and the raceways. When a rolling element encounters a surface defect, such as a spall, the normal balance of the preload forces on the rolling element is disrupted and the trajectory of the rolling element or raceway is suddenly altered. The normally occurring bearing loads also contribute to this effect, similar to a car tire rolling over a pothole. The result is a short time duration impulse input into the bearing system. The frequency at which rolling elements traverse a defect is the characteristic defect frequency, and this frequency can be directly calculated if the bearing geometry and the defect location are known (Barkov 1995). This periodic train of impulses into the system causes a regularly occurring wide band excitation of the structural vibration modes of the bearing and the surrounding machine components. Each impulse then produces a ringing in the various machine components which decays due to system damping. Examination of the various ringing and impulse frequencies of the system vibration can yield insight to the nature of the bearing defect (Harker and Sandy 1989). Bearing monitoring and fault detection strategies which rely on the monitoring of vibration signals employ methods such as statistical analysis, FFT and spectrum analysis, neural networks, and wavelets. In general, bearing defects can be classified into localized and distributed defects. Localized defects include pits, cracks and spalls caused by fracture on the rolling surface. On the other hand, distributed defects include waviness, surface roughness and misaligned races.

In this work, the prediction of the bearing remaining useful life will be based on a development of a localized defect.

# CHAPTER 3. VIBRATION DATA ANALYSIS USING EXPERIMENTAL DATA

As mentioned earlier, vibration data analysis is the most common commonly used condition monitoring technique. In this work, vibration data analysis will be applied to acceleration experimental data in order to perform a life prediction. In order to have a data that captures the behavior of the bearings, the data acquisition process should be performed effectively. Data acquisition is the process of sampling physical conditions (e.g., pressure, temperature and vibration) and conversion of the samples into a format that can be manipulated by a computer. Typically, it involves the conversion of analog waveforms into digital values for processing purposes. The main components of a data acquisition system are shown in **Figure 3.1**. See **Appendix A** for more details.

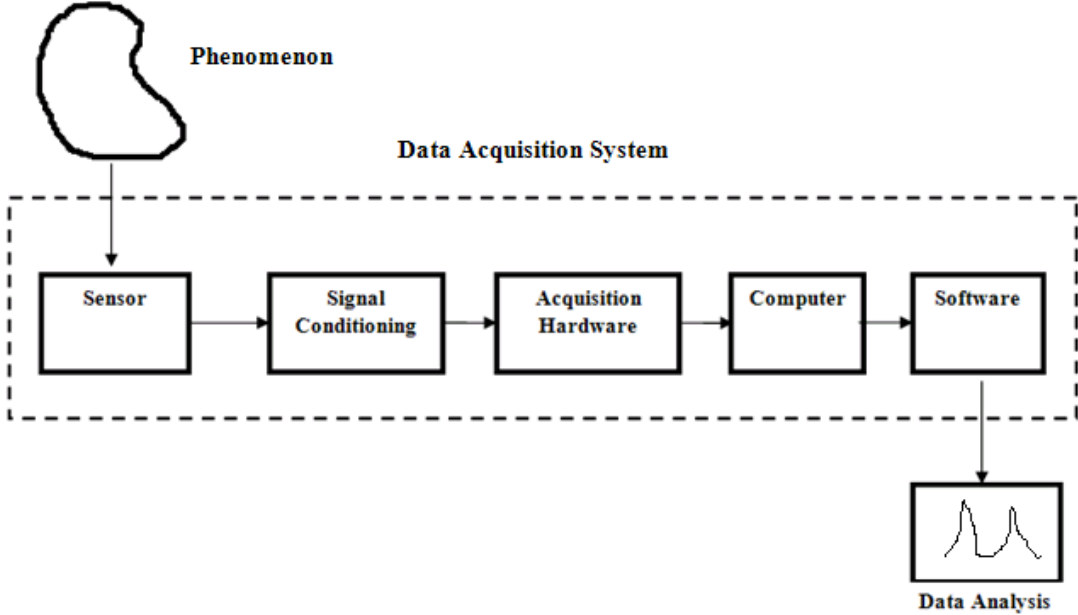


**Figure 3.1:** Components of a data acquisition system

## 3.1 DATA ANALYSIS METHODS

### 3.1.1 Statistical Analysis

A fault detection method called *Bicoherence* which is based in part on statistical analysis and in part on spectral analysis has been developed (Li et al 1995; Li et al 1996). Li et al (1995, 1996) describe the method in detail, beginning with an explanation of bispectrums. The bispectrum of a signal is defined as the double Fourier transform of the third moment of the signal and it measures the statistical dependence among three frequency components. In this case, these three frequencies will be multiples or a sum of the defect frequencies. Then, the quadratic coupling of these frequencies is examined. Bicoherence is an indication of the degree of quadratic coupling. Consequently, the bicoherence spectrum should have large values for frequency pairs which are multiples of the defect frequency. It follows that the magnitude of the bicoherence at these frequencies is a measure of the severity of the defect(s). Li et al. (1995, 1996) claim that localized defect detection by bicoherence analysis is so sensitive to the presence of a localized defect that it can detect a defect using signals in a low frequency band which is full of mechanical noise.

### 3.1.2 FFT and Spectral Analysis

Spectral analysis is used to transform a signal from the time domain to the frequency domain and vice versa. The spectral content of a periodic function is obtained by applying a Fourier Transform to the function. The Fourier transform of a periodic function  $x(t)$  is given by (Press et al 1992):

$$X(f) = \int_{-\infty}^{\infty} x(t)e^{i\omega t} dt \quad (3.1)$$

where  $\omega$  equals  $2\pi f$  and  $f$  is the frequency component of the signal. The resultant function  $X(f)$  is a sum of sine and cosine functions of varying frequencies.

In practical situations, the function  $x(t)$  is sampled, and Equation (3.1) does not apply. In such cases, the discrete Fourier Transform (DFT) is applied. The discrete Fourier Transform of  $N$  even sampled points of amplitude  $h_k$  is given by (Press et al 1992):

$$X_k(n) = \sum_{k=0}^{N-1} h_k e^{i\frac{2\pi kn}{N}} \quad (3.2)$$

where  $X_k$  are the Fourier components and  $N$  is the number of samples per record (or sample size). The independent variable  $n$  can be related to the frequency by the relation  $f_n = (n/Nh)$ , where  $h$  is the sampling interval between adjacent points and  $T=Nh$  is the total record length. The discrete Fourier Transform of  $N$  sampled values typically requires  $N^2$  computations.

If the sample size  $N$  is a power of 2, a variant of the DFT, called the Fast Fourier Transform (FFT) is used to find the discrete Fourier Transform of  $N$  sample values in only  $N \log_2 N$  computations. This translates to a difference between 30 seconds of CPU time and 2 weeks of CPU time on a microsecond cycle time computer (Press et al 1992).

FFT and spectrum analysis methods for determining bearing condition have also been proposed with claims of success. Researchers in the field of rolling element bearing diagnostics all agree that a strong correlation exists between the health of a bearing and the spectral content of its vibration. An early attempt at something more sophisticated than simply looking at spectral output and searching for defect frequencies involves decomposing the vibration signal into a sum of different periodic signals and random components, and then computing the RMS value of frequency components which correspond to bearing defect frequencies (Braun and Datner 1979). Bearing damage status can then be ascertained by examining these RMS values, with RMS values of the bearing defect frequencies increasing with increasing damage. Braun and Datner (1979) claim that this method is less dependent on sensor location than simply examining the spectral data and searching for the magnitude of the spectrum at the defect frequencies. A similar, albeit slightly more sophisticated, detection method is outlined by Koizumi and Taniguchi (1986).

A simple FFT based approach is described by Kuhnell and Rees (1987). Simply put, accelerometers are attached directly to the bearing housing, the vibration data is sent periodically to a computer, and the computer calculates the FFT of the data and stores the spectral data. The system automatically produces reports, which include the original vibration spectral data, the most recent spectral data, and the current spectrum being collected. Ultimately, the computer operator must make the analysis decisions based on defect frequency analysis. A similar method is reported by Rao (1990) in which the author states that the choice of window for an FFT represents a tradeoff between time and frequency resolution. A Wigner distribution is a joint time-frequency signal representation which mitigates this tradeoff. The Wigner distribution is the Fourier spectrum of an inner product kernel derived from the input signal. Using this method, long-term transient spectral phenomena can be observed, specifically events near the defect frequencies.

Berry (1986) contends that spectral content, not vibration magnitude, is the key to revealing bearing condition. He showed that L10 bearing life is significantly reduced when significant dynamic loads are present, thus neither vibration magnitude nor life calculations are sufficient to determine bearing life. The vibration spectra of defective bearings are described to include: random, ultrasonic frequencies; natural frequencies, rotational defect frequencies; and sum and difference frequencies. He also discussed details of several defect frequencies are described, and optimal sensor placement. Real-world failure scenarios are presented with emphasis on analyzing frequency data in order to predict the remaining life in a bearing. In particular, the defect frequencies and their migrations are examined.

A method similar to Envelope Analysis is presented by Li et al (1995) in which estimations are made of the rate and strength of impulsive vibrations, which may be the result of localized faults. If the pulse generating frequency is close to any of the characteristic defect frequencies and the strength of the impulse train is significant, the bearing will be classified as damaged. The digital vibration data passes through a high pass filter and a median smoother, and is then processed by both a zero-crossing rate filter and a short-time energy filter. Both of these filtered data sets are then passed through an auto-correlation and peak locator. The amplitude of the resulting digital signals is a measure of the strength of the vibration signal. The two digital

signals are then sent to a frequency comparator and compared to the calculated defect frequencies.

### 3.2 BEARING TYPES

Rolling element bearings are an assembly of several parts: an outer race, an inner race, a set of rollers or balls and a cage or retainer. The cage maintains even spacing of the rolling elements. Bearings have very little rolling resistance and sliding. The purpose of this section is to summarize the different types of bearings and presents the bearing type considered for the analysis of this work. Bearings can be grouped into the following categories:

#### 1. Ball

- a. Radial
- b. Angular Contact
- c. Thrust

#### 2. Roller

- a. Cylindrical
- b. Spherical

In this work, the vibration data analysis has been performed on experimental data of a Rexnord ZA-2115 Spherical Double Row Bearing. Bearing characteristics are shown in **Table 3.1**.

**Table 3.1:** Bearing characteristics.

<i>Rexnord ZA-2115 Double Row Bearing Characteristics</i>	
Number of rollers	16 per row (32 total)
Contact angle	15.17°
Pitch diameter	2.815 in.
Rolling element diameter	0.331 in.

### 3.3 BEARING FAULT FREQUENCIES

Vibration data provides some of the most reliable quantitative indicators of gear, bearing and rotating component fatigue. Vibration sensors work within a particular range of frequencies. Before the selection of vibration sensor(s), we need to know the frequencies we want to analyze for detecting possible faults in bearings or gears. Byington et al (2006) develop a feature extraction and analysis driven system that integrates high frequency vibration/acoustic emission data to assess the health of bearings and gearboxes in turbine engines. They examined frequency domain features known as Bearing Fault Frequencies. These frequencies are geometry and RPM dependent and are produced by a bearing defect. Li et al (2000) used these frequencies to develop an approach for motor rolling bearing fault diagnosis using neural networks and time/frequency-domain bearing vibration analysis. Stack et al (2003) also used these frequencies in their research that introduces the notion of categorizing bearing faults as either single-point defect or generalized roughness.

Rolling bearings are composed of two concentric rings called the outer raceway and inner raceway with a set of rolling elements running in their races. Generally, there are five basic frequencies, as shown in **Figure 3.4**, that can be used to describe of a bearing movement and each motion generates a unique frequency response. If we define  $V_o$ ,  $V_c$  and  $V_i$  as the liner velocities of the outer raceway, cage and outer raceway, respectively, we can derive the equations for the bearing fault frequencies. **Figure 3.2** shows the location of the linear velocities. Before the derivation of these equations, let's define some additional variables that are related to the geometry of the ball bearing.  $D$ ,  $\alpha$  and  $d$  represent the pitch diameter, contact angle and rolling element diameter, respectively. **Figure 3.3** shows a schematic of the ball bearing geometry. In this work we will use bearing fault frequencies in order to provide early fault indication. These equations can be applied to either ball or roller bearings.

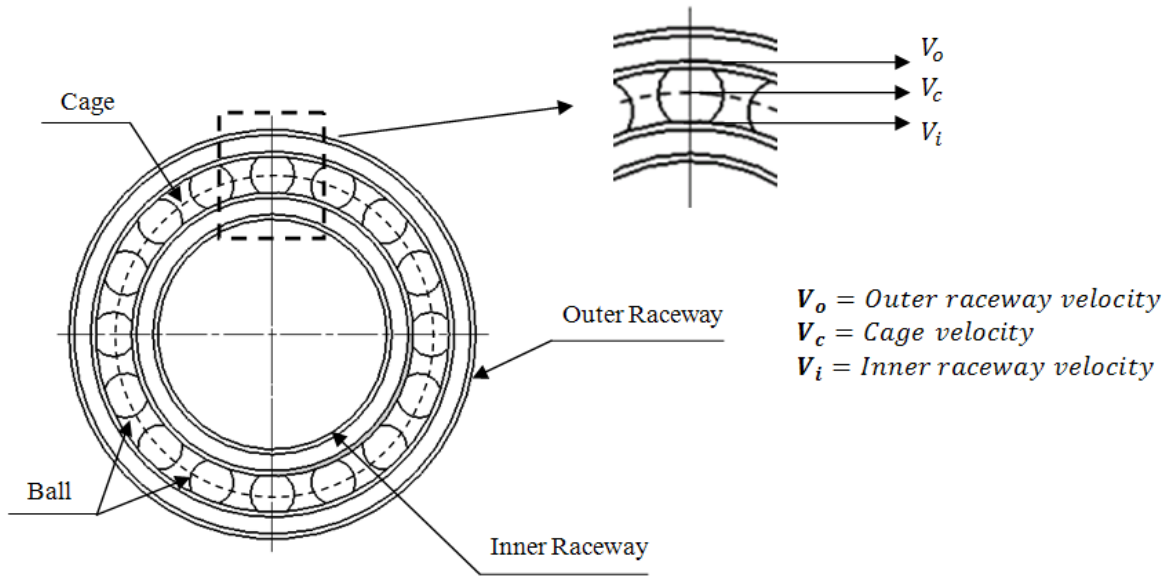


**Figure 3.2:** Bearing dynamics

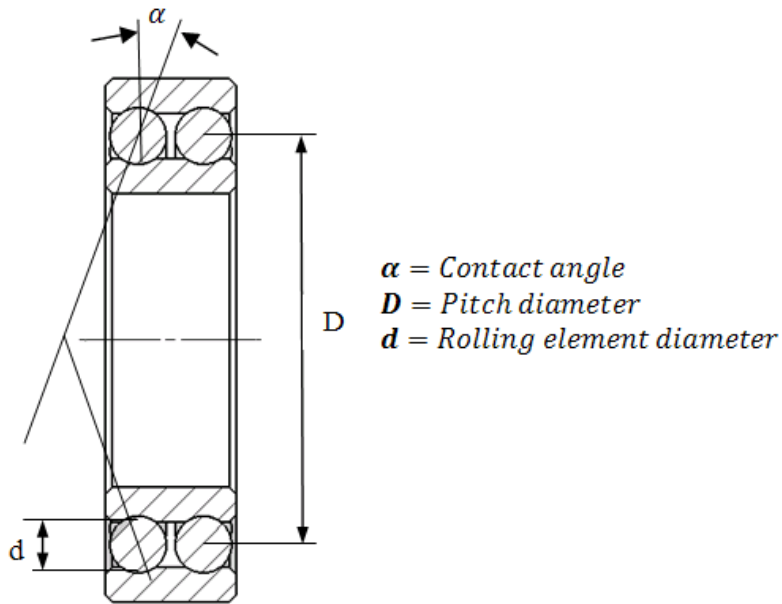


**Figure 3.3:** Bearing geometry

## 1. Shaft Rotational Frequency ( $F_S$ )

The rotational frequency of the shaft is very important because bearings are often used to form a bearing-rotor system. We can express the bearing fault frequencies as a function of this frequency. The shaft rotational frequency is given by:

$$F_S = \frac{\text{shaft speed (rpm)}}{60} \quad (\text{Hz}) \quad (3.3)$$

## 2. Fundamental Cage Frequency ( $F_{FCF}$ )

The fundamental cage frequency is the rotational frequency of the cage. It is the frequency at which the retainer operates and can be derived from the linear velocity of the cage  $V_C$ . The velocity of the cage is defined as the mean of the linear velocity of the outer raceway and the inner raceway:

$$V_C = \frac{V_o + V_i}{2} \quad (3.4)$$

If we divide Equation (3.4) by the radius of the cage  $R_c = D/2$  we get the fundamental cage frequency:

$$F_{FCF} = \frac{V_C}{R_C} = \frac{V_o + V_i}{D} \quad (3.5)$$

We can express the linear velocities  $V_o$  and  $V_i$  in terms of their respective rotational frequencies  $F_o$  and  $F_i$  multiplied by the outer raceway and inner raceway radius respectively. The outer raceway  $R_o$  and inner raceway  $R_i$  radius are given by:

$$R_o = R_c + \frac{d \cos \alpha}{2} \quad (3.6)$$

$$R_i = R_c - \frac{d \cos \alpha}{2} \quad (3.7)$$

Substituting Equations (3.6) and (3.7) into (3.5) we get the following:

$$F_{FCF} = \frac{V_o + V_i}{D} = \frac{F_o R_o + F_i R_i}{D} = \frac{1}{D} \left( F_o \frac{D + d \cos \alpha}{2} + F_i \frac{D - d \cos \alpha}{2} \right) \quad (3.8)$$

### 3. Ball Pass Inner Raceway Frequency ( $F_{BPIF}$ )

The ball pass inner raceway frequency is the rate at which the balls pass a point on the track of the inner raceway. This is the frequency at which a single defect in the inner race will be detected and is equal to the number of bearing balls  $N_B$  multiplied by the difference between the fundamental cage frequency and the inner raceway frequency:

$$F_{BPIF} = N_B |F_{FCF} - F_i| \quad (3.9)$$

$$= N_B \left| \frac{F_i R_i + F_o R_o}{D} - F_i \right| \quad (3.10)$$

Substituting (3.6) and (3.7) into (3.10) we get:

$$= N_B \left| \frac{F_i \left( R_c - \frac{d \cos \alpha}{2} \right) + F_o \left( R_c + \frac{d \cos \alpha}{2} \right)}{D} - F_i \right| \quad (3.11)$$

$$= N_B \left| \frac{F_i \left( \frac{D - d \cos \alpha}{2} \right) + F_o \left( \frac{D + d \cos \alpha}{2} \right)}{D} - F_i \right| \quad (3.12)$$

$$= N_B \left| \frac{F_i(D - d \cos \alpha) + F_o(D + d \cos \alpha) - 2DF_i}{2D} \right| \quad (3.13)$$

$$= \frac{N_B}{2} \left| F_i \left( 1 - \frac{d \cos \alpha}{D} \right) + F_o \left( 1 + \frac{d \cos \alpha}{D} \right) - 2F_i \right| \quad (3.14)$$

$$= \frac{N_B}{2} \left| F_o \left( 1 + \frac{d \cos \alpha}{D} \right) + F_i \left( 1 - \frac{d \cos \alpha}{D} - 2 \right) \right| \quad (3.15)$$

$$= \frac{N_B}{2} \left| F_o \left( 1 + \frac{d \cos \alpha}{D} \right) + F_i \left( \frac{-D - d \cos \alpha}{D} \right) \right| \quad (3.16)$$

$$= \frac{N_B}{2} \left| F_o \left( 1 + \frac{d \cos \alpha}{D} \right) - F_i \left( 1 + \frac{d \cos \alpha}{D} \right) \right| \quad (3.17)$$

$$= \frac{N_B}{2} \left| (F_o - F_i) \left( 1 + \frac{d \cos \alpha}{D} \right) \right| \quad (3.18)$$

$$= \frac{N_B}{2} \left| (F_i - F_o) \left( 1 + \frac{d \cos \alpha}{D} \right) \right| \quad (3.19)$$

#### 4. Ball Pass Outer Raceway Frequency ( $F_{BPOF}$ )

The ball pass outer raceway frequency is the rate at which the balls pass a point on the track of the outer raceway. This is the frequency at which a single defect in the outer race will be detected and is equal to the number of bearing balls  $N_B$  multiplied by the difference between the fundamental cage frequency and the outer raceway frequency:

$$F_{BPOF} = N_B |F_{FCF} - F_o| \quad (3.20)$$

$$= N_B \left| \frac{F_i R_i + F_o R_o}{D} - F_o \right| \quad (3.21)$$

Substituting (3.6) and (3.7) into (3.21) we get:

$$= N_B \left| \frac{F_i \left( R_C - \frac{d \cos \alpha}{2} \right) + F_o \left( R_C + \frac{d \cos \alpha}{2} \right)}{D} - F_o \right| \quad (3.22)$$

$$= N_B \left| \frac{F_i \left( \frac{D - d \cos \alpha}{2} \right) + F_o \left( \frac{D + d \cos \alpha}{2} \right)}{D} - F_o \right| \quad (3.23)$$

$$= N_B \left| \frac{F_i(D - d \cos \alpha) + F_o(D + d \cos \alpha) - 2DF_o}{2D} \right| \quad (3.24)$$

$$= \frac{N_B}{2} \left| F_i \left( 1 - \frac{d \cos \alpha}{D} \right) + F_o \left( 1 + \frac{d \cos \alpha}{D} \right) - 2F_o \right| \quad (3.25)$$

$$= \frac{N_B}{2} \left| F_i \left( 1 - \frac{d \cos \alpha}{D} \right) + F_o \left( 1 + \frac{d \cos \alpha}{D} - 2 \right) \right| \quad (3.26)$$

$$= \frac{N_B}{2} \left| F_i \left( 1 - \frac{d \cos \alpha}{D} \right) + F_o \left( \frac{-D + d \cos \alpha}{D} \right) \right| \quad (3.27)$$

$$= \frac{N_B}{2} \left| F_i \left( 1 - \frac{d \cos \alpha}{D} \right) - F_o \left( 1 - \frac{d \cos \alpha}{D} \right) \right| \quad (3.28)$$

$$= \frac{N_B}{2} \left| (F_i - F_o) \left( 1 - \frac{d \cos \alpha}{D} \right) \right| \quad (3.29)$$

## 5. Ball Rotational Frequency ( $F_B$ )

The ball rotational frequency is the rate of rotation of a ball about its own axis in a bearing. It is the frequency at which a single defect on a rolling element will be detected and is given by:

$$F_B = \left| (F_i - F_{FCF}) \frac{R_i}{R_b} \right| \quad (3.30)$$

Since  $R_b = d/2$  we get:

$$= \left| (F_i - F_{FCF}) \frac{\left( R_C - \frac{d \cos \alpha}{2} \right)}{\frac{d}{2}} \right| \quad (3.31)$$

$$= \left| (F_i - F_{FCF}) \frac{\left(\frac{D - d \cos \alpha}{2}\right)}{\frac{d}{2}} \right| \quad (3.32)$$

$$= \left| (F_i - F_{FCF}) \left(\frac{D - d \cos \alpha}{d}\right) \right| \quad (3.33)$$

Substituting (3.8) into (3.33) we get:

$$= \left| \left( F_i - \frac{F_o R_o + F_i R_i}{D} \right) \left( \frac{D - d \cos \alpha}{d} \right) \right| \quad (3.34)$$

$$= \left| \left[ F_i - \frac{F_i \left(\frac{D - d \cos \alpha}{2}\right) - F_o \left(\frac{D + d \cos \alpha}{2}\right)}{D} \right] \left( \frac{D - d \cos \alpha}{d} \right) \right| \quad (3.35)$$

$$= \left| \left[ \frac{2DF_i - F_i(D - d \cos \alpha) - F_o(D + d \cos \alpha)}{2D} \right] \left( \frac{D - d \cos \alpha}{d} \right) \right| \quad (3.36)$$

$$= \frac{1}{2d} \left| \left[ \frac{2DF_i - DF_i + F_i d \cos \alpha - F_o(D + d \cos \alpha)}{D} \right] (D - d \cos \alpha) \right| \quad (3.37)$$

$$= \frac{1}{2d} \left| \left[ \frac{DF_i + F_i d \cos \alpha - F_o(D + d \cos \alpha)}{D} \right] (D - d \cos \alpha) \right| \quad (3.38)$$

$$= \frac{1}{2d} \left| \left[ F_i \left( 1 + \frac{d \cos \alpha}{D} \right) - F_o \left( 1 + \frac{d \cos \alpha}{D} \right) \right] (D - d \cos \alpha) \right| \quad (3.39)$$

$$= \frac{1}{2d} \left| (F_i - F_o) \left( 1 + \frac{d \cos \alpha}{D} \right) (D - d \cos \alpha) \right| \quad (3.40)$$

$$= \frac{D}{2d} \left| (F_i - F_o) \left( 1 - \frac{d^2 \cos^2 \alpha}{D^2} \right) \right| \quad (3.41)$$

Assuming that the outer raceway is stationary and the inner raceway is rotating at the speed of the shaft,

$$F_i = F_s , F_o = 0$$

Therefore, the bearing fault frequencies equations become:

$$F_{FCF} = \frac{F_s}{2} \left( 1 - \frac{d \cos(\alpha)}{D} \right) \quad (Hz) \quad (3.42)$$

$$F_{BPIF} = \frac{N_B F_s}{2} \left( 1 + \frac{d \cos(\alpha)}{D} \right) \quad (Hz) \quad (3.43)$$

$$F_{BPOF} = \frac{N_B F_s}{2} \left( 1 - \frac{d \cos(\alpha)}{D} \right) \quad (Hz) \quad (3.44)$$

$$F_B = \frac{D F_s}{2d} \left( 1 - \frac{d^2 \cos^2(\alpha)}{D^2} \right) \quad (Hz) \quad (3.45)$$

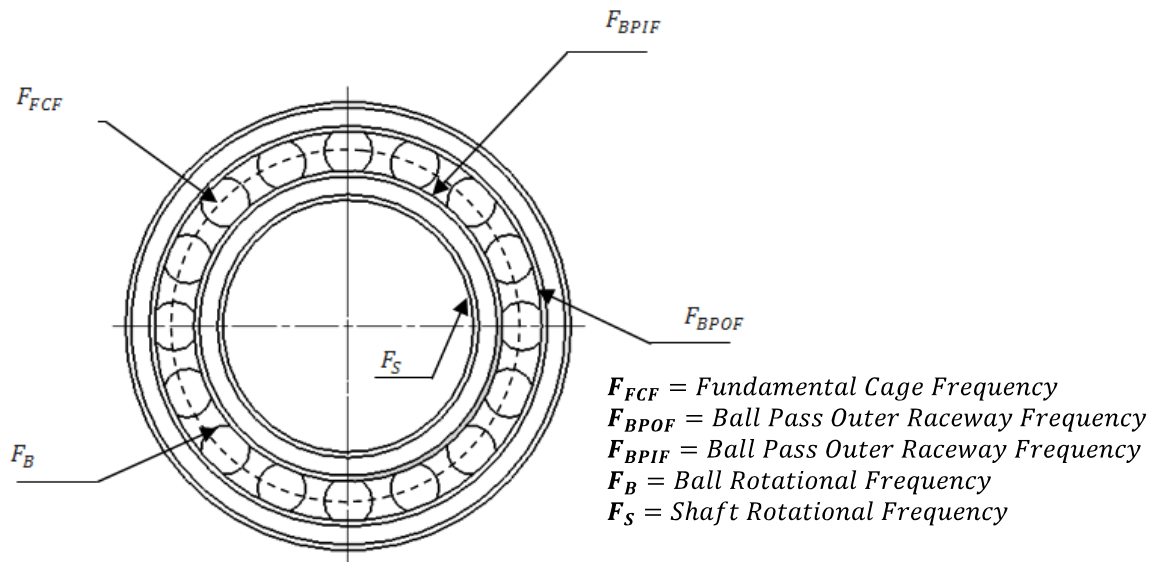


**Figure 3.4:** Frequencies in a bearing

Specific fault frequencies are clearly identifiable in the vibro-acoustic regime of 1 through 100 kHz (Byington et al 2006). Therefore, for this work we will the dimensions of the bearings in the EMA to calculate the fault frequencies in order to know the vibro-acoustic regime that our sensors should be capable of identify specific faults. Also, by knowing these frequencies we can design optimum filters to start filtering the data measured from sensors in order to focus on the magnitude of specific fault frequencies.

Another feature of fault frequencies is their harmonics. Higher harmonics of these frequencies are also important indicators of faults. When a defect is generated on one of the parts of the bearing, related frequency, its sidebands, its orders, etc. may take place in a spectrum graph (Orhan et al 2006). In order to diagnose and isolate the fault, extraction of the energy or power level at these fault frequencies from a FFT or power spectral density (PSD) plot can be very useful. We can compare the magnitudes of the frequencies against known baselines to start tracking a specific fault. If we measure a larger than expected magnitude at a bearing fault frequency, it confirms a fault in that specific bearing component. It is expected that those magnitudes increase as the severity of the fault increases.

For defects on the raceway of a rolling bearing, each time a roller hits the defective raceway, the corresponding ball pass outer raceway frequency,  $F_{BPOF}$ , or ball pass inner raceway frequency,  $F_{BPIF}$ , will be generated (Li et al 1998). If the defective area is large, the harmonics of  $F_{BPOF}$  and  $F_{BPIF}$  will also be generated. Therefore, the existence of these harmonics can help to indicate the severity of the defect. The simplest spectrum for bearing vibration is the one caused by bearing looseness. Only fundamental cage frequency ( $F_{FCF}$ ) or shaft rotational frequency ( $F_S$ ) and their harmonics exist for this case. **Table 3.2** shows a list of bearing vibration frequency characteristics for different faults.

**Table 3.2:** Vibration frequency characteristics.

Location of fault	Frequency	Observations
Rolling elements	$F_{BPOF}, F_{BPIF}$	Modulated by $2 F_B, F_{FCF}$
Bearing looseness	$F_S, F_{FCF}$	Harmonics of $F_S, F_{FCF}$
Outer raceway	$F_{BPOF}$	-- An increase in the severity of the defects produces higher order harmonics -- Frequency shift in the spectrum
Inner raceway	$F_{BPIF}$	

Bearing fault frequencies may not always be visible because a bearing tends to be a low-energy device compared to the remainder of the rotating machine. The fault frequencies are visible when the bearings are on their way to destruction. The chances of picking up an inner race fault are small unless the load direction of the bearing coincides with the location of the accelerometer. Any impact between a rolling element and the inner race must transmit across the rolling element, through an oil film, through the outer race, through the bearing housing, to the accelerometer. Therefore, the transmission path of the vibration is longer for the inner race. Also, the inner race is displaced away from the load zone causing that the amplitude of the impact is lower. The difficulty of the transmission path from the inner race to the housing helps

to explain why an outer race fault tends to be the easiest one to observe. The same type of defect produces a larger level of vibration in the outer race than in the inner race. Sensors are commonly placed in the outer part of the bearing. Experts in health monitoring have shown that inner race failures produce catastrophic breakdowns earlier than any other type faults (Duque et al 2005). The most common bearing failures take place in the following elements, listed in order of importance:

1. Inner race
2. Outer race
3. Rolling elements
4. Cage

A spall on a ball of a ball bearing will not always contact the inner and outer race, because sometimes the spall may be oriented in the axial direction and miss a race. Therefore, this effect may be extremely difficult to detect. Some papers on the vibration monitoring of bearings state that bearings are least likely to fail because of ball problems. It is far more likely, however, that ball failures are least likely to be observed until severe damage has occurred on the races as well as on the balls. This problem of observation does not appear in roller bearings because the rollers always maintain the same orientation with respect to the races. When the bearing cage is deteriorated enough to cause a measurable amount of unbalance at the accelerometer, it is likely that total failure occurs within a short time. Note that a bearing that is loose in its housing will spin at about half shaft speed, causing a peak at that frequency.

A confusing phenomenon in bearing analysis that the fault frequencies equations fail in their accuracy is when bearing components slip along each other on an oil film, rather than maintaining rolling contact. Although slippage is usually only a few percent, it has been observed to be almost fifty percent during some modes of operation of a gas turbine engine in flight.

## 3.4 CONDITION INDICATORS

Condition indicators have been widely used for machine condition monitoring purposes. The use of CIs helps us to detect specific faults in gearboxes and some of them enable us to track the vibration level of the system. Therefore, the role of CIs is extremely important in the design of a health monitoring system. The differences between these CIs are in the signal from which the calculations are performed. Another difference is that some CIs use time-domain data and others frequency-domain data. In this chapter, some CIs were calculated using the vibration data in order to see how it behaves and been able to detect when the fault began to initiate.

### 3.4.1 Kurtosis

Kurtosis is a measurement used to determine the "peakedness" of a data distribution. It measures whether the data is sharp or flat relative to a normal distribution. If a vibration signal contains sharp peaks with a higher value, we can say that its distribution function will be sharper. One method for predicting bearing condition is based on this statistical parameter (Dyer and Stewart 1978). The results of this method are based on an experimental study in which the acceleration is measured in close proximity to the outer ring of the test bearing. The measured acceleration is then used to calculate the values of kurtosis. In general, vibration signals of healthy bearings are Gaussian in distribution, regardless of load and speed, therefore the value of the kurtosis is close to three for the vibration signals of healthy bearings<sup>2</sup>. The appearance of a fatigue crack or a spall on the bearing surfaces resulted in kurtosis values that were significantly greater than three. As damage became severe, kurtosis values settled back to three. As a result, the extent of bearing damage may be assessed by examining the distribution of the kurtosis in selected frequency ranges.

It is for that reason that Kurtosis has been used by many researchers for health monitoring purposes. Kurtosis value analysis brings out variations in the vibration characteristics of machine bearing through estimation of change in shape of important frequency components of the vibration spectrum. Kurtosis is recognized to be the sensitive good parameter for machine diagnosis. It has a value of 3.0 under normal conditions and the value generally goes up as the

---

<sup>2</sup> The kurtosis values in this study are normalized such that the kurtosis of a square-wave equals 1, the kurtosis of a sine-wave equals 1.5, and the kurtosis of a waveform with a Gaussian amplitude distribution equals 3.

deterioration increases. However, there are cases that kurtosis value goes up and then goes down when damages increase as time passes. The mathematical definition of kurtosis is given by:

$$Kurt = \frac{N \sum_{i=1}^N (s_i - \bar{s})^4}{[\sum_{i=1}^N (s_i - \bar{s})^2]^2} \quad (3.46)$$

where

$N$  = is the number of points in the history of signal  $s$

$s_i$  = is the  $i^{\text{th}}$  point in the time history of signal  $s$

Using the above definition and our time-domain data, we proceed to calculate the kurtosis value for bearing 1 in  $X$ -direction (Test 2). We used a MATLAB built-in function named *kurtosis* (for more details see **Appendix C**). **Figure 3.5** shows the results. We can see that the variation of kurtosis value is moderate until it reaches approximately 6500 minutes that starts to increase.

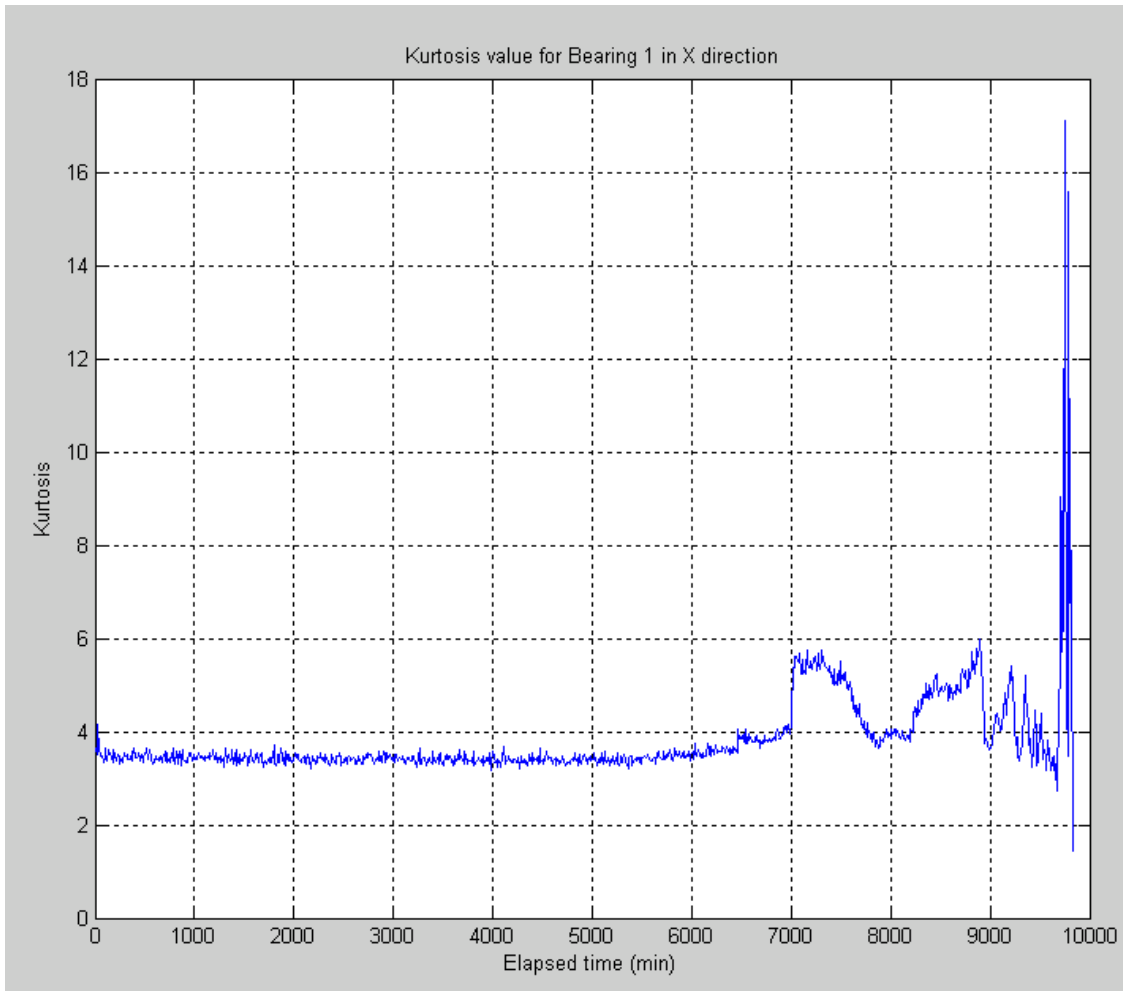


**Figure 3.5:** Kurtosis value for bearing 1 in X-direction.

### 3.4.2 Root Mean Square Value (*RMS*)

The *RMS* value has been used for track the vibration level of a system. In gearboxes, this value is used to monitor the overall vibration level. The *RMS* value of the vibration signal is a very good descriptor of the overall condition of the tested gearboxes. The *RMS* value is given by the following equation:

$$S_{rms} = \sqrt{\frac{1}{N} \sum_{i=1}^N (S_i)^2} \quad (3.47)$$

where

$N$  = is the number of points in the history of signal  $s$

$S_i$  = is the  $i^{\text{th}}$  member of data set  $S$

We applied the above equation to our accelerometer time-domain data in order to calculate the *RMS* as a function of elapsed time. **Figure 3.6** shows the results for the *RMS* value. We can note that like the previous case of kurtosis analysis, there is a significant change in the *RMS* value around 6500 minutes.

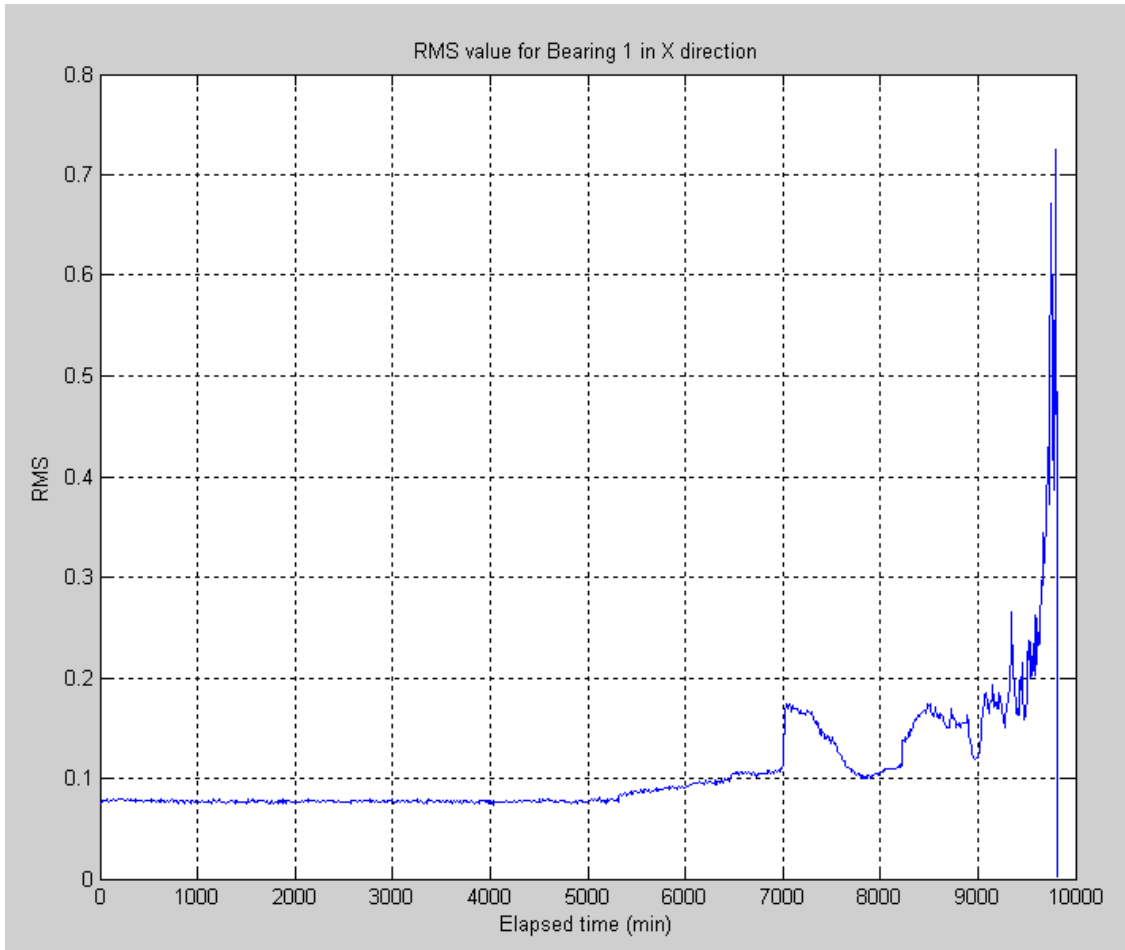


**Figure 3.6:** *RMS* value for bearing 1 in *X*-direction.

### 3.5 THE FAST FOURIER TRANSFORM (FFT) PROCEDURE

The frequency components of a time-domain signal are extracted by performing a Fast Fourier Transform (FFT) to convert the data to the frequency-domain. After obtain the FFT, then we can perform Power Spectral Density (PSD) plots of the signal. But before obtain the PSD plots, we need to understand the procedure of the FFT. Since we have a discrete signal from accelerometers, we need to use the definition of the Discrete Fourier Transform or DFT. The DFT is a special case of the discrete-time Fourier transform or DTFT. For a causal signal  $x(k)$ , the DTFT is defined as follows:

$$X(f) = \sum_{k=0}^{\infty} x(k) \exp(-jk2\pi fT), \quad -\frac{f_s}{2} < f \leq \frac{f_s}{2} \quad (3.48)$$

where  $f_s$  is the sampling frequency and  $T = 1/f_s$

We can simplify the previous expression by restricting our analysis to signals of finite duration. The DTFT converges for time signals that are absolutely summable (Schilling and Harris 2005). If  $x(k)$  is absolutely summable, then  $|x(k)| \rightarrow 0$  as  $k \rightarrow \infty$ . Therefore, the DTFT can be approximated by:

$$X(f) \approx \sum_{k=0}^{N-1} x(k) \exp(-jk2\pi fT) \quad (3.49)$$

Then we evaluate  $X(f)$  at  $N$  discrete values of  $f$ ,

$$f_i = \frac{if_s}{N} \quad (3.50)$$

By substituting the previous expression and  $T = 1/f_s$  into the DTFT equation, we get a more general version of the DTFT expression,

$$X(f) \approx \sum_{k=0}^{N-1} x(k) \exp\left(\frac{-jk2\pi i}{N}\right), \quad 0 \leq i < N \quad (3.51)$$

MATLAB uses a built-in function called *fft* that calculates the discrete Fourier transform. Our goal is to verify the results using both the MATLAB function and the definition (see **Appendix C**). Before we can proceed, we need to rewrite the definition because MATLAB does not accept zero or negative indices. Therefore, the definition of the DFT becomes:

$$X(f) \approx \sum_{k=1}^N x(k) \exp\left(\frac{-j2\pi(k-1)(i-1)}{N}\right), \quad 0 \leq i < N \quad (3.52)$$

### 3.6 BASELINES

In order to diagnose the fault, the PSD plots need to be examined to extract the power level of the bearing fault frequencies. The extraction of the power level of critical frequencies allows us to compare them against known baselines. A larger than allowable value at a bearing fault frequency confirms a fault in that corresponding bearing component. It is for that reason that the selection of baselines or the use of a reference standard plays an important role in diagnosing the fault. One of the standards that can be considered is the ISO 10816 used for evaluation of vibration severity.

### 3.7 ANALYSIS ON TEST 2

On the second test, which was performed from 02/12/2004 until 02/19/2004, they found that an outer race failure occurred on bearing 1. Therefore, we took data from the second test in order to analyze the frequency components of bearing 1. Each data set contains information about both bearing 1 and bearing 2 and represents one second snapshot sampled at 20 kHz. However, we

are focusing on bearing 1. **Figure 3.7** and **3.8** show the accelerometer data recorded on 02/12/2004 and 02/18/2004, respectively.

We learned how to take a time-domain signal and convert it to its frequency domain by developing a MATLAB algorithm that reads the data set, perform a FFT and obtain the Power Density Spectrum. Also, our algorithm calculates statistical features like Kurtosis and *RMS*. To confirm a failure in the outer race of bearing 1, we expect to see a change in magnitude on the power spectrum for the ball pass outer race frequency component (BPOF).

Based on bearing dimensions and shaft speed, the MATLAB algorithm calculates the bearing fault frequencies. **Table 3.3** shows the calculated frequencies. The fault frequencies for both bearings are the same since the bearings are identical and rotate at the same speed. Then the algorithm extracts the bearing data from the text files.

**Table 3.3:** Fault frequencies based on bearing dimensions.

<i>Bearing Fault Frequencies (Hz)</i>	
BPOF	236.4
BPIF	296.9
FB	139.9
FCF	14.8

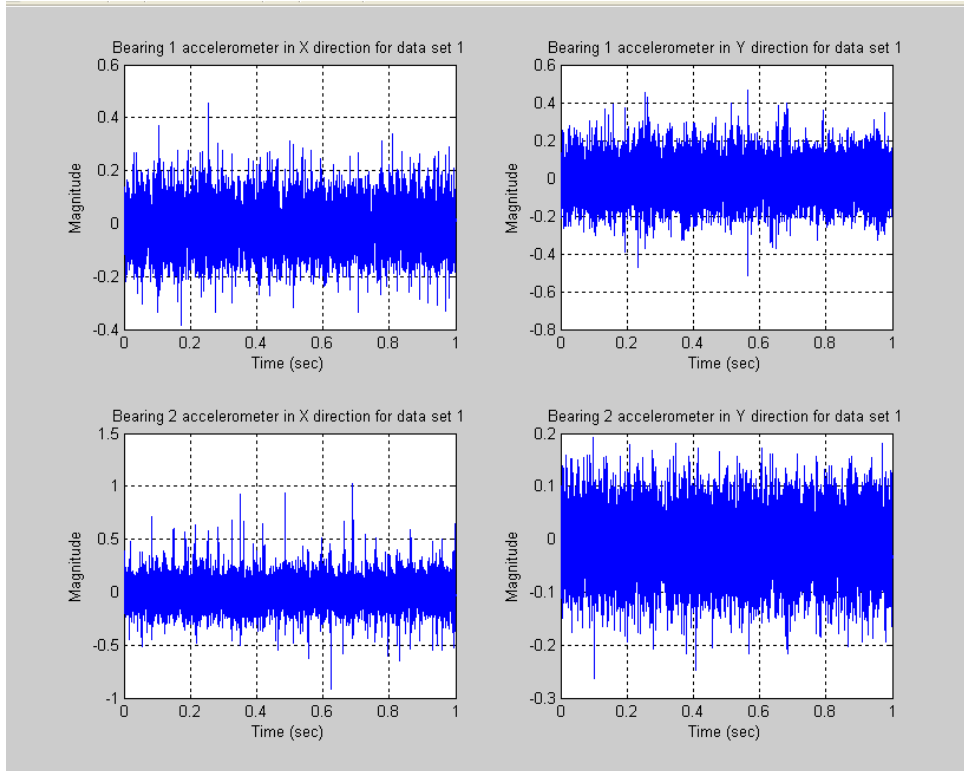


**Figure 3.7:** Vibration signal recorded on 02/12/2004.

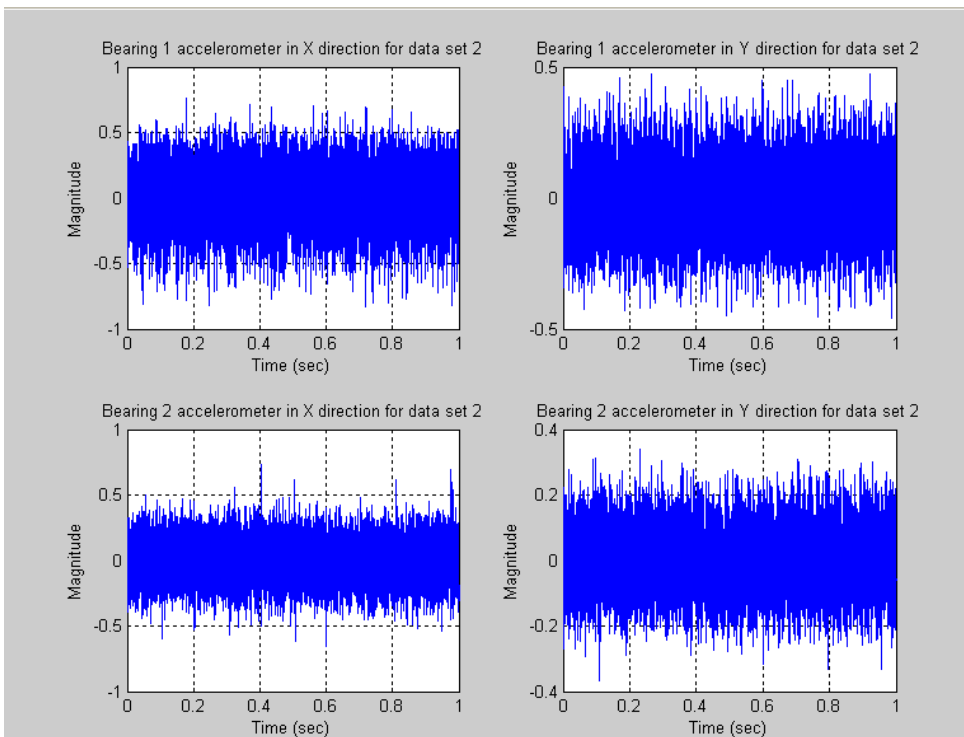


**Figure 3.8:** Vibration signal recorded on 02/18/2004.

**Bearings failure mode:** Small spalling or cracks were formed and were later smoothed by the continuous rolling contact.

**Bearings state:** Healthy or undamaged bearings were used at the time of testing.

### 3.7.1 Creation of Frequency Data Windows

Before the creation of any data window, we need to establish the center frequency. Then the window is created around this frequency. Since we want to track the damage progression of the outer race of bearing #1, our interested frequency is the Ball Pass Outer Race (BPOF). Based on the test operating conditions, this frequency has the value of 236.4 Hz. For our analysis on Kurtosis and *RMS* values, we considered two data windows: 1)  $\pm 15\%$  BPOF and 2)  $\pm 25\%$  BPOF. The purpose of these windows is to filter the data in order to focus on the interested frequency. Therefore, we can track the vibration level for a specific frequency range. In order to extract the data of a specific vector for the desired frequency range or window we used a MATLAB built-in function called *find* (see **Appendix C**). The objective of this function is to extract all the element indices of a vector subjected to the specified conditions. This function acts as an ideal bandpass filter as shown in **Figure 3.9**. After obtained the element indices, these indices were used to extract the values of different vectors such as PSD or Amplitude RMS corresponding to the frequency window. In this case, the indices of the frequency axis vector for both frequency ranges were extracted. Below there is an example for both data windows:

```
% Create frequency range
freq_axis=(Fs/2)*linspace(0,1,(N/2)+1);

± 15% BPOF window

% Create a window for ± 15% BPOF
freq_window=find(BPOF-(0.15*BPOF)<freq_axis & freq_axis<BPOF+(0.15*BPOF));

± 25% BPOF window

% Create a window for ± 25% BPOF
freq_window=find(BPOF-(0.25*BPOF)<freq_axis & freq_axis<BPOF+(0.25*BPOF));
```

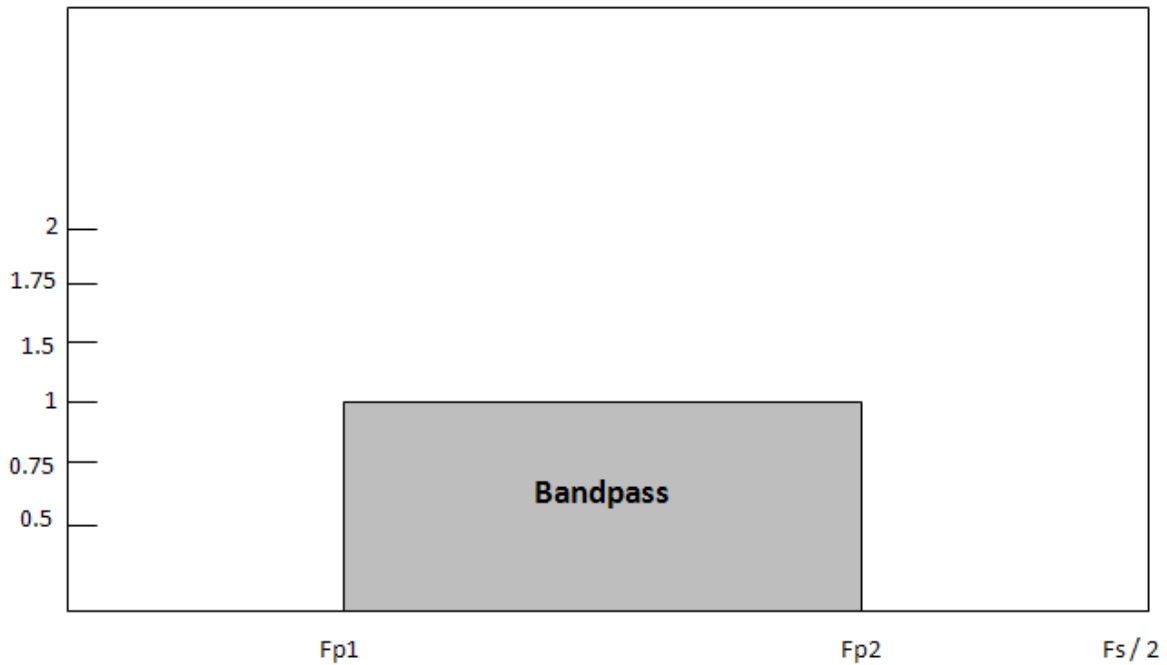


**Figure 3.9:** Ideal bandpass filter

### 3.7.2 PSD Plots Comparison

In this section we took two files at different times of testing to track the change in amplitude of BPOF. At the beginning of the test this amplitude should be low and when the bearing enters the damage initiation phase, we expected that this amplitude starts to increase. We used a window of  $\pm 15\%$  around the center frequency which in this case is BPOF. The selected files were #3 (30 min of testing) and # 350 (350 min of testing). **Figure 3.10** shows the PSD plot for file #3. The large peak around approximately 1000 Hz corresponds to a natural frequency of the system. This frequency remained stable during the test. **Figure 3.11** shows the PSD plot for the selected window. Then we proceeded to obtain the PSD plot of the file #350. **Figure 3.12** shows the PSD plot for file #350. From this figure we can see that amplitudes in the frequency range of 0 to 1000 Hz started to increase. To confirm that these change in amplitude correspond to a frequency around BPOF, we obtained the PSD plot for the frequency range of  $200.94 < f < 271.86$  Hz. **Figure 3.13** shows the PSD plot for the selected frequency range. In this figure we can see a shift in BPOF that can be related to the "leakage" phenomenon. This phenomenon means that the spectral power that should be concentrated at the critical frequency has spread out

or "leaked" into adjacent frequencies. The increase in amplitude indicates an existence of damage.

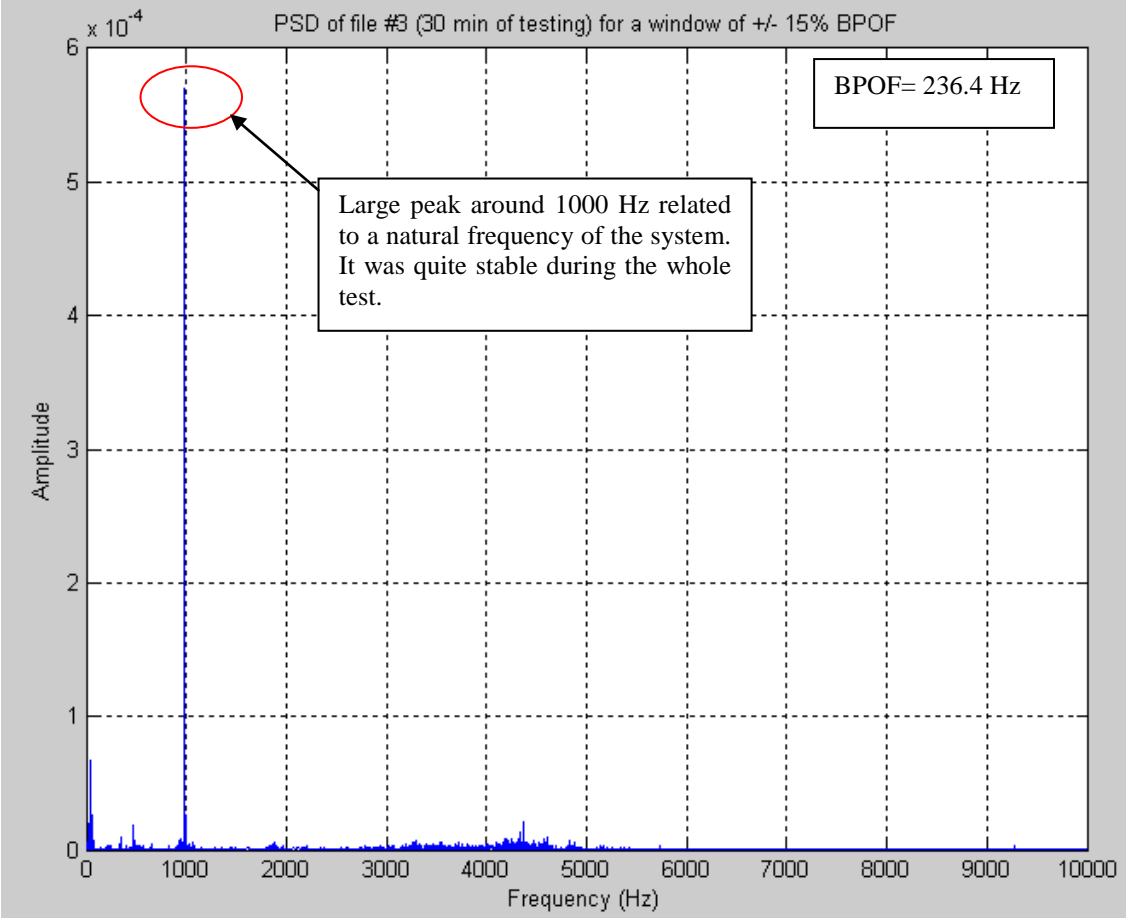


**Figure 3.10:** PSD plot for the file #3.

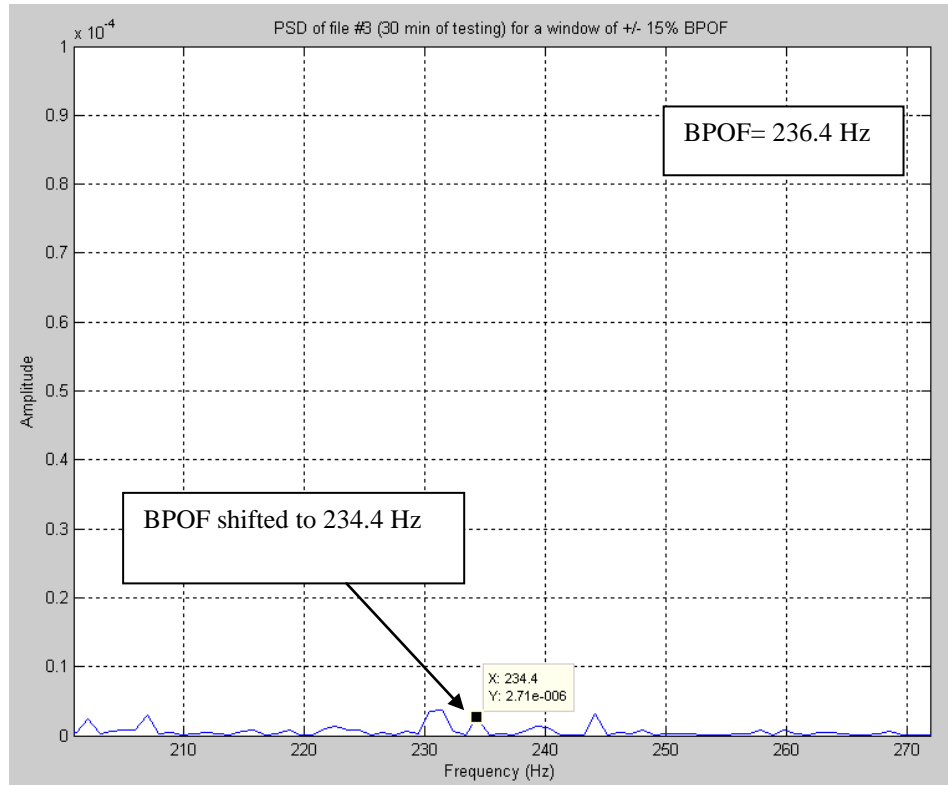


**Figure 3.11:** PSD plot of file #3 for the selected frequency range ( $200.94 < f < 271.86$  Hz).

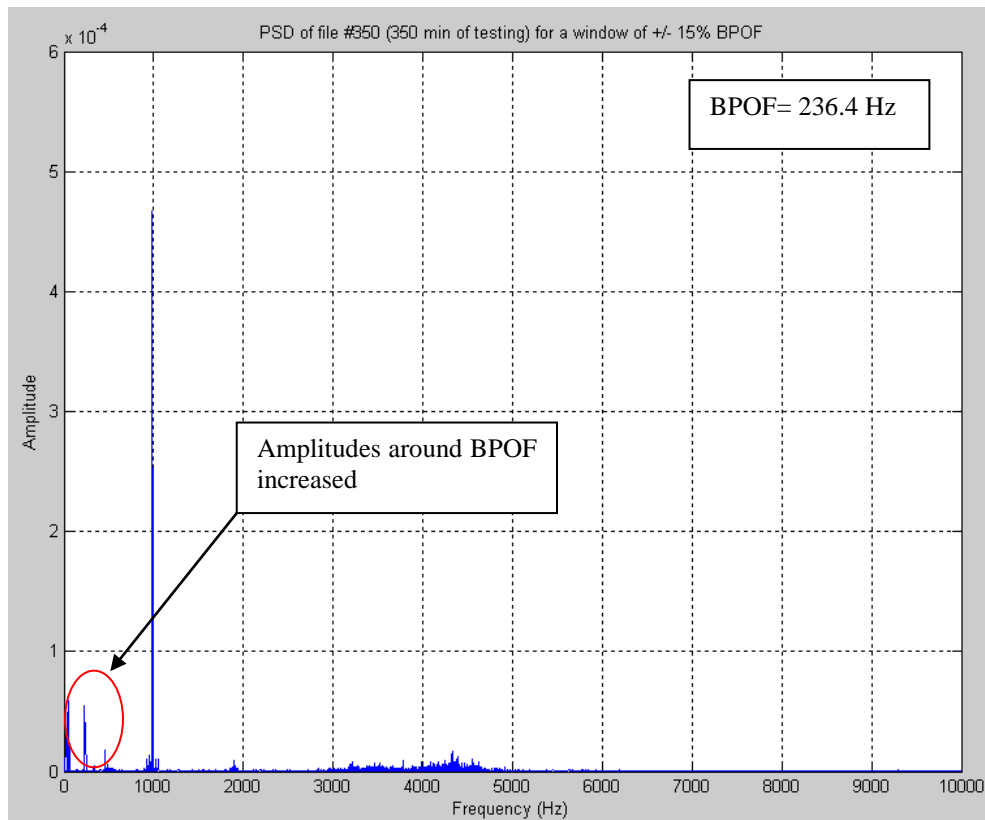


**Figure 3.12:** PSD plot for the file #350.

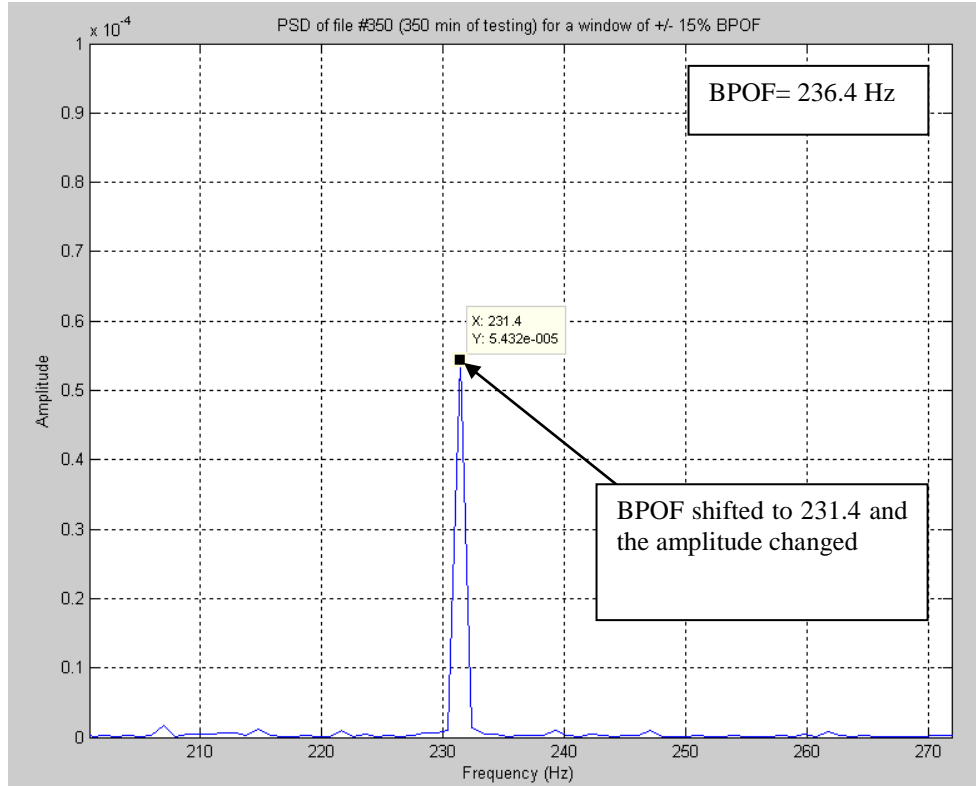


**Figure 3.13:** PSD plot of file #350 for the selected frequency range ( $200.94 < f < 271.86$  Hz).

### 3.7.3 Kurtosis of BPOF

In this part, the Kurtosis evolution of BPOF using two different windows,  $\pm 15\%$  BPOF and  $\pm 25\%$  BPOF was calculated. We considered both  $X$  and  $Y$  accelerometer directions. It is important to state that we calculated the Kurtosis using all 984 files (complete test) for bearing 1. **Figure 3.14** shows the Kurtosis for both data windows for bearing 1 in  $X$ -direction. **Figure 3.15** shows the Kurtosis for both data windows for bearing 1 in  $Y$ -direction. By comparing both figures, we can see that the data in the  $X$ -direction gives more relevant results than  $Y$ -direction. We can see that an approximately 7000 minutes there is an increase in the Kurtosis. This increase in Kurtosis can be related to a damage initiation on the bearing. After 7000 minutes the Kurtosis value starts to fluctuate and then increases dramatically reaching a higher value. This phase can be related to damage progression until bearing failure.

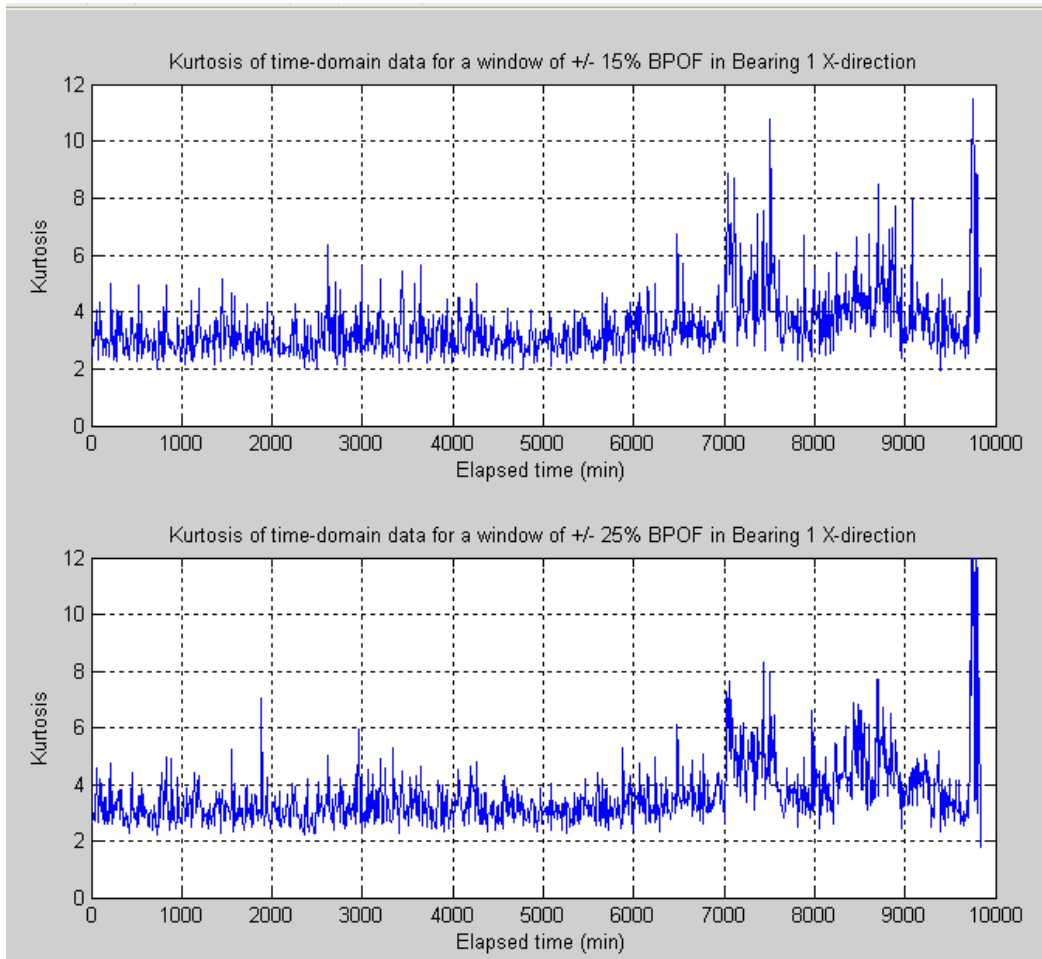


**Figure 3.14:** Kurtosis of time-domain data for Bearing 1 in X-direction.

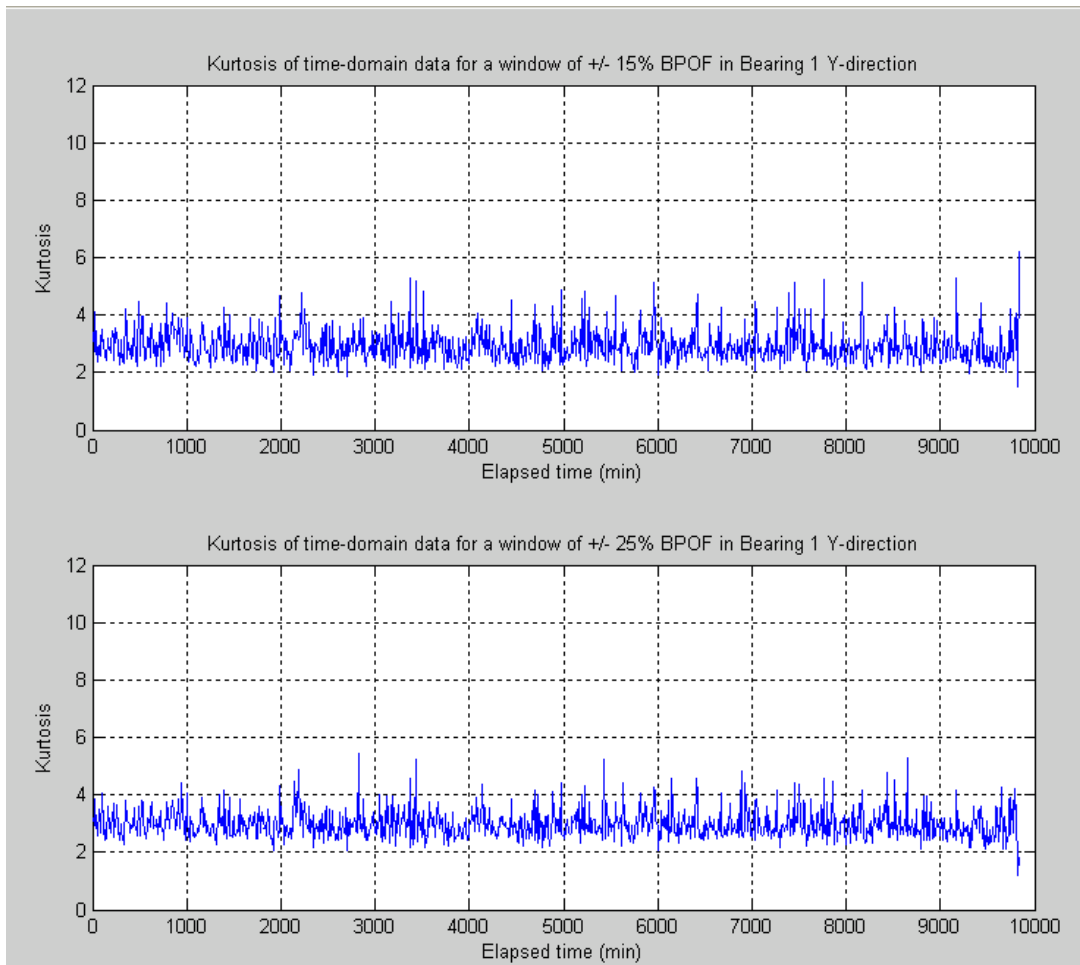


**Figure 3.15:** Kurtosis of time-domain data for Bearing 1 in Y-direction.

### 3.7.4 RMS of BPOF

In this section, the *RMS* value using the time-domain for both data windows was calculated. **Figure 3.16** shows the *RMS* for both data windows for bearing 1 in X-direction. From this figure we can note that by using a window of  $\pm 15\%$  we get a better trend in the *RMS* value. Like in the Kurtosis trend against time, the *RMS* value starts to increase at approximately 7000 minutes indicating a presence of damage. **Figure 3.17** shows the *RMS* for both data windows for bearing 1 in Y-direction. By comparing both Kurtosis and *RMS*, we can see that the *RMS* condition indicator captures the vibration behavior of the bearing better than Kurtosis.

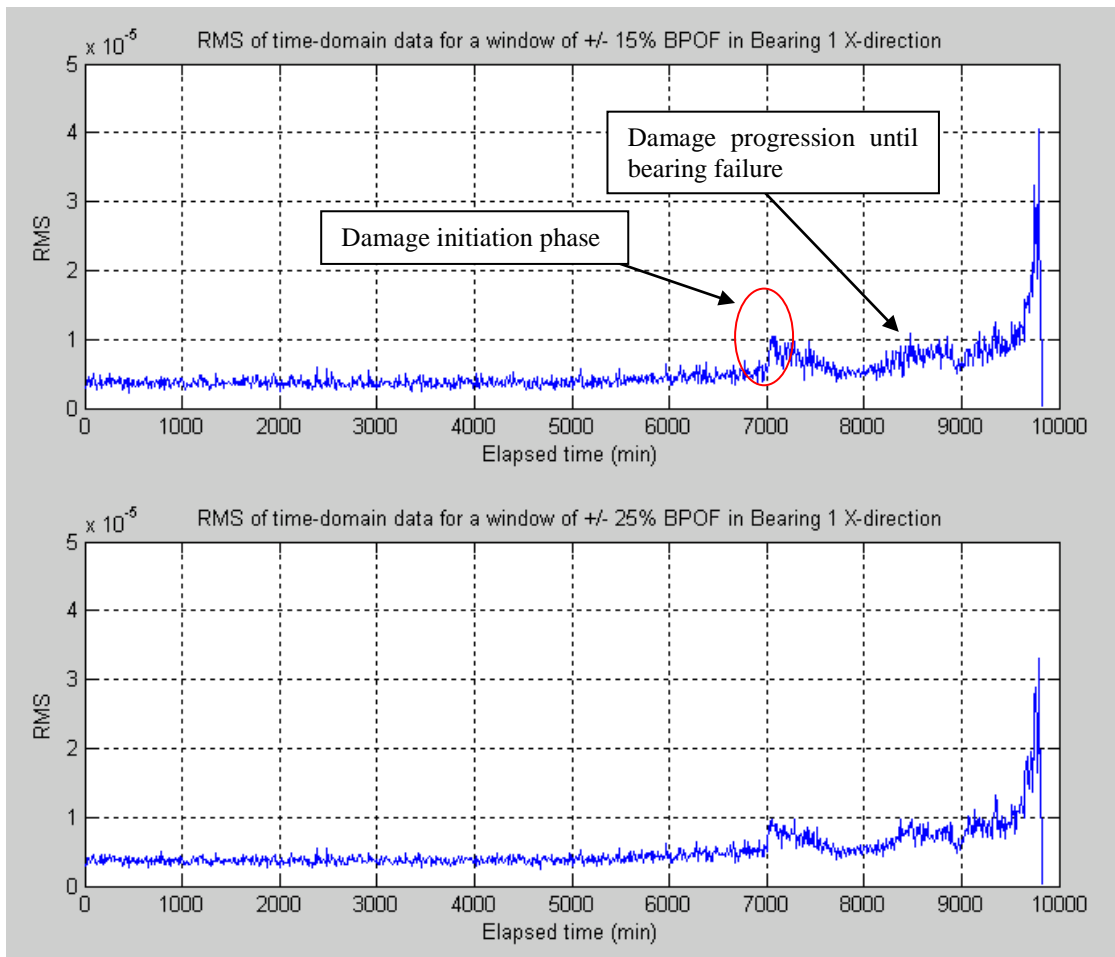


**Figure 3.16:** RMS of time-domain data for Bearing 1 in X-direction.

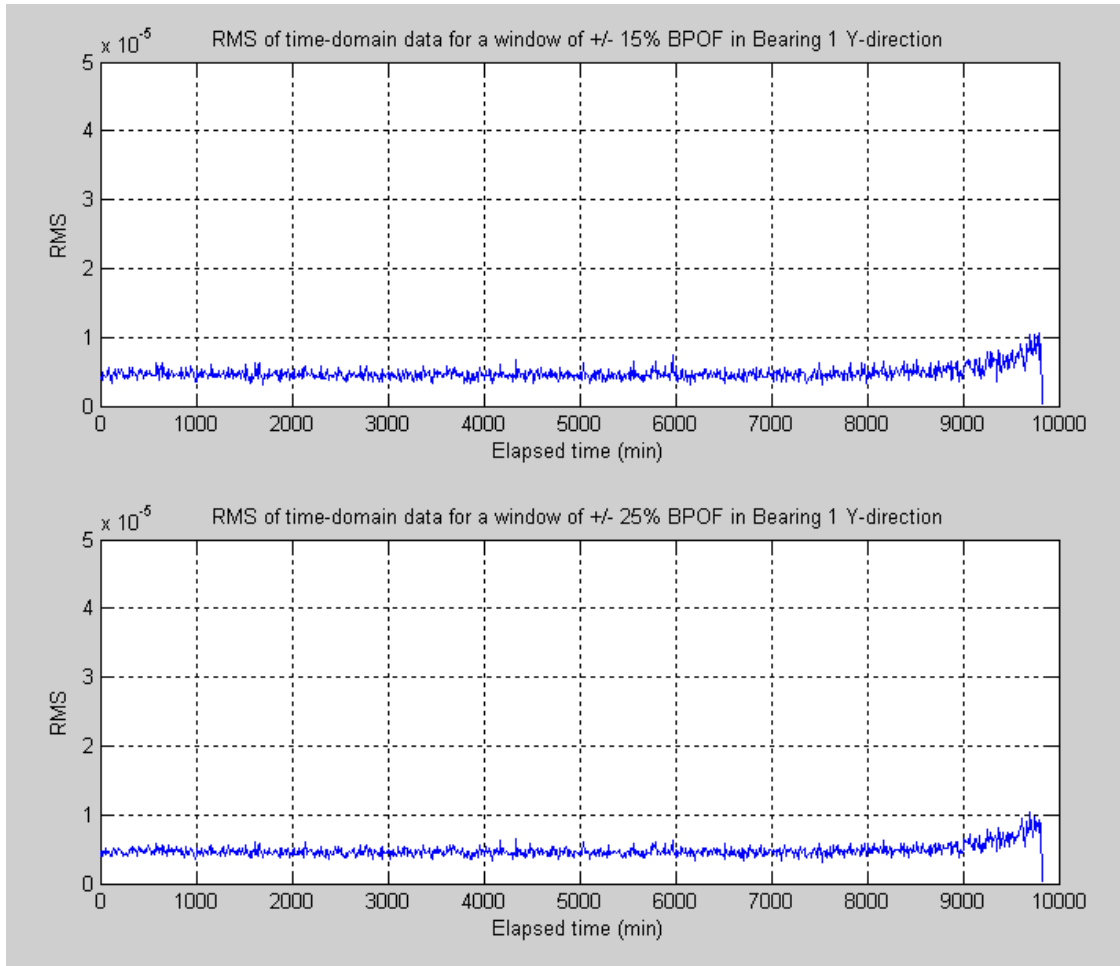


**Figure 3.17:** RMS of time-domain data for Bearing 1 in Y-direction.

### 3.7.5 Trending the Power of BPOF

As part of the diagnosis of the fault, the energy level of the selected bearing frequency becomes an important parameter for comparison against baselines. As we mentioned before, we selected the BPOF as our critical frequency because we want to confirm an outer race failure on bearing 1. The value of this frequency is 236.4 Hz. The objective of trending the power of BPOF is to plot the magnitude value vs. time in order to identify when the power level exceeds the acceptable limit. As we know, the BPOF can experience a shift in the frequency spectrum due to the "leakage" phenomenon. It is for that reason we selected a window around BPOF in order to extract the maximum amplitude value in that frequency range. After obtain that power value for all data files then we can perform the plot of BPOF Power vs. Time. We selected a window of  $\pm 15\%$  BPOF (approximately  $\pm 35.5$  Hz). Usually, the frequency shift is not more than 35 Hz and

our objective is to extract the power of the BPOF. Therefore, by selecting a window of  $\pm 15\%$  BPOF we are ensuring that the power extracted in that frequency interval correspond to the BPOF. **Figure 3.18** shows the results for bearing 1 in both directions. In addition to the power of BPOF, the amplitudes of BPIF, FB and FCF are trended over time to compare them against the power of BPOF. **Figures 3.19 to 3.21** show the results for the power of BPIF, FB and FCF. It is evident that the amplitude of BPOF is much greater than the amplitude of the other defect frequencies. Thus, these results confirm a failure due to a defect on the outer race.

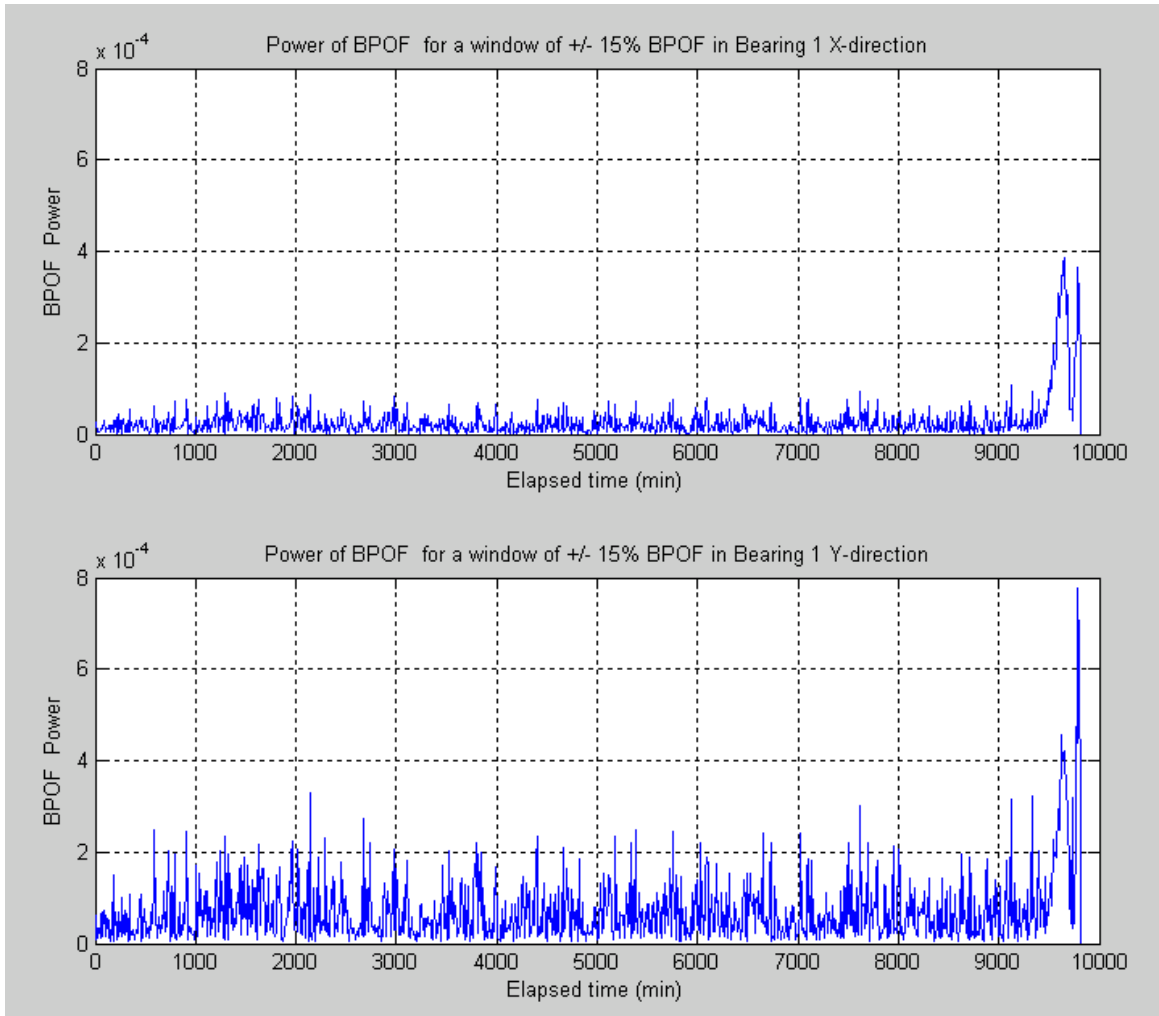


**Figure 3.18:** BPOF power trend for bearing 1 in both X and Y directions.

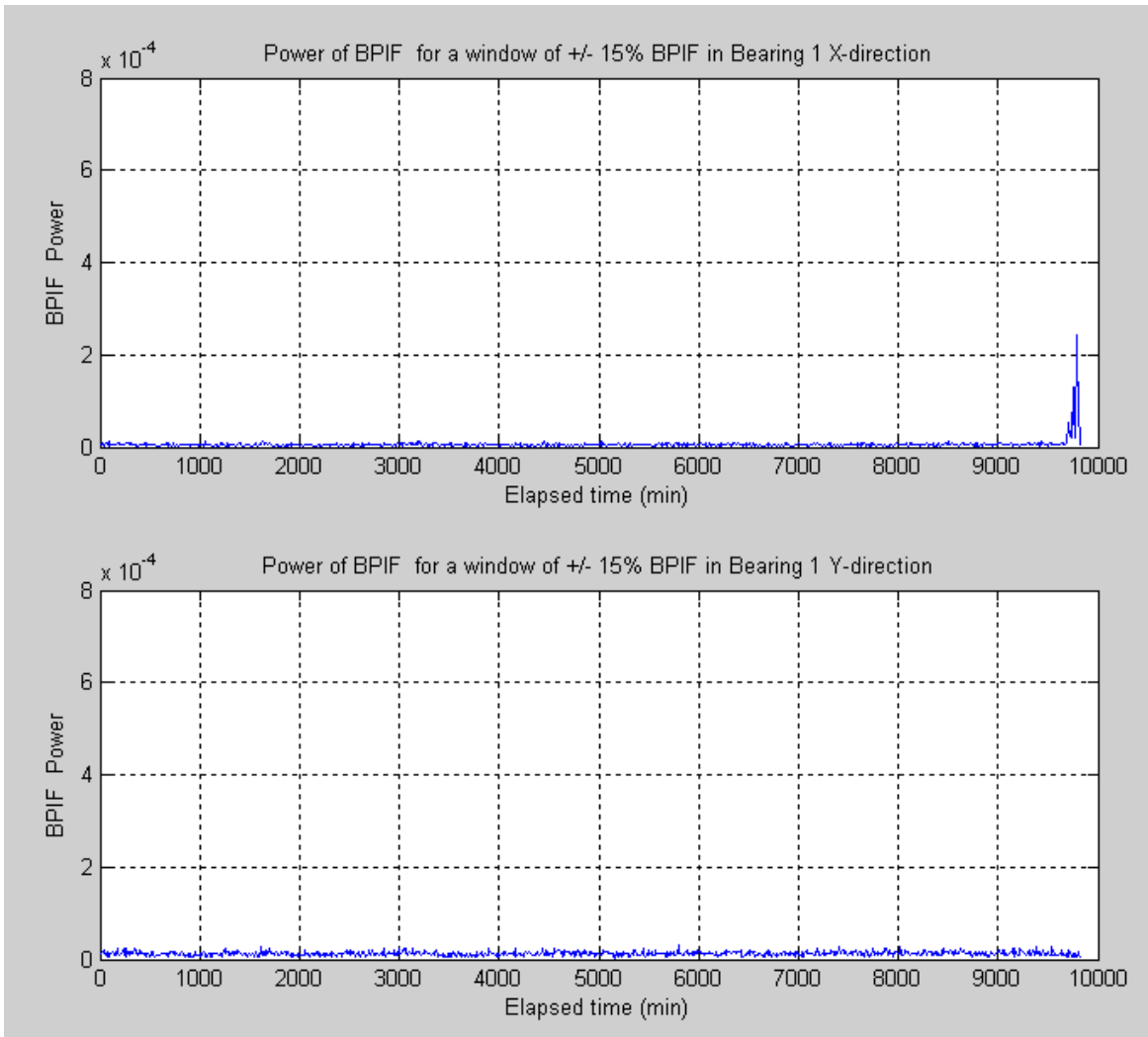


**Figure 3.19:** BPIF power trend for bearing 1 in both X and Y directions.

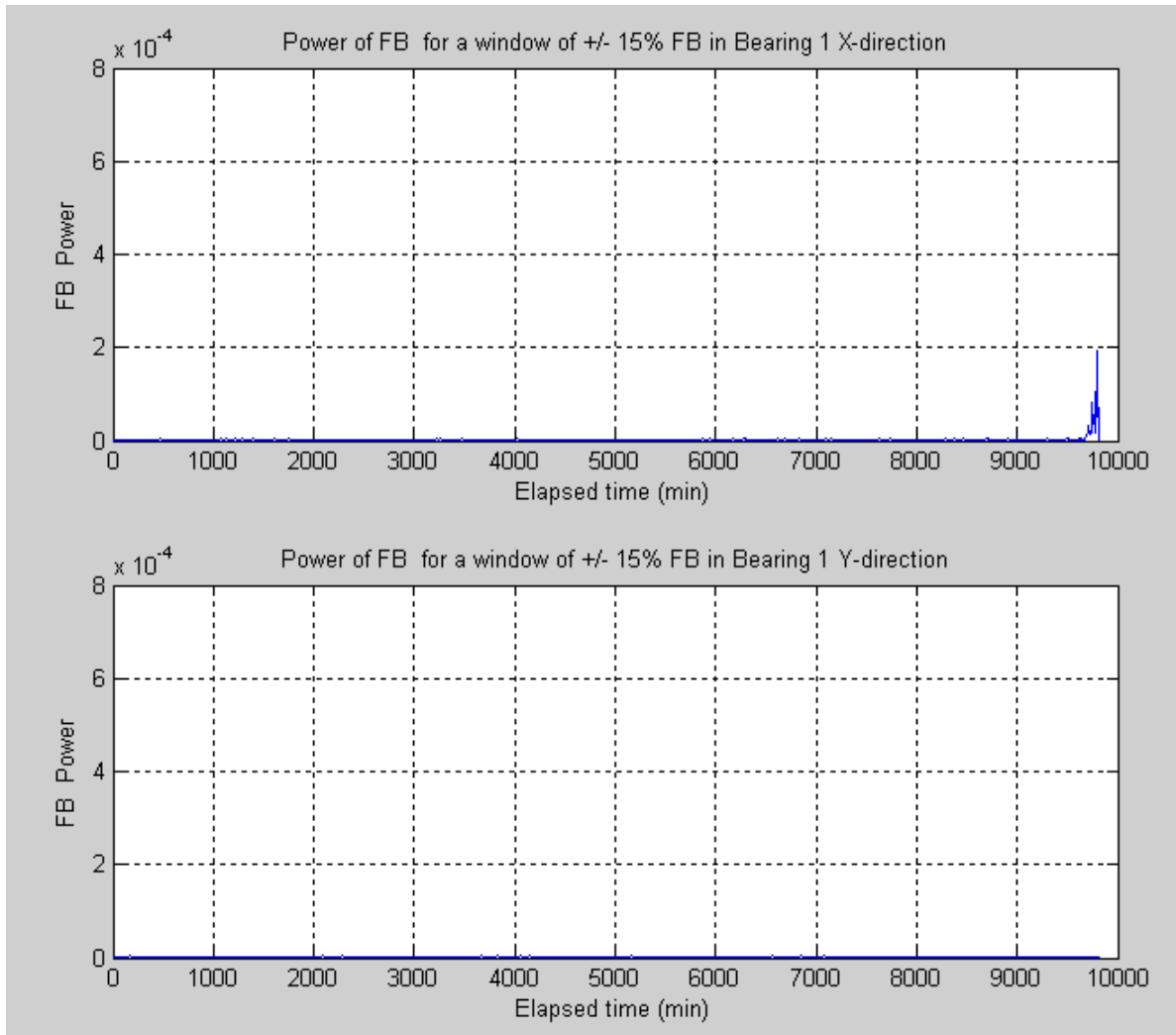


**Figure 3.20:** FB power trend for bearing 1 in both X and Y directions.

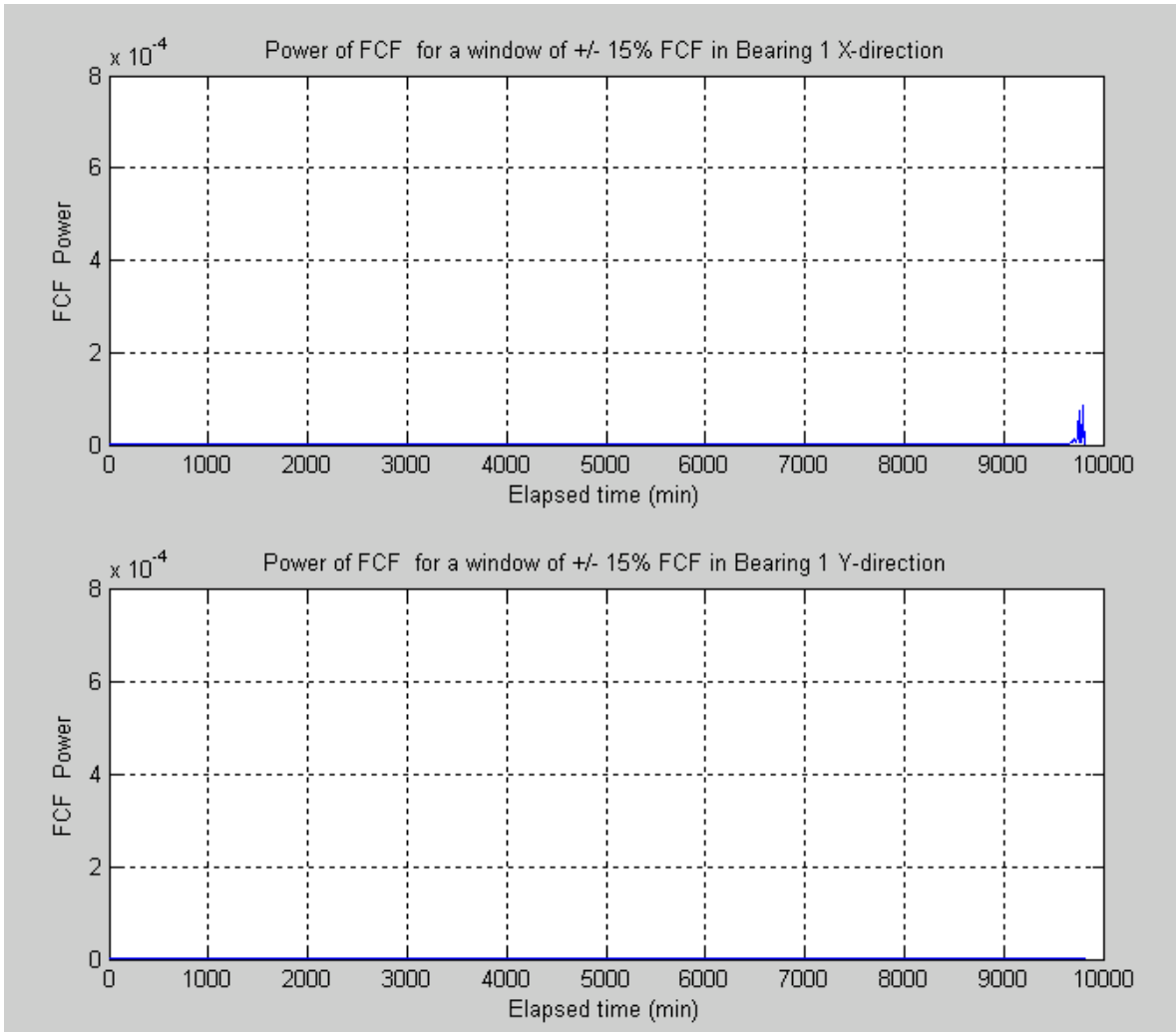


**Figure 3.21:** FCF power trend for bearing 1 in both X and Y directions.

### 3.8 DEGRADATION SIGNAL SELECTION

The focus of this section is the prediction of the remaining useful life of the ball bearing using measured data. As we presented before, bearing fault frequencies are associated with different bearing components (i.e. outer raceway, inner raceway, etc.) and every time that a specific component develops a defect, it excites its corresponding frequency. Before the life prediction process, we need to select a signal that captures the evolution of bearing's degradation. Therefore, this signal can be used to predict the bearing's remaining useful life. This type of signal is called a *degradation signal*. According to Gebraeel et al (2004), a good degradation signal must capture the physical transitions that the bearing undergoes during different stages of

its life; it must possess a trend that reflects the deterioration of the bearing, a low signal-to-noise ratio and must be easy to compute. Finally, it must be possible to define a reasonable failure threshold which is a signal amplitude indicating failure. **Figure 3.22** shows an example of the proposed approach. The degradation signal we considered was the *RMS* vibration level over time. In our approach, instead of calculate the *RMS* vibration across the entire spectrum; we calculated it around the interested frequency and its first five harmonics using a window of  $\pm 15\%$ . Then we calculated the average of these *RMS* values and this became the degradation signal that we trended over time. The purpose of doing this is because the amplitude of the defect frequency is typically an indication of a defect and the presence of the harmonics of the defect frequency is also another indication of degradation and spall formation.

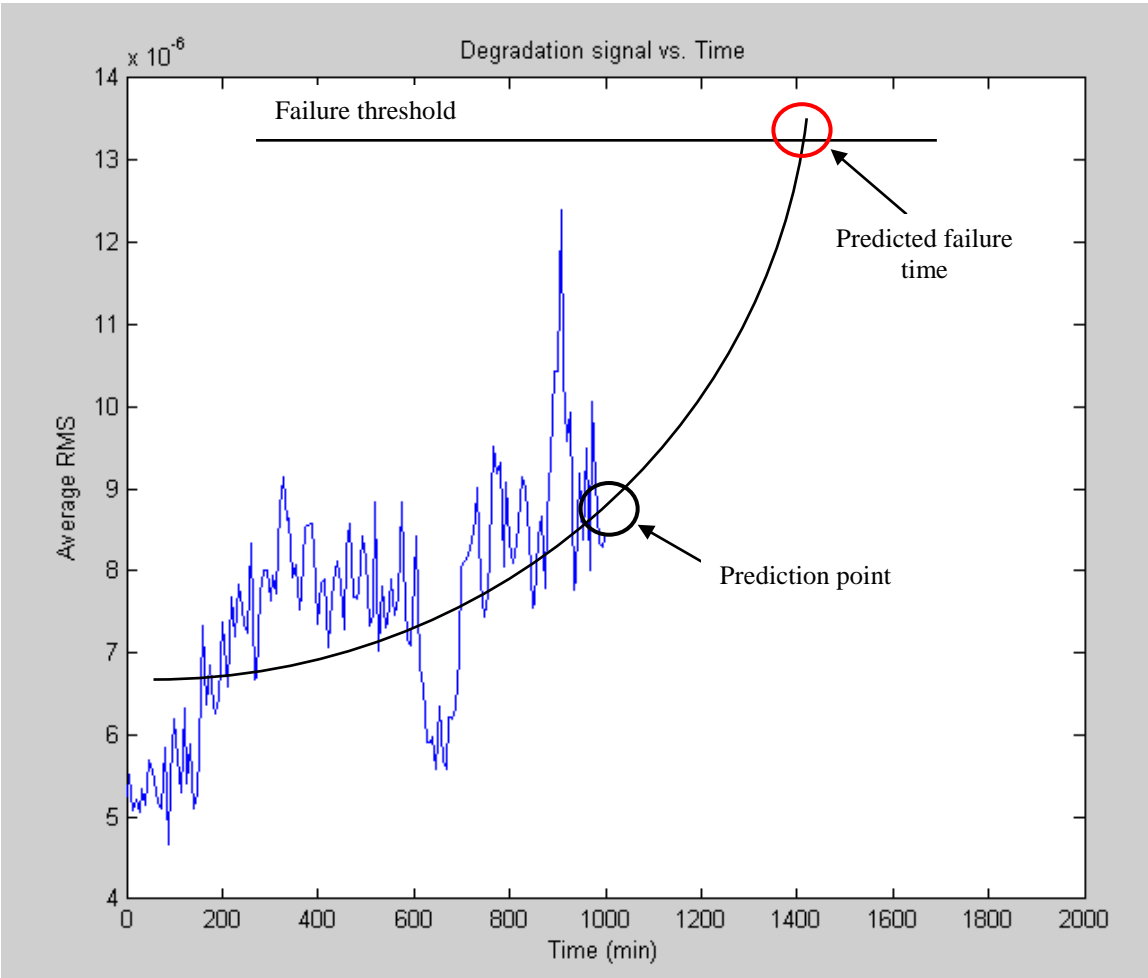


**Figure 3.22:** Example of the proposed approach to calculate bearing's remaining useful life.

### 3.9 REMAINING USEFUL LIFE PREDICTION ON TEST 2

In this test, we calculated the *RMS* vibration around the BPOF and its first five harmonics using a window of  $\pm 15\%$ . As we mentioned earlier, then we calculated the average of these *RMS* values and this became the degradation signal that we trended. **Figure 3.23** shows the average of *RMS* for bearing 1 in both *X* and *Y* directions for the entire test. If we compare the data in both directions, we can say that the data in *X* direction captures the degradation of the bearing and it is for that reason that we used this data to predict bearing's remaining life.

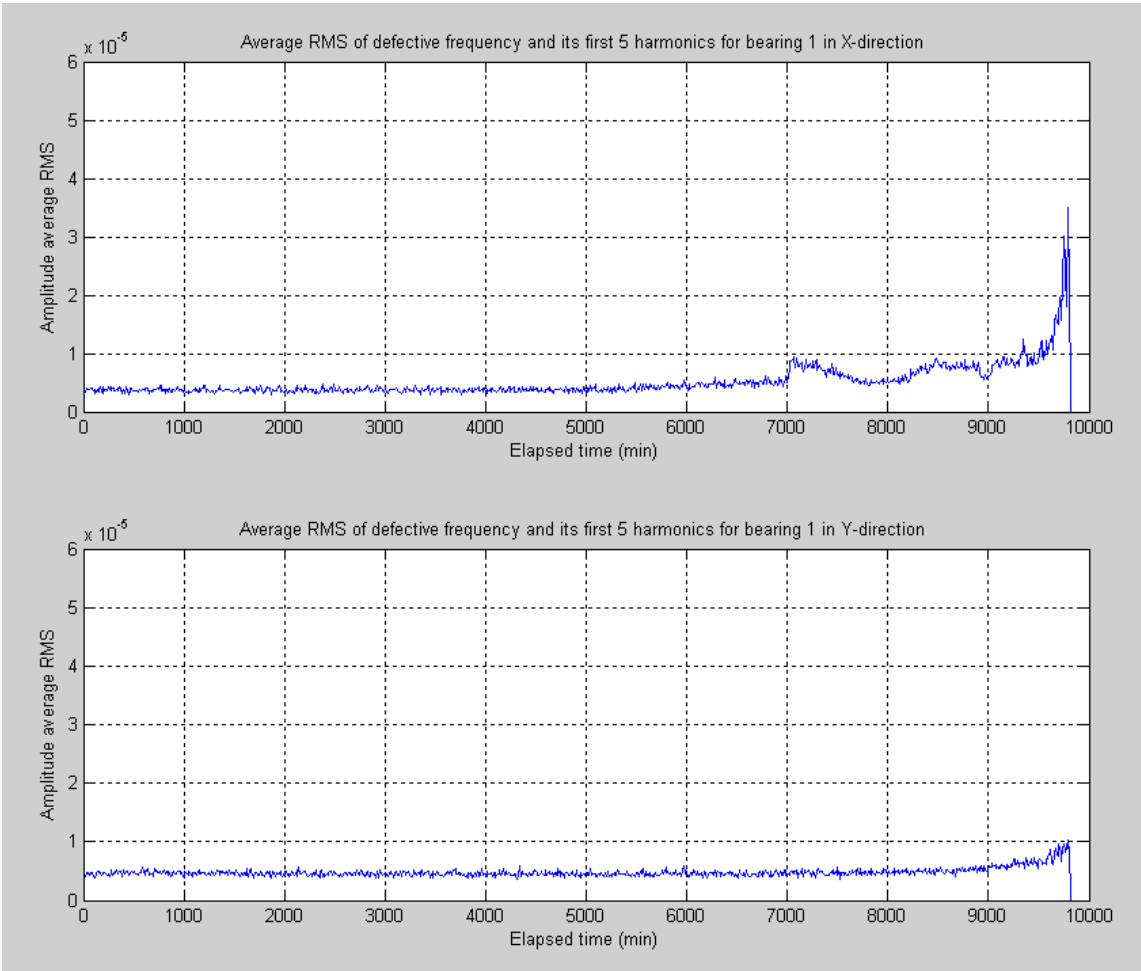


**Figure 3.23:** Average *RMS* for bearing 1 in both *X* and *Y* directions using a window of  $\pm 15\%$ .

**Figure 3.24** shows the average *RMS* vibration level of the BPOF and its five harmonics for the entire test. From this figure we can observe two distinct regions in the signal. The first one is characterized by a flat region representing normal or defect-free bearing operation. The second region is characterized by a fluctuating signal with an increasing trend. This region is associated with spall initiation and propagation along raceway's surface and extends until bearing failure. Also, we can note that the signal possess an exponential behavior at the time of damage initiation. Therefore, we will use an exponential model in order to predict bearing life. The objective is to apply the best exponential fit on the degradation signal.

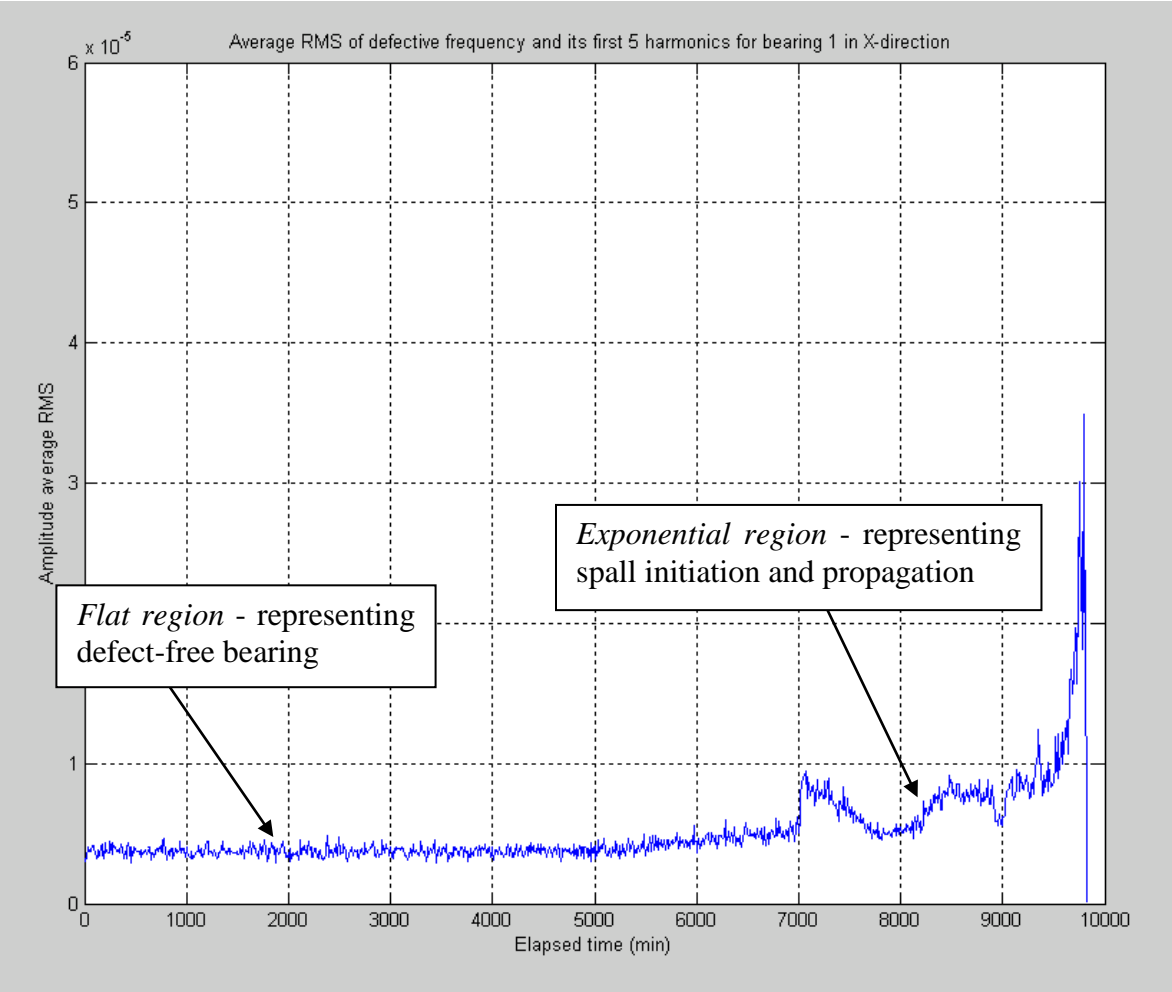


**Figure 3.24:** Average *RMS* for bearing 1 in X-direction.

### 3.9.1 Vector Scaling

In this section we discussed the process of vector scaling for the values of the  $Y$ -axis. From previous plots we can see that the magnitudes of Average  $RMS$  values are much less than 1. Therefore, we applied a scaling process to avoid having such small numbers. In order to achieve that, all the Average  $RMS$  values were divided by the failure threshold and then multiplied by 100. Therefore, the values of the  $Y$ -axis will be a percentage of the failure threshold and failure will occur when the percentage is 100. **Figure 3.25** shows the plot of the Average  $RMS$  after the scaling process.

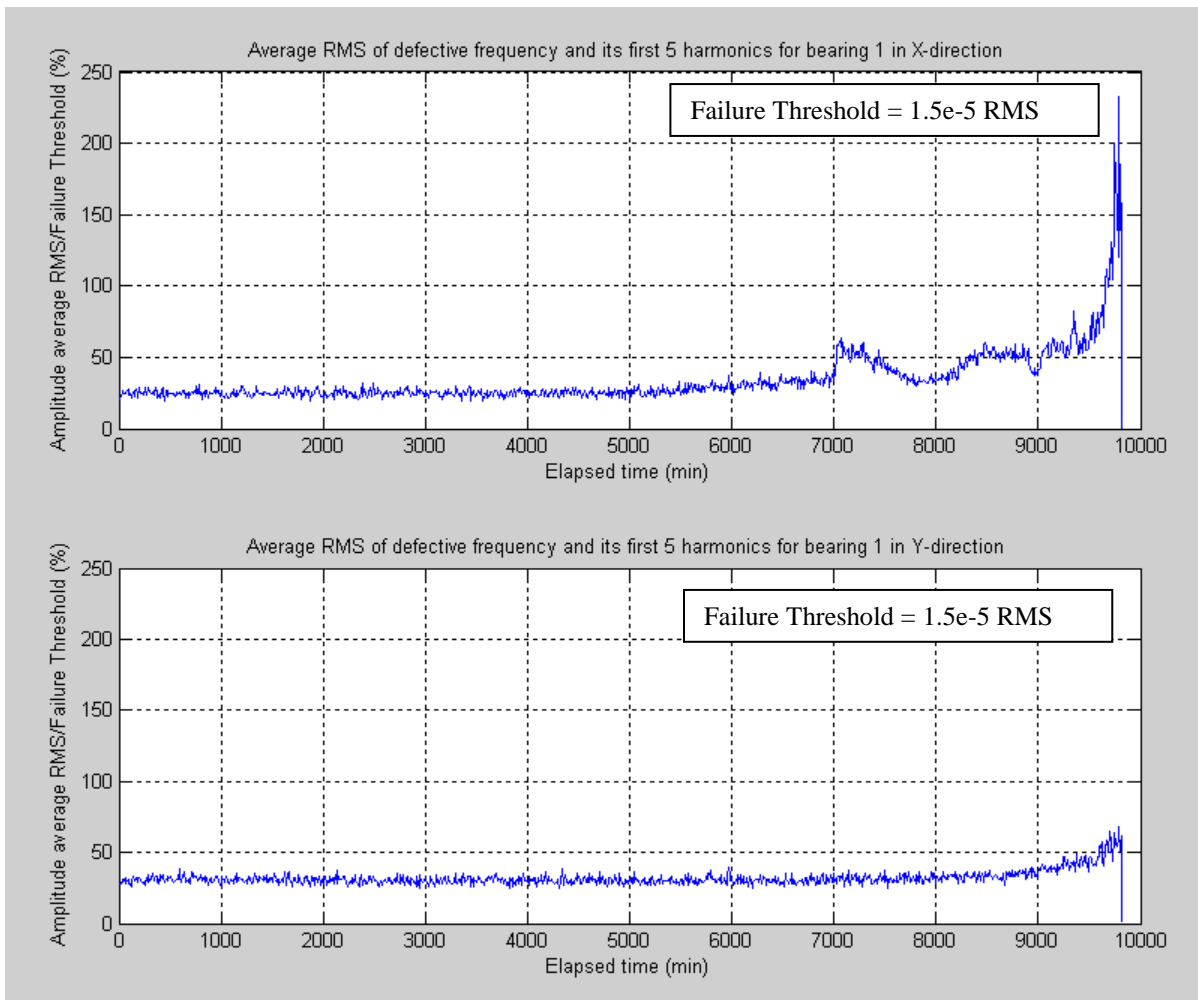


**Figure 3.25:** Average RMS/Failure Threshold (%) for bearing 1 in both X and Y directions

### 3.9.2 Development of a Moving Window Algorithm

As part of the development of the health monitoring tool, a moving window algorithm has been developed in order to track behavior changes in the degradation signal. This algorithm detects changes in the average and slope values for each time step. The time step is defined as the selected time interval to perform the calculations. The purpose of divide the data into time steps is to iteratively calculate the value of the degradation signal and perform a continuous comparison against initial conditions. For example, if the time step is chosen as 100 minutes, our tool will calculate key features every 100 minutes and make comparisons against initial values of those features. Therefore, by creating a moving window algorithm is that we can analyze with more detail the evolution of the degradation signal as a function of each time step. Also, by using this type of algorithm, when the degradation signal starts to experiment an abnormal behavior we can perform a better fit through the data. As we mentioned in the previous section, our selected degradation signal is the *RMS* vibration level over time. The harmonics were also considered because when damage is present, the harmonics of the fault frequency contain certain amount of energy that we are interested to capture.

One of the goals is to develop the algorithm most generic as possible. In order to achieve that, certain baselines were established based on the available experimental data. The data used in this analysis was extracted from the second test of the NASA experimental data. As discussed before, the data from bearing 1 in *X*-direction contained more useful information than data in *Y*-direction because it captured the changes in the vibration signal due to damage initiation. Therefore, the data from *X*-direction was used to establish the limits for future random data. **Figure 3.26** shows the average *RMS* vibration level as a function of elapsed time. For establish our limits, a window width of 500 minutes was selected because we can calculate the average and slope of each time step more accurately. Sometimes, in an interval of 1000 minutes we can have both positive and negative slopes. Therefore, if the window is reduced to 500 minutes these variations can be better tracked. If we consider two window widths, i.e. 500 and 1000 min, at the time of life prediction using the 500 min width we will have more time between the prediction point and failure point. By having more time between the prediction point and the failure point, an appropriate maintenance action can be scheduled. Before life calculations, we need to establish a failure threshold which means that when the signal reaches this value, the bearing is

considered failed. Based on the behavior of the degradation signal, the bearing is considered failed after 9700 minutes of testing. This time will be the actual failure time of the bearing. The failure threshold for that corresponding time is  $1.5e-5$  RMS. For future analyses, the threshold should be established based on the type of measurement, machine size and operating speed.

From **Figure 3.26** we can see the differences in average and slope values for two different regions. The first one is a flat region which is stable. For this zone (files 1-50), average and slope values were 25.0% and 0.0018%/min respectively. The second region is where damage propagation occurs. We selected this zone to establish our limits because at this point both the step average and slope values increased dramatically in comparison to the first zone. For the second zone (files 801-850), average and slope values were 43.4% and 0.0485%/min respectively.

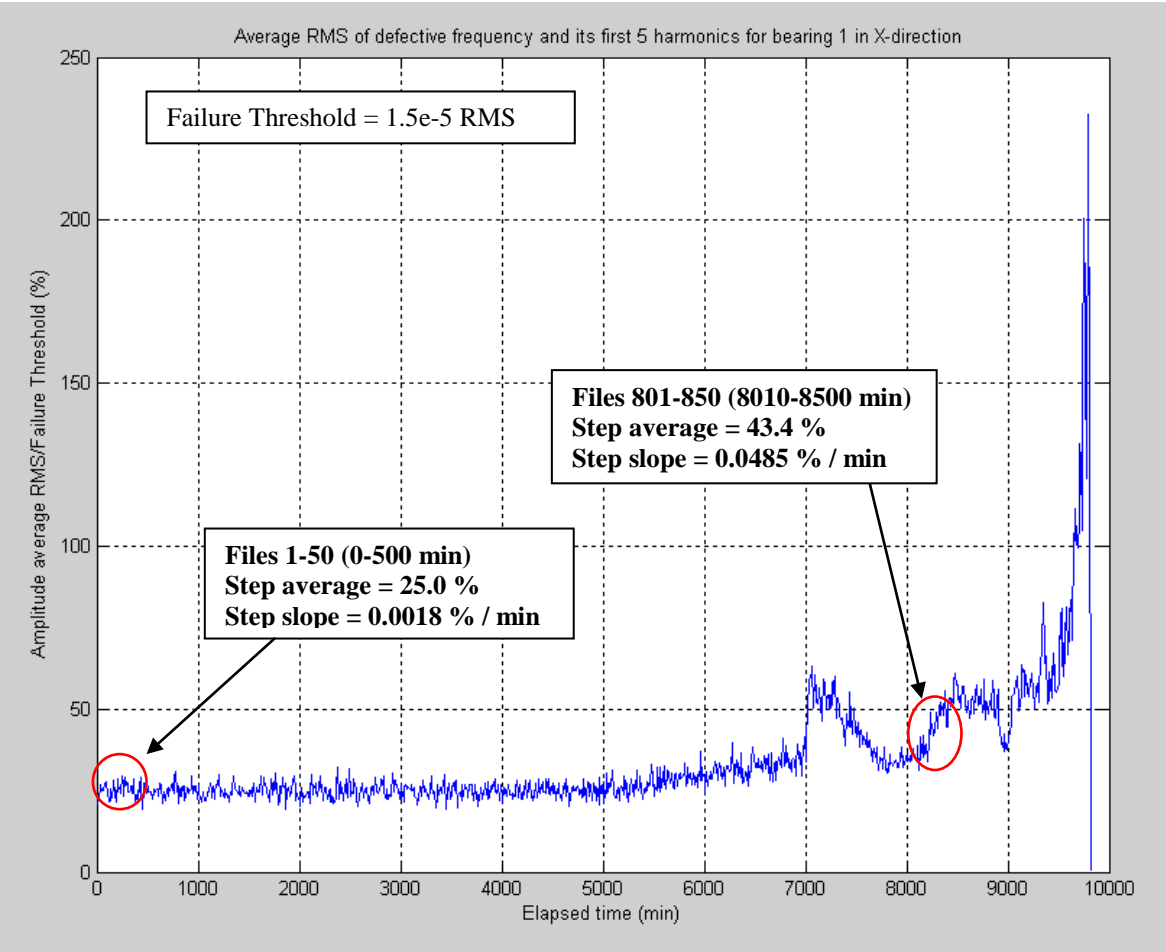


**Figure 3.26:** Average RMS/Failure Threshold (%) in X-direction

By comparing both zones, we can note that the step average of the second zone is approximately 1.7 times the step average of the first zone and also it is approximately 43% of the failure threshold. Therefore, we considered this relationship for our generic algorithm. However, as a safety factor, we established our maximum step average as 40% of the failure threshold. As mentioned before, the slope for the second zone is 0.0485%/min that is approximately 27 times the slope of the first zone. Again we applied a safety factor and we selected a slope threshold of 26 times the initial slope.

**Table 3.4:** Signal limits added into the tool.

<i>Degradation Signal Limits Integrated into the Tool</i>	
Damage initiation	35% failure threshold
Prediction point	40% failure threshold 26.0×initial slope

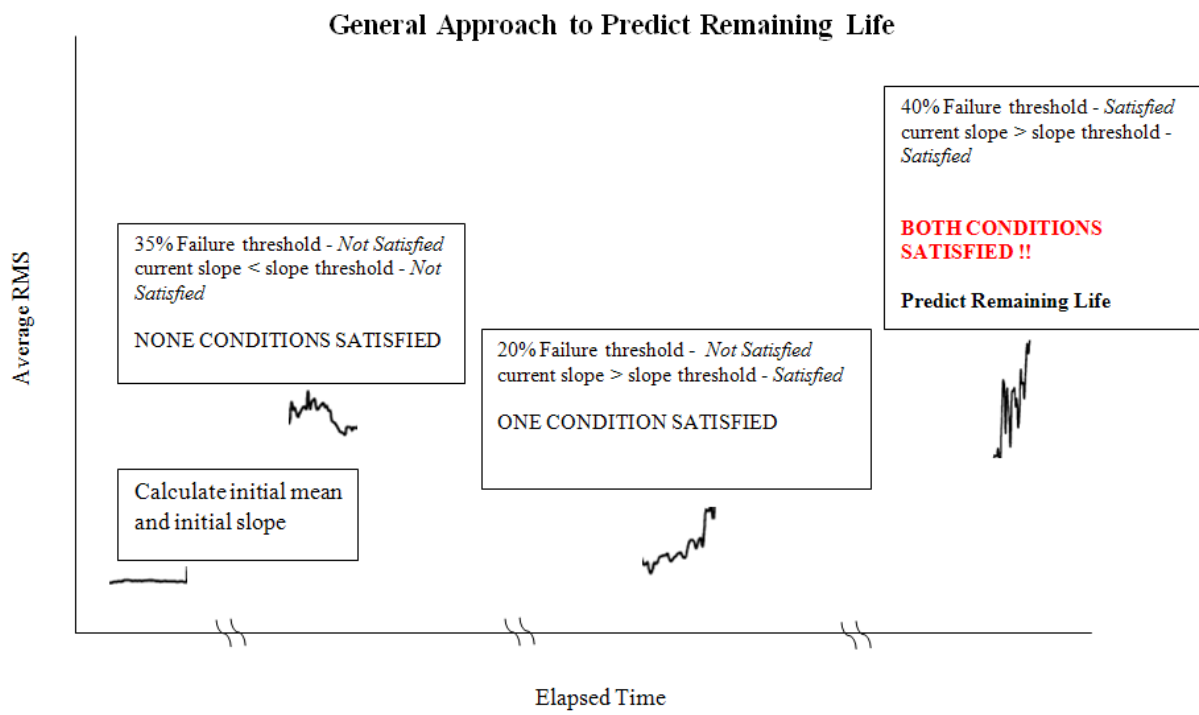


**Figure 3.27:** General approach used into the algorithm.

Another feature of our tool is that it is capable of predict the time where damage initiation occurs. As mentioned before, the degradation signal behaves in a stable manner and eventually starts to increase indicating a presence of damage. Since it is of our interest the time when damage occurs, our tool compares each time step average against the initial time step average. We can assume that the increase in the degradation signal is more noticeable when the average is 35% of the failure threshold. Therefore, when our algorithms detect that condition the tool display the corresponding time. **Table 3.4** shows the signal limits added into the tool.

After established the permissible limits, we proceeded to incorporate these limits into our generic algorithm. At the beginning of the algorithm, it calculates the average for the first time step and stored it into memory. Then it gets into a loop which calculates the average and slope for each time step. It then compares these values with the permissible limits. For a certain time step, if the average is 40% of the failure threshold and the slope reached the slope threshold, the loop stops and proceeds to perform the curve fitting in order to predict the remaining life. It is important to clarify that both conditions **must** be satisfied. These conditions are evaluated in both *X* and *Y* accelerometer directions. The loop stops when the conditions are satisfied in either of the directions. **Figure 3.27** shows the schematic of the used approach.

When the loop stops, our algorithm performs an exponential fit trough the data points of the last time step. In order to perform the exponential fit in MATLAB, we used the command *fit* with the exponential model as an option. Below there is an example of the command line in MATLAB.

```
exponential_fit=fit(elapsed_time,rms_average_X_percent,'expl');
```

After the algorithm performed the nominal failure curve or exponential fit through the data, it proceeded to calculate 95% confidence upper and lower curve. The two types of confidence bounds are observation and functional respectively. Observation bounds are wider than functional bounds because they measure the uncertainty of predicting the fitted curve plus the random variation in the new observation. Therefore, in this work observation bounds are used. By ensuring that the upper and lower curve encompasses 95% of the data, the time-to-failure (TTF) will have 95% confidence for the threshold we selected. In MATLAB, we performed this using the command *predint*. Below there is an example of the command line.

```
[c1,ypred1] = predint(exponential_fit,total_time,0.95,'obs','on');
```

Just the last time step is used to fit the exponential curve because sometimes the slope at previous time steps shows a fluctuating pattern leading in negative slope values causing that the upper confidence bound never reaches the failure threshold. The algorithm calculate the remaining life for both  $X$  and  $Y$  directions. The minimum of these TTF's is the predicted remaining life. **Figures 3.28** and **3.29** show the predicted TTF's. Based on the results, the predicted remaining life is 362 minutes. In the algorithm, confidence bounds for new observations were used. Confidence bounds for new observations are wider than functional bounds because they measure the uncertainty of predicting the fitted curve plus the random variation in the new observation. After the prediction point, we don't exactly what would be the behavior of the data because it can tend toward the threshold or away from it. In **Figure 3.29** we can see that the upper bound never crossed the threshold indicating that the average RMS was stable and didn't have any signs of increase dramatically because of its slope. From **Figure 3.28** we can see that the prediction point is 8500 minutes. Therefore, the tool predicts that the bearing will fail at 8862 minutes of testing. This value can be compared to the actual bearing failure time as follows:

$$relative\ error = \frac{|actual\ failure\ time - predicted\ failure\ time|}{actual\ failure\ time} \times 100$$

$$relative\ error = \frac{|9700 - 8862|}{9700} \times 100 = 8.6\ %$$

According to the results, there is an 8.6 percent error between the actual and predicted bearing failure time.

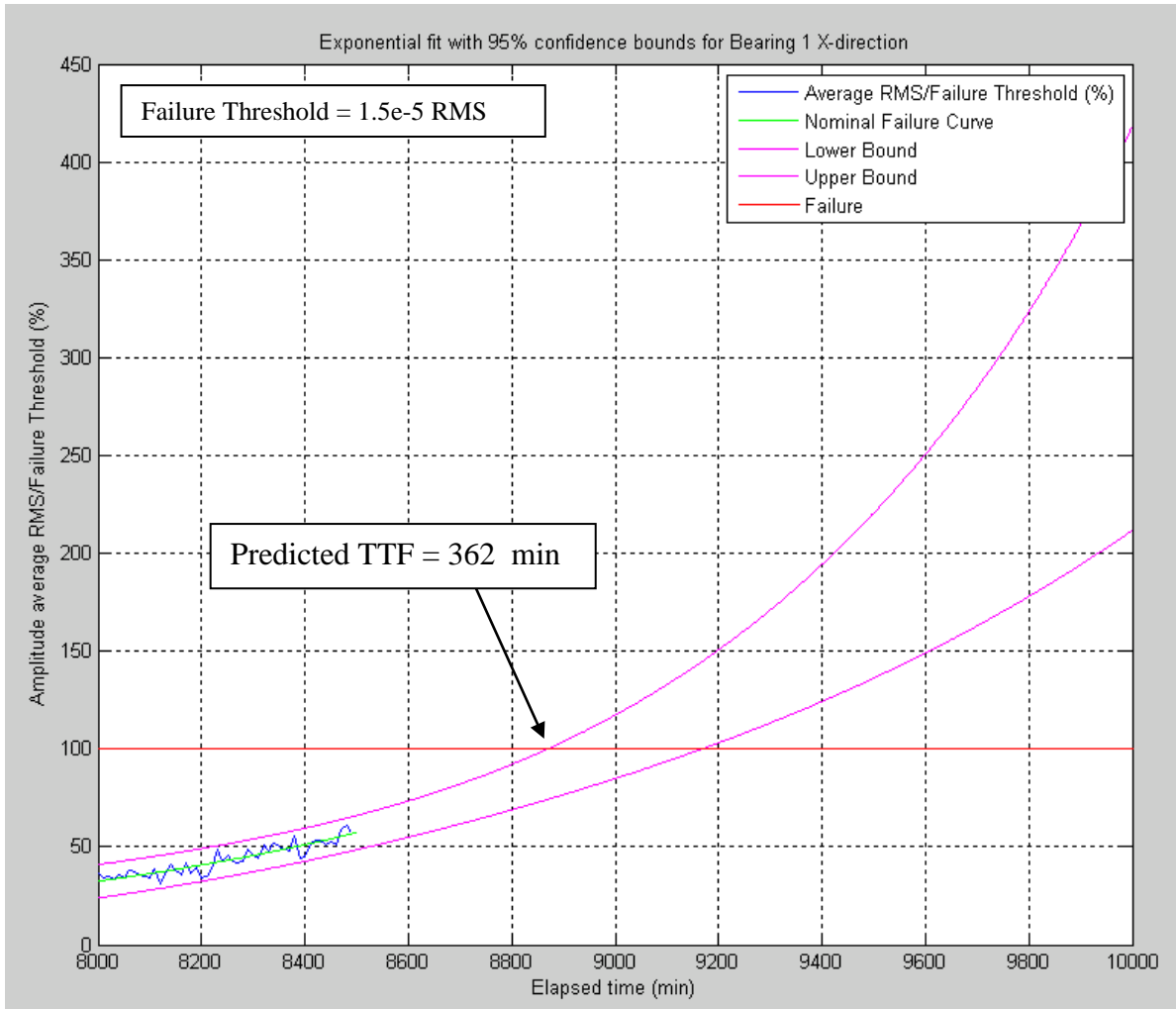


**Figure 3.28:** Exponential fit with 95% confidence bounds for X-direction.

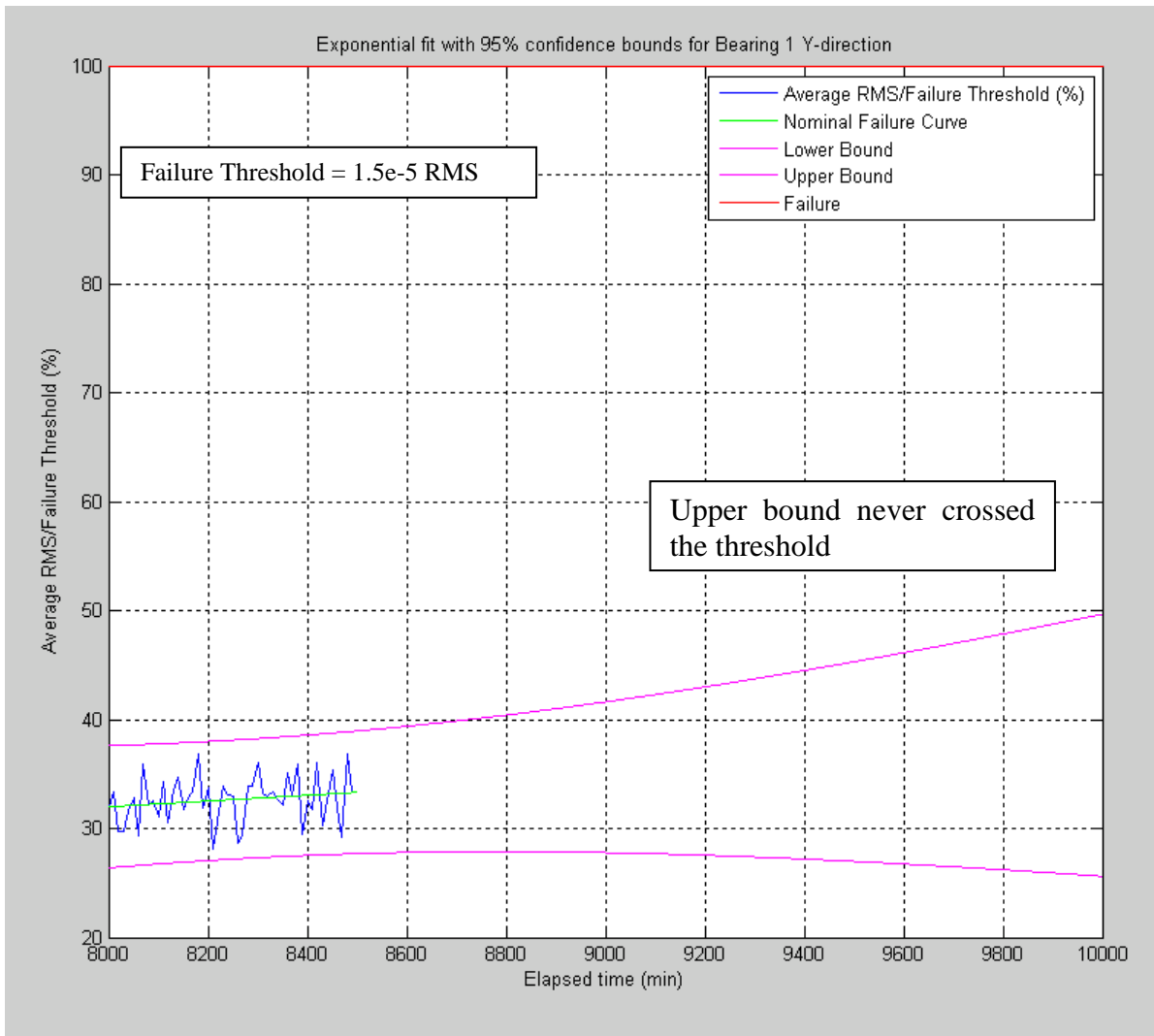


**Figure 3.29:** Exponential fit with 95% confidence bounds for Y-direction.

### 3.10 BEARINGS PROGNOSTIC TOOL

After proving that the developed algorithms can predict the remaining life, they were incorporated together to develop a generic bearings prognostic tool using the Graphical User Interface (GUI) in MATLAB. The structure of the developed code is shown in **Figure 3.30**. First, the code loads the bearing data. Then, it calculates the critical frequencies based on system conditions and bearing geometry. After calculate the frequencies, data filtering is achieved using data windows around the selected frequency and its harmonics. Then, it calculates the slope and mean of the average RMS for the initial time step. Finally, the code enters into analysis phase that is about trending the condition indicators (Kurtosis, RMS and Power of defective frequency) and predicting the remaining life based on the evolution of the average RMS. See **Appendix B** for more details about the subroutines and functions used in the code.

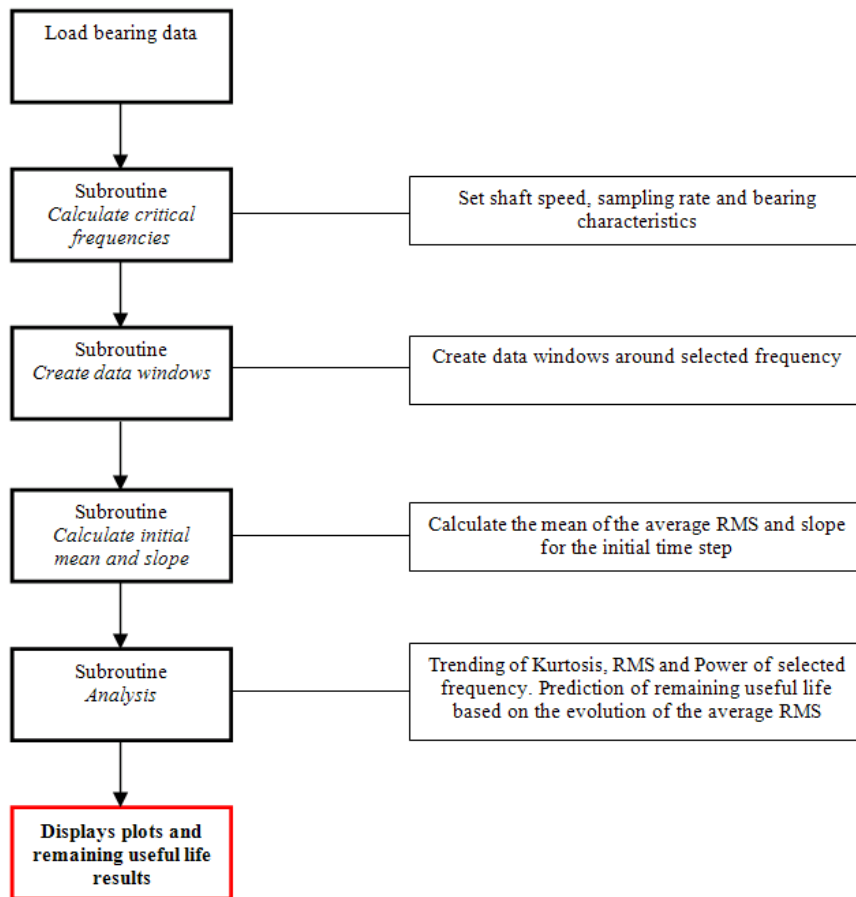


**Figure 3.30:** Structure of the code

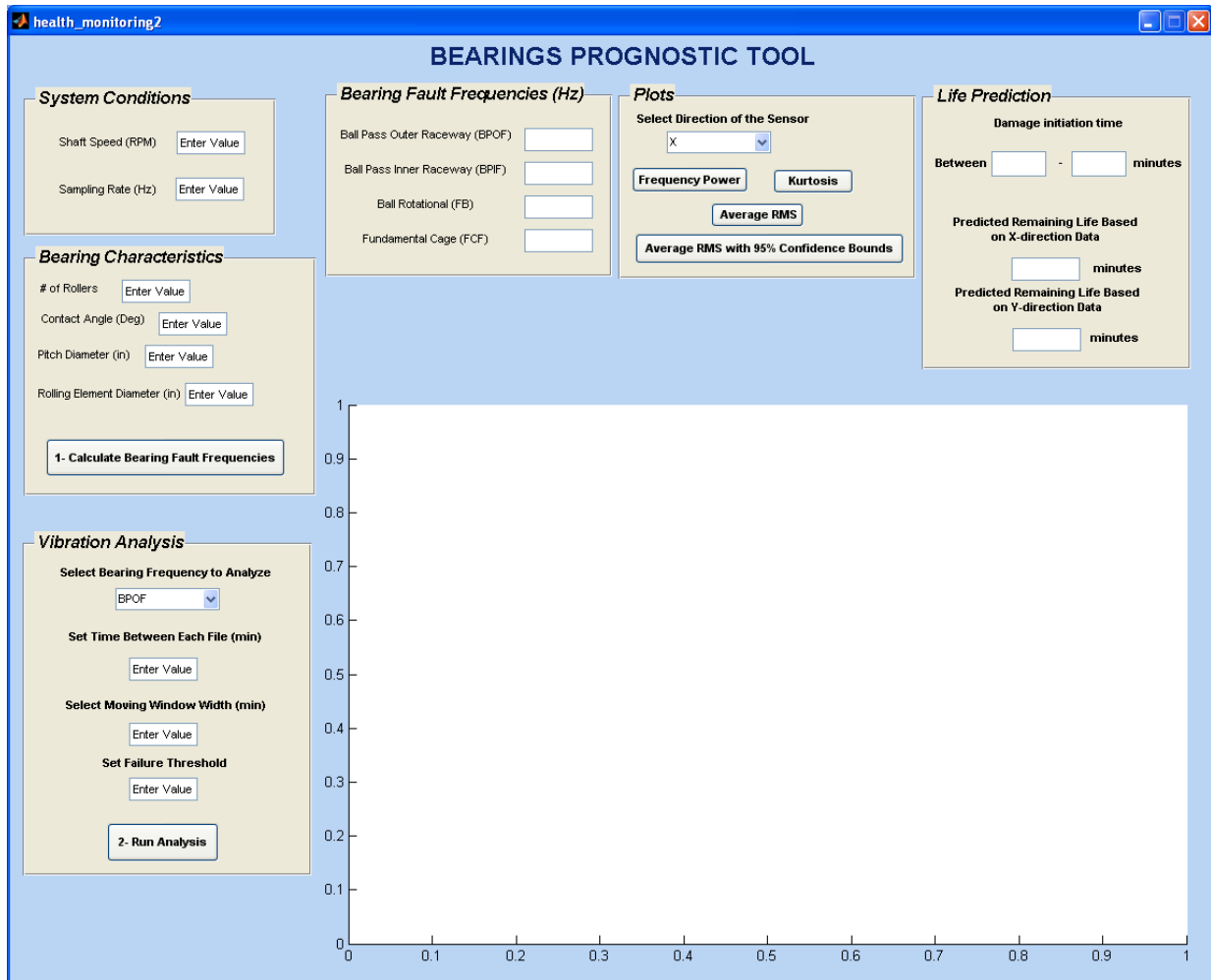
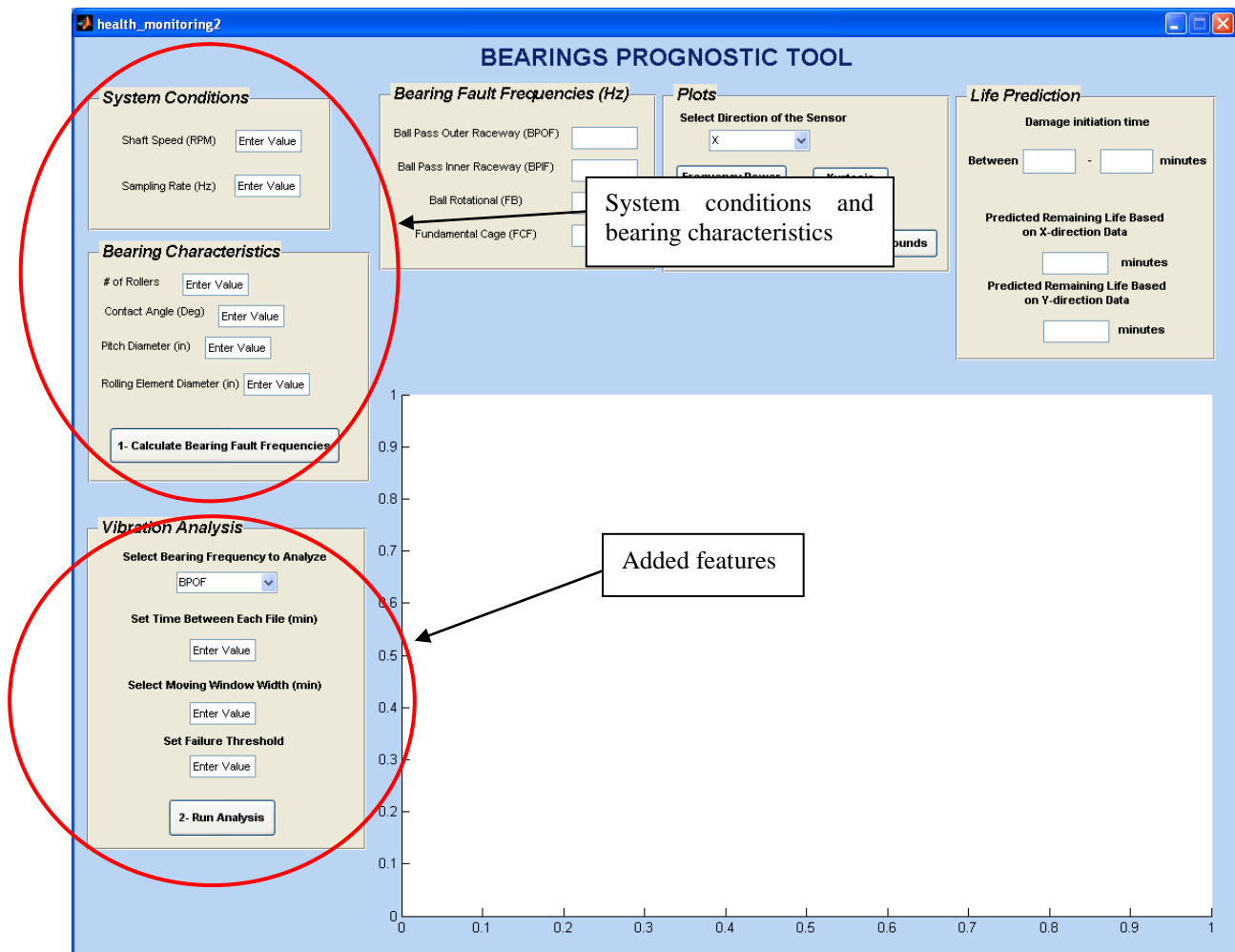


Figure 3.31: General view of the bearing prognostic tool for bearings.

This version of the GUI is very generic and it is capable of analyze both X and Y directions at the same time. After the sensor data is loaded and saved in a *.mat* file, the tool reads the data and performs the analysis. **Figure 3.31** shows the prognostic tool applicable for bearings. The tool has several features making it more flexible for the user. The user can select the bearing fault frequency to analyze, moving window width and failure threshold. The failure threshold is selected based on the type of measured data. There are different standards that establish different threshold values based on machine size and speed. The user needs to input the time between each of the recorded data file. **Figure 3.32** shows the features of the tool. **Table 3.5** shows the capabilities and limitations of the developed tool.



**Figure 3.32:** Features within bearings prognostic tool.

After run the analysis, the tool displays the exponential fit along with 95% confidence bounds. Also, it displays the predicted TTF's for both directions. The user can choose the direction of the measured data for plotting purposes. In the plots panel, the user can select to view the Kurtosis, Frequency Power, Average *RMS* (the first five harmonics are included) and Average *RMS* with 95% confidence bounds for bearing life prediction. **Figure 3.33** shows the Kurtosis value as a function of elapsed time. **Figure 3.34** shows the power of the defect frequency. **Figure 3.35** shows the average *RMS* as a function of elapsed time. **Figure 3.36** shows the Average *RMS* plot along with the exponential fit.

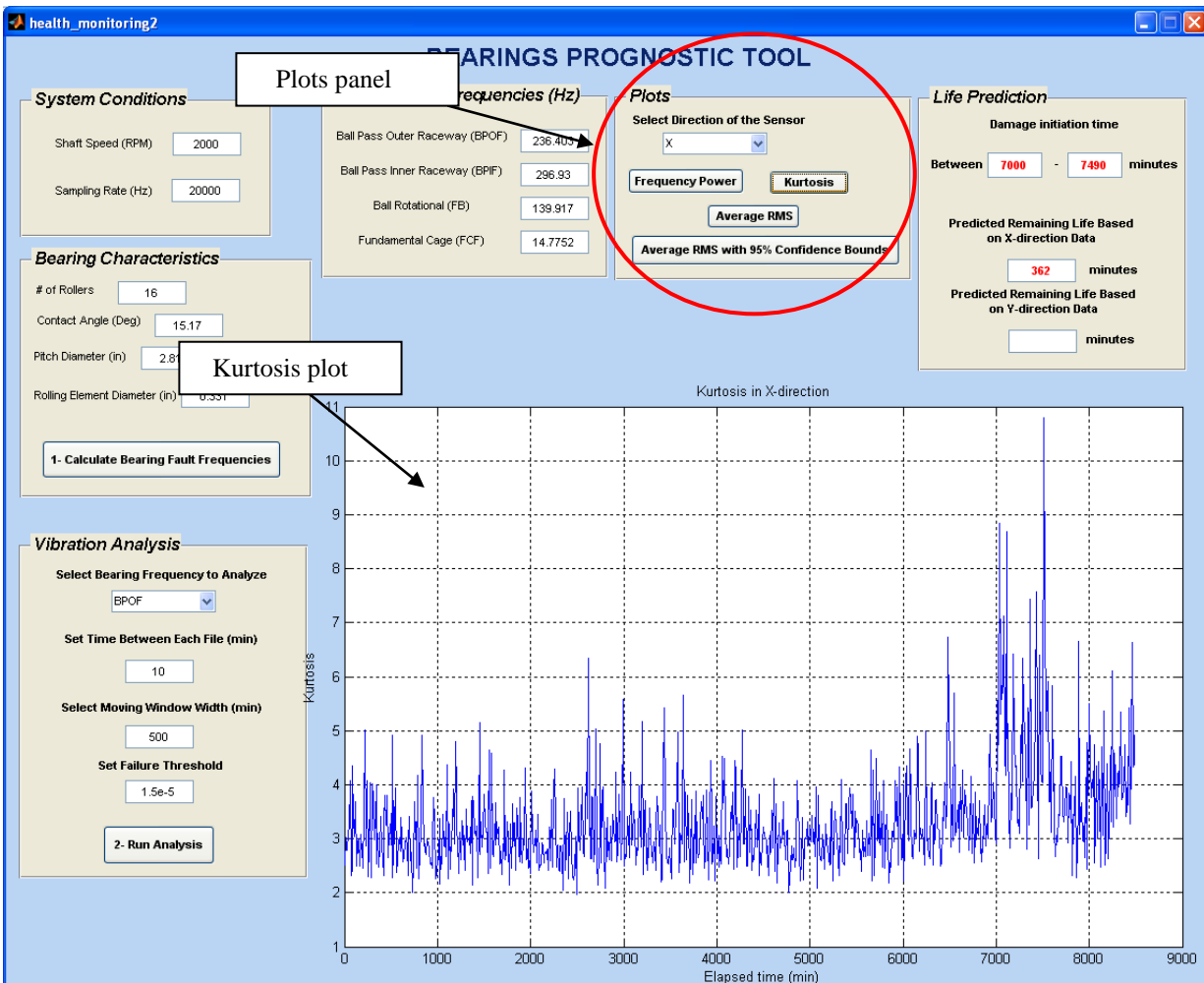


**Figure 3.33:** Bearings prognostic tool showing the Kurtosis plot.

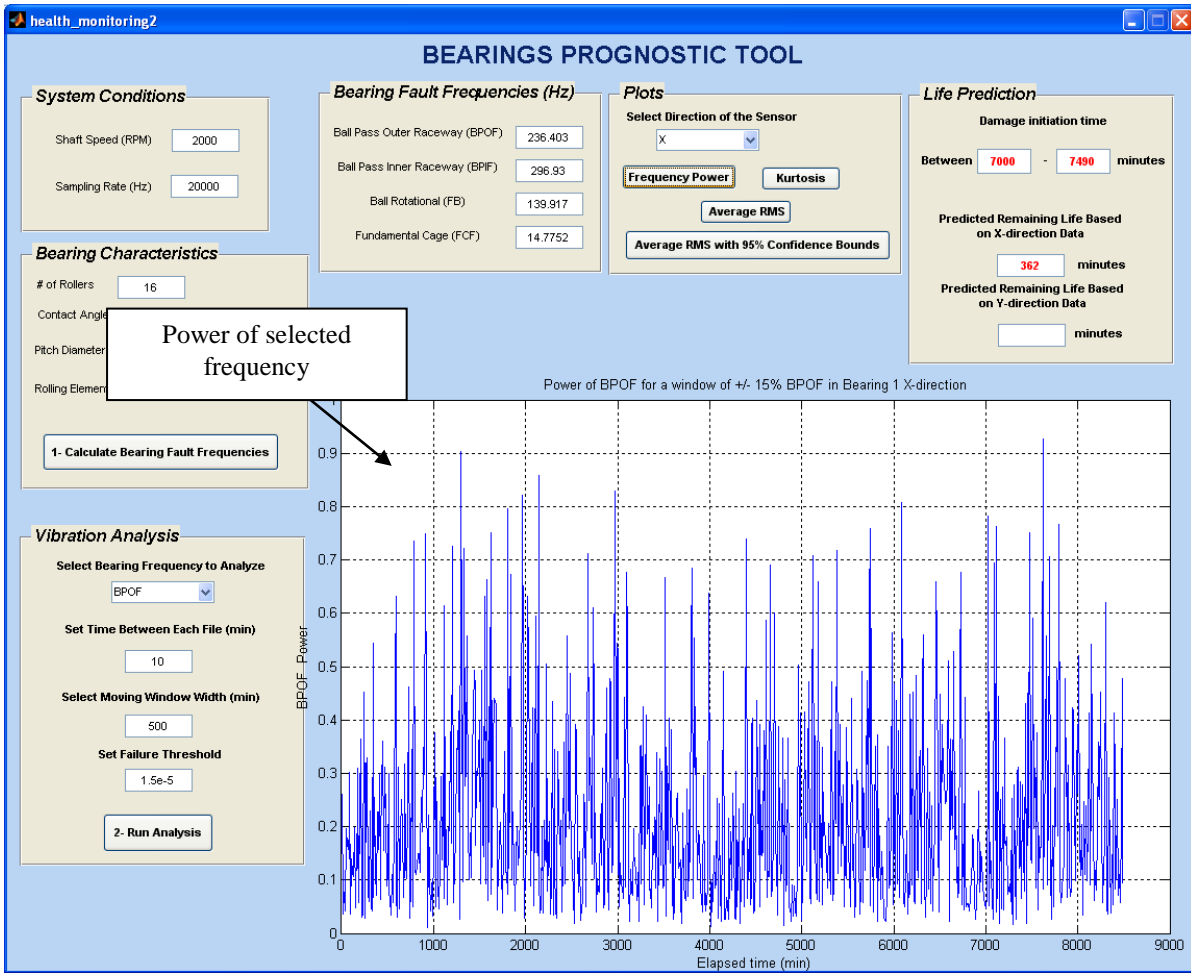
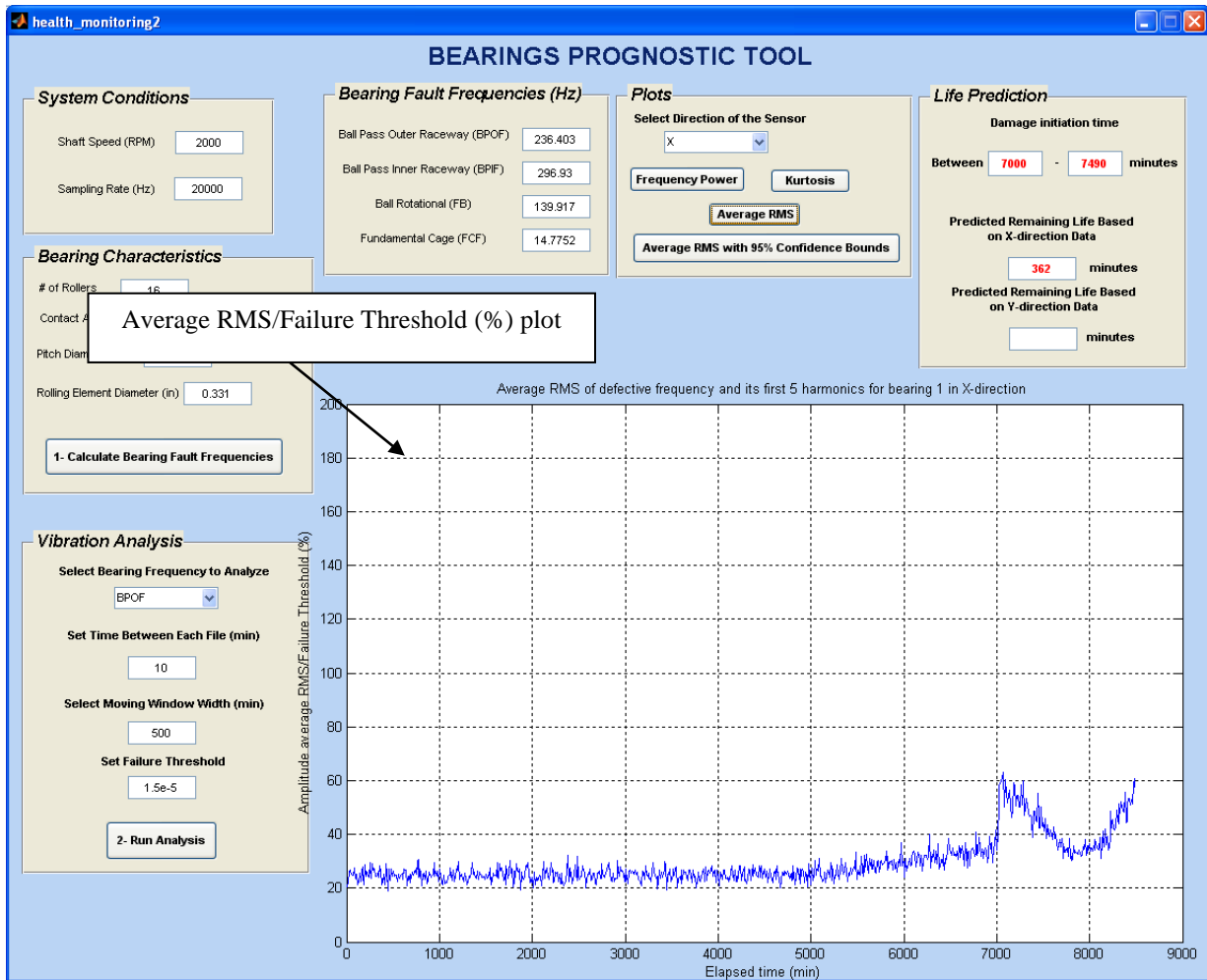


Figure 3.34: Bearings prognostic tool showing the power of selected frequency.



**Figure 3.35:** Prognostic tool showing the Average *RMS* / Failure Threshold (%) as a function of elapsed time.

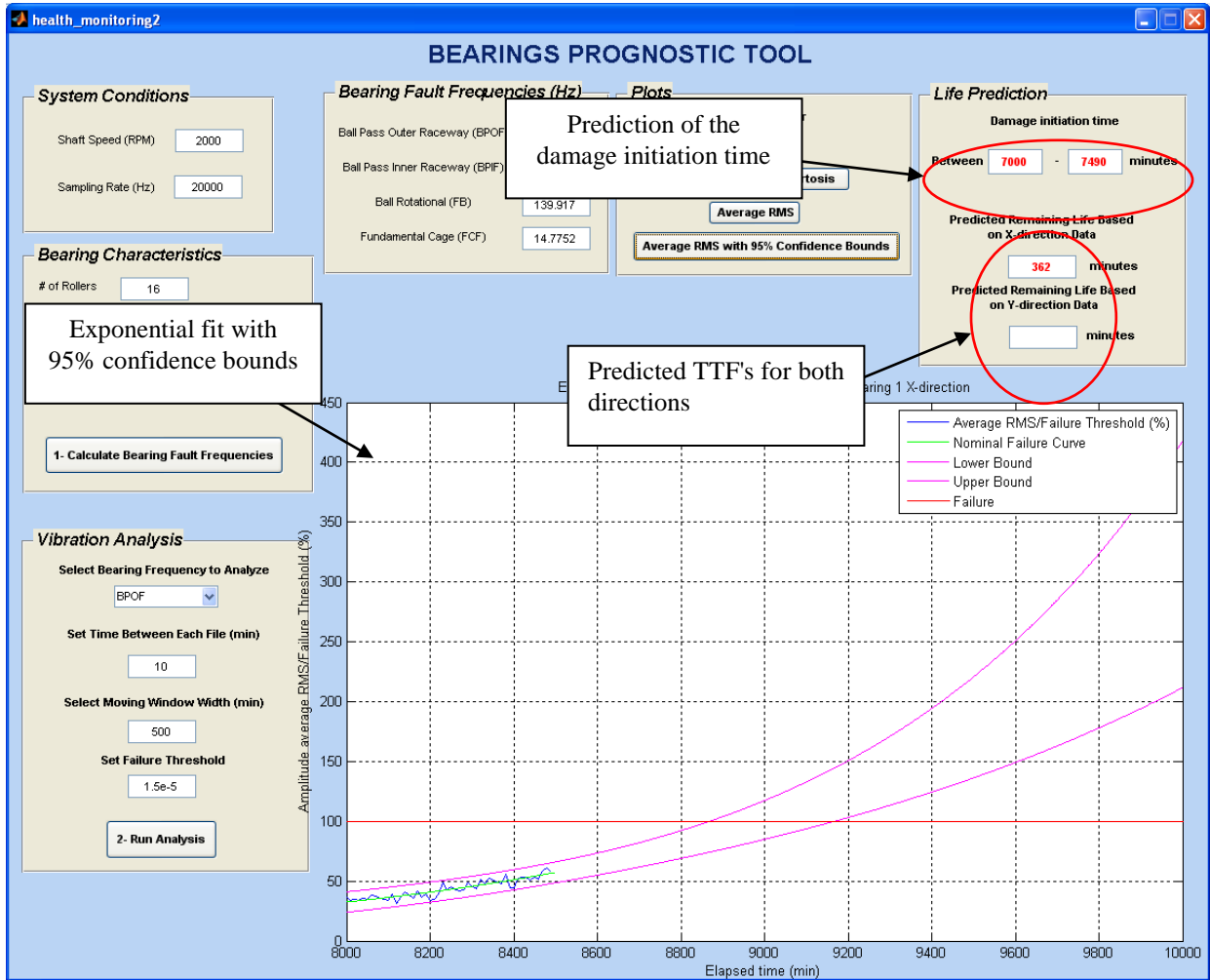


Figure 3.36: Predicted TTF's and exponential fit with 95% confidence bounds plot.

**Table 3.5:** Capabilities and limitations of the bearings prognostic tool

<b>Capabilities and Limitations of the Tool</b>	
<i>Capabilities</i>	<i>Limitations</i>
-- Analyze data in two accelerometer directions in parallel. -- System conditions can be selected. -- Multiple trending plots. -- Indicates damage initiation time and predict remaining useful time	-- Analyses need to be done individually for each critical frequency -- Data files need to be converted into <i>.mat</i> format before loading them into the tool.

## CHAPTER 4. CONCLUDING REMARKS

---

### 4.1 CONCLUSIONS

A data-driven life prediction model for bearings failure has been developed. The tool was created using the Graphical User Interface (GUI) within MATLAB® and it is capable to analyze accelerometer data measured in two different directions. The major contribution of this work is that life prediction of bearings can be achieved just by using experimental data measured from accelerometers. This method is cost effective because it does not require any expensive or complicated sensor technology. The analysis was performed using bearing data obtained from the NASA Prognostics Repository. They performed three run-to-failure tests under normal load conditions and data was measured using accelerometers which were placed on  $X$  and  $Y$  directions. At the end of the second test they found a failure in the outer race of bearing 1. Therefore, the developed tool in this work was tested using experimental data from the second test in order to confirm a failure on the outer race of bearing 1 and perform a remaining useful life prediction.

A set of algorithms were incorporated within the tool and it is capable of calculate the bearing fault frequencies and trend several condition indicators such as Kurtosis, RMS and Power of the defective frequency. Since the damage occurred in the outer race, the Ball Pass Outer Raceway Frequency (BPOF) was selected to perform the life prediction. The technical approach used into the algorithms was well documented. The remaining useful life prediction was based on the evolution of a selected degradation signal. The selected degradation signal was the RMS vibration level of the defective frequency and its first five harmonics. Then the average of these RMS values was calculated and this became the degradation signal trended over time. The objective of consider the harmonics is because the change in amplitude of the defect frequency is typically an indication of a defect and the presence of the harmonics of the defect frequency is also another indication of degradation and spall formation. For these RMS calculations a window of  $\pm 15\%$  was used in order to consider the frequency shift due to the

"leakage phenomenon". Vector scaling was also applied to the data in order to avoid small numbers. Based on the trend of the RMS vibration level we were able to identify the damage initiation and damage propagation phases. After run the tool using the data from Test 2, the remaining life was predicted using 95 % confidence bounds. According to the results, damage initiation occurred at approximately 7000 minutes of testing and when the degradation signal enters into the damage propagation phase, the tool indicated a time-to-failure (TTF) of 362 minutes after the prediction point. The values for the actual and predicted bearing life were 9700 and 8862 minutes respectively. Therefore, the relative error between the failure times was 8.6 %. In the future, the tool can be applied to different experimental data sets to test its accuracy. The proposed method in this work was not compared against other methods because they are not based just on acceleration data and require several additional parameters.

In practical situations, the user of the methodology will only need to know three main things: the parameters (or failure mechanisms) to be concerned about, the worst-case loads in the life cycle environment (to prevent damage to the sensors and the monitored part as well as to aid in the selection of the proper sensing equipment), and the frequencies of interest, if the user is interested in monitoring vibration. If an entirely new product is being monitored, all parameters of the life cycle environment should be considered.

## **4.2 RECOMMENDED FUTURE WORK**

Future work necessary for the improvement of the remaining useful life assessment is summarized as follows:

1. Develop EMA's components finite element models such as gears and bearings with the failure mechanism in order to obtain the response due to damage.
2. Asses fault diagnosis and remaining life prediction for bearings and gears based on EMA's varying motor speeds.

### Vibration Data Analysis Approach for Variable Shaft Speeds

Through this work we have focused our attention to a fixed shaft speed. However, this is not true in real systems. Hence, we would like to recommend an approach for vibration data analysis under a variable shaft speed scenario. Before we get into the analysis, note that a certain speed cycle needs to be assumed. Speed cycles can be represented as different functions such sinusoidal, linear, etc. For simplicity purposes, let's assume that the speed cycle can be represented as a step function as shown in **Figure 4.1**.

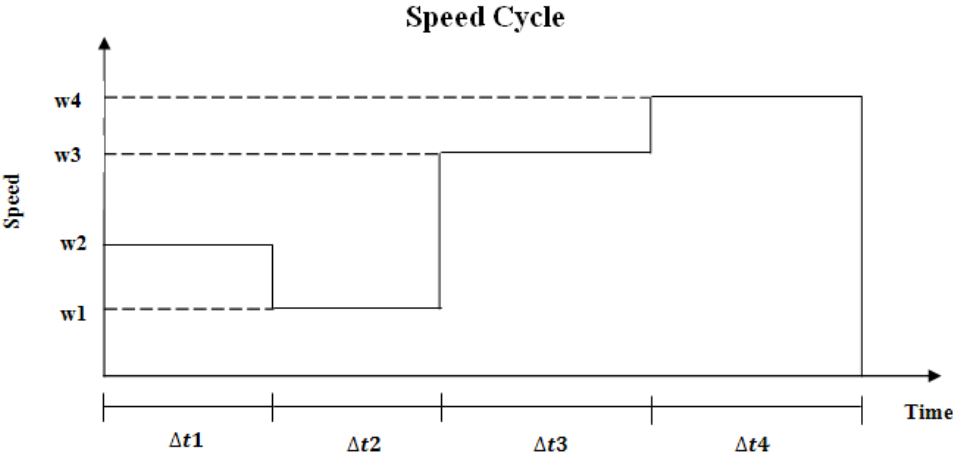


**Figure 4.1:** Arbitrary speed cycle

For each time step, the number of snapshots has to be established. In order to know the time between snapshots for each time step, the time step has to be divided by the number of desired snapshots. It is important to state that the sampling rate needs to be established based on the highest critical frequency. Due to speed changes, the bearing fault frequencies vary for each time step. Therefore, the trending of the selected degradation signal and condition indicators will be based on the updated critical frequencies.

## REFERENCES

---

- Afshari, N. 1996. Model-Based Techniques for Real-Time Monitoring of Rolling Element Bearings, Ph.D. Dissertation. *Case Western Reserve University*.
- Barkov, A. and N Barkova. 1995. Condition assessment and life prediction of rolling element bearings, part 2. *Sound and Vibration*. pp. 27-31.
- Beder, S. 1993. Making Engineering Design Sustainable. *Transactions of Multi-Disciplinary Engineering Australia*. Vol. GE17, No. 1, pp. 31-35.
- Berry, J. 1986. How to Track Rolling Element Bearing Health with Vibration Signature Analysis. *Sound and Vibration*. pp. 10-17.
- Braun, S. and B. Datner. 1979. Analysis of roller/ball bearing vibrations. *Journal of Mechanical Design*. Vol. 101, pp. 118-25.
- Byington, C.S., Orsagh, R., Kallappa P., Sheldon J., DeChristopher M., Amin S., and J. Hines. 2006. Recent case studies in bearing fault detection and prognosis. *IEEE*.
- Carr, J.J. 1993. *Sensors and Circuits*. PTR Prentice-Hall, New Jersey, pp. 5-8.
- Choy, F.K., Mugler, D.H., and J. Zhou. 2003. Damage Identification of a Gear Transmission Using Vibration Signatures. *Journal of Mechanical Design*. Vol. 125, pp. 394-402.
- Duque, O., Perez, M., and D. Mornigo. 2005. Detection of bearing faults in cage induction motors fed by frequency converter using spectral analysis of line current. *IEEE*.
- Dyer, D., and R. Stewart. 1978. Detection of rolling element bearing damage by statistical vibration analysis. *Journal of Mechanical Design*. Vol. 100, pp.229-35.
- Gebraeel, N., Lawley, M., Liu R., and V. Parmeshwaran. 2004. Residual Life Predictions From Vibration-Based Degradation Signals: A Neural Network Approach. *IEEE*.
- Guyer Jr. R.A. 1996. *Rolling bearing handbook and troubleshooting guide*.
- Harker, R. and J. Sandy. 1989. Rolling element bearing monitoring and diagnostics techniques. *Journal of Engineering for Gas Turbines and Power*. Vol. 111, pp. 251-256.
- Harris, T.A. 1991. *Rolling Bearing Analysis*. 3rd ed., John Wiley & Sons.

- Heng, A., Zhang, S., Tan C.C. A., and J. Mathew. 2009. Rotating machinery prognostics: State of the art, challenges and opportunities. *Mechanical Systems and Signal Processing*. 23, pp. 724-739.
- Kelkar, N., Dasgupta, D., Pecht, M., Knowles, I., Hawley, M., and D. Jennings. 1997. Smart Electronic Systems for Condition-Based Health Management. *Quality and Reliability Engineering International*. Vol. 13, pp. 3-7.
- Khemili, I. and M. Chouchane. 2005. Detection of rolling element bearing defects by adaptive filtering. *European Journal of Mechanics A/Solids*. pp. 293-303.
- Koizumi, T., and R. Taniguchi. 1986. Preventive maintenance for roller and journal bearings of induction motor based on the diagnostic signature analysis. *Journal of Vibration, Acoustics, Stress, and Reliability in Design*. Vol. 108, pp.26-31.
- Kuhnell, B. and F. Rees. 1987. Monitoring system to predict machine failure. *Information and Software Technology*. Vol. 29, pp. 6-7.
- Li, B., Chow, M., Tipsuwan, Y. and J.C. Hung. 2000. Neural-Network-Based Motor Rolling Bearing Fault Diagnosis. *IEEE*.
- Li, B., Goddu G., and Mo-Yuen Chow. 1998. Detection of Common Motor Bearing Faults Using Frequency-Domain Vibration Signals and a Neural Network Based Approach. *American Control Conference*.
- Li, C., Ma, J., and B. Hwang. 1995. Bearing localized defect detection by bicoherence analysis of vibrations. *Journal of Engineering for Industry*. Vol. 117, pp.625-629.
- Li, C., Ma, J., and B. Hwang. 1996. Bearing condition monitoring by pattern recognition based on bicoherence analysis of vibrations. *IMechE Publication, Journal of Mechanical Engineering Science*. Vol. 210, pp.277-85.
- Marble, S. and B. P. Morton. 2006. Predicting the Remaining Life of Propulsion System Bearings. *IEEE*.
- Mitchell, J.S. 1993. *An Introduction to Machinery Analysis and Monitoring*. Tulsa:PennWell Books.
- Orhan, S., Aktürk N., and V. Çelik. 2006. Vibration monitoring for defect diagnosis of rolling element bearings as a predictive maintenance tool: Comprehensive case studies. *NDT&E International*. pp. 293-298.

- Pecht, M., Dube, M., Natishan, M., and I. Knowles. 2001. An Evaluation of Built-In Test. *Transactions on Aerospace and Electronic Systems*. Vol. 37, No. 1, pp. 266-272.
- Press, W.H., Teukolsky, S.A., Vetterling, W.T. and B.P. Flannery. 1992. *The Fast Fourier Transform, Numerical Recipes in C: the Art of Scientific Computing*. Cambridge University Press, New York. pp. 505.
- Qiu, H., Lee, J., Lin, J. and G. Yu. 2006. Wavelet filter-based weak signature detection method and its application on rolling element bearing prognostics. *Journal of Sound and Vibration*. pp. 1066-1090.
- Qiu, J., Zhang, C., Seth, B.B and S.Y. Liang. 2002. Damage mechanics approach for bearing lifetime prognostics. *Mechanical Systems and Signal Processing*. 16(5), pp.817-829.
- Randall, R.B. 2004. Detection and diagnosis of incipient bearing failure in helicopter gearboxes. *Engineering Failure Analysis*. pp. 177-190.
- Rao, P., and F. Taylor. 1990. Real time monitoring of vibration using the Wigner distribution. *Sound and Vibration*. pp. 22-121.
- Shilling R.J., and S.L. Harris. 2005. *Fundamentals of digital signal processing using MATLAB*.
- Stack, J.R., Habetler, T.G. and R.G. Harley. 2003. Fault Classification and Fault Signature Production for Rolling Element Bearings in Electric Machines. *Symposium on Diagnostics for Electric Machines, Power Electronics and Drives*.
- Wade, Richard, A. 2005. A Need-focused Approach to Air Force Engine Health Management Research. *IEEE Aerospace Conference, Big Sky, Montana*.

# APPENDICES

# A. DATA ACQUISITION

The principal role of analysis and signal processing of vibration for health monitoring is to quantify signal changes. These vibration changes can be related to changes in component condition. Structural changes caused by friction and wear in a component lead to changes in its dynamic motion and hence the vibration that you can measure using sensors. In this work, accelerometers were used to capture those changes in the behavior of the bearing. If we have a machine with several components, the measured vibration is a composite of vibrations from each component. However, the focus of this work is to monitor the vibration behavior of the bearings. **Figure A.1** shows the part of the approach that focuses on sense the condition of the system.

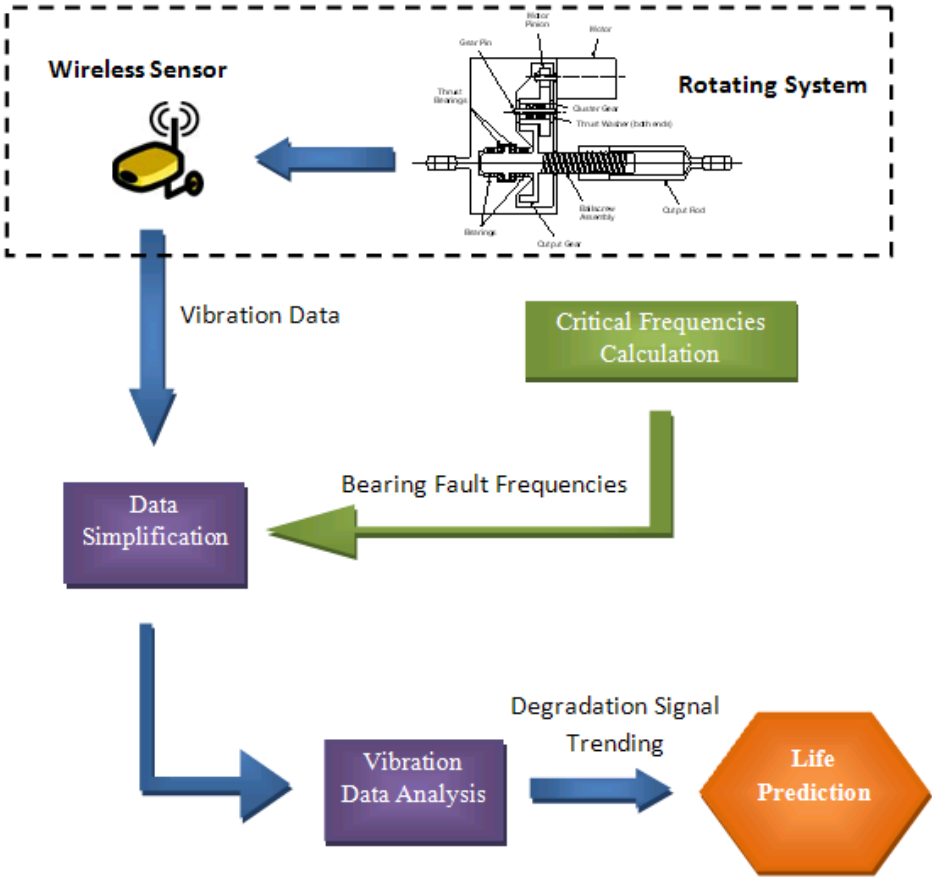


**Figure A.1:** Sensor data acquisition.

## ACCELEROMETER MOUNTING

One of the most important considerations is the location of the accelerometer. When measuring vibration, the accelerometer needs to be as close as possible to the bearing. One typical location is on the bearing housing close to the point of interest. Another consideration is the measuring direction. The NASA experimental data was obtained using accelerometers in both horizontal  $X$  direction and vertical  $Y$  direction. **Figure A.3** shows the accelerometer used to capture the data. The purpose of this section is to provide a description of a possible mounting scenario for measuring experimental data. Guyer (1996) discusses the importance of the measuring direction. He stated that horizontal measurements typically show the greatest vibration because the machine is more flexible in the horizontal plane. On the other hand, vertical measurements show less vibration than horizontal because of the stiffness due to mounting and gravity. However, in order to be capable of capture the whole vibration behavior of the bearing, we should consider both directions. Then, vibration data analysis in both directions can be done to compare which direction captures the vibration better. **Figure A.2** shows a mounting schematic for the accelerometers.

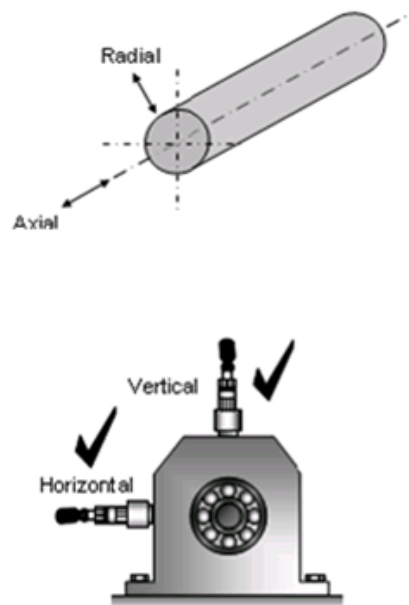


**Figure A.2:** Accelerometers mounting <sup>3</sup>

---

<sup>3</sup> [www.commtest.com](http://www.commtest.com)



**Figure A.3:** PCB 353B33 High Sensitivity Quartz ICP Accelerometer<sup>4</sup>

## DATA ACQUISITION

NASA experimental data was acquired using a National Instruments DAQCard-6062E data acquisition card. **Figure A.4** shows the data acquisition card. Data collection was conducted by a National Instruments LabVIEW program. For future analyses, the data acquisition toolbox within MATLAB also supports data acquisition hardware from National Instruments.

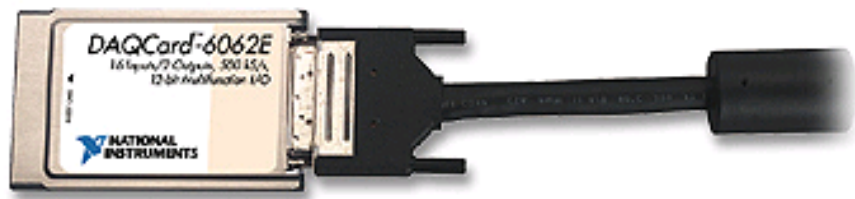


**Figure A.4:** National Instruments data acquisition card<sup>5</sup>

---

<sup>4</sup> [www.pcb.com](http://www.pcb.com)

<sup>5</sup> [www.ni.com](http://www.ni.com)

## SAMPLING RATE

Most signals behave as continuous phenomena over their period of acquisition and provide a history of the measured parameter as a function of time. Sampling is the process of obtaining a series of discrete numerical values from a continuous function. Electronic sampling circuits observe a source signal at intervals of time and convert the source into an electrical signal with a numerical value analogous to the source signal.

The sampling interval is the most important consideration during the sampling process. Sampling points that are too close will result in a redundant data, while sampling points that are too far apart will lead into confusion between the low and high frequency components of the signal. For example, consider the time record shown in **Figure A.5**. Suppose that the record is sampled such that the time interval between adjacent sampling points is  $d$  seconds. The sampling rate is therefore  $1/d$  samples per second. Since at least two sample points are required to define a cycle (i.e., one point for the start and for the end of a cycle), the number of cycles per second (or the frequency of sampling) is  $1/2d$ . Therefore, the highest frequency component that can be defined by sampling at the rate of  $1/d$  samples per second is  $1/2d$ . The cutoff frequency  $f_c$  (equal to  $1/2d$ ) is called the Nyquist frequency and the corresponding time between samples  $d$  is called the Nyquist interval.

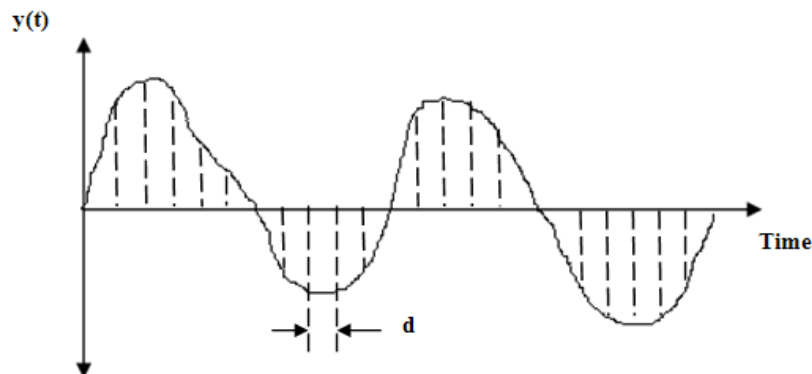


**Figure A.5:** Sampling of a continuous time record.

Any frequency  $f$  above  $f_c$  contained in the signal will be “folded” back into the frequency range from 0 to  $f_c$  and will be confused with data within the low-frequency range. This problem, called *aliasing*, is a potential source of error in sampling. For any frequency  $f$  in the range  $0 \leq f \leq f_c$ , the frequencies that will be aliased with  $f$  are  $2kf_c \pm f$ , where  $k$  is number from 1 to  $N$ . To prove this, consider a sampling interval  $t = 1/2f_c$ . Then,

$$\cos 2\pi (2kf_c \pm f) \frac{1}{2f_c} = \cos \left( 2k\pi \pm \frac{2\pi f}{2f_c} \right) = \cos 2\pi f \frac{1}{2f_c} = \cos 2\pi f t \quad (\text{A.1})$$

Thus, all data at frequencies  $(2kf_c \pm f)$  have the same cosine function amplitude as the data at frequency  $f$  when sampled at times  $1/2f_c$  apart, and hence all data at the higher frequencies will be superimposed (or aliased) on data at frequency  $f$ . For example, data at frequencies 250 Hz, 350 Hz, 450 Hz, 600 Hz will be aliased with data at 100 Hz if  $f_c = 200$  Hz. Therefore, the sampling interval  $h$  should be carefully chosen to prevent aliasing.

As discussed above, during the data acquisition process, a continuous-time or analog signal,  $y(t)$ , is measured and we will take samples of that analog signal to produce a discrete-time signal,  $y(k)$ , in order to obtain the frequency spectrum of the bearings. Therefore, the sampling rate plays an important role during this process because we want to extract all the necessary information of the original signal. To ensure the optimum sampling rate, we will incorporate the use of the Shannon Sampling Theorem. The theorem states as follows:

*Suppose a continuous-time signal  $y(t)$  is bandlimited to  $B$ . Let  $y(k) = y(kT)$  be the  $k$ th sample of  $y(t)$  using a sampling frequency of  $f_s = 1/T$  where  $T$  is the sampling interval. If  $f_s > 2B$ , then all the essential information about  $y(t)$  is contained in the samples  $y(k)$ .*

Therefore, if our signal has a certain frequency  $B$ , we will use a sampling rate of  $2B$  in order to ensure that our data contains all the information necessary to extract the features needed in the frequency spectrum.

## B. CODE FLOWCHARTS

---

---

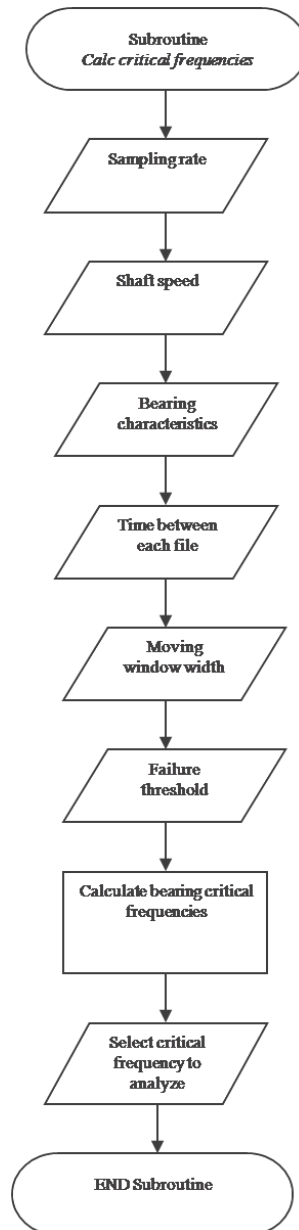


**Figure B.1:** Subroutine: Calculate critical frequencies

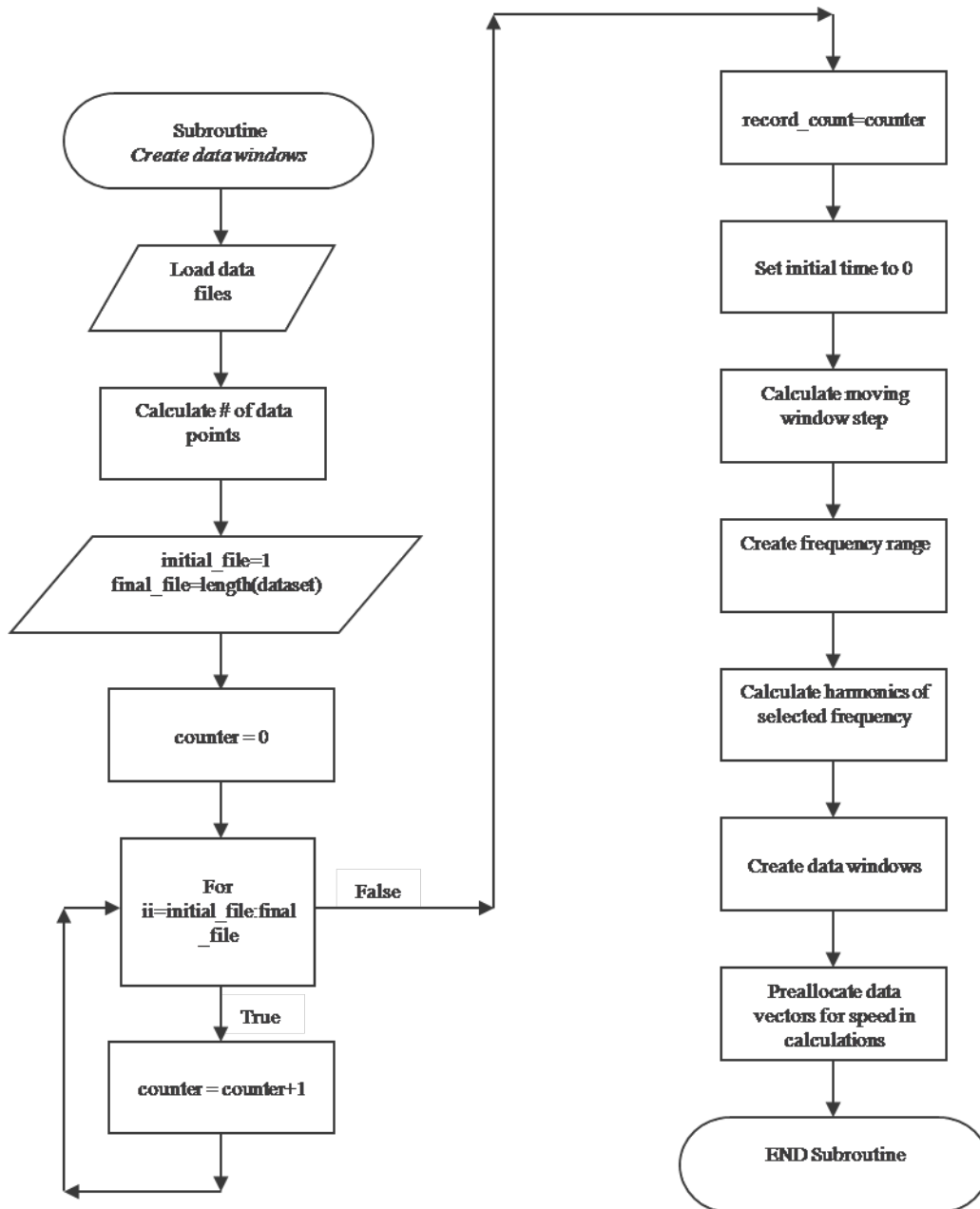


**Figure B.2:** Subroutine: Create data windows

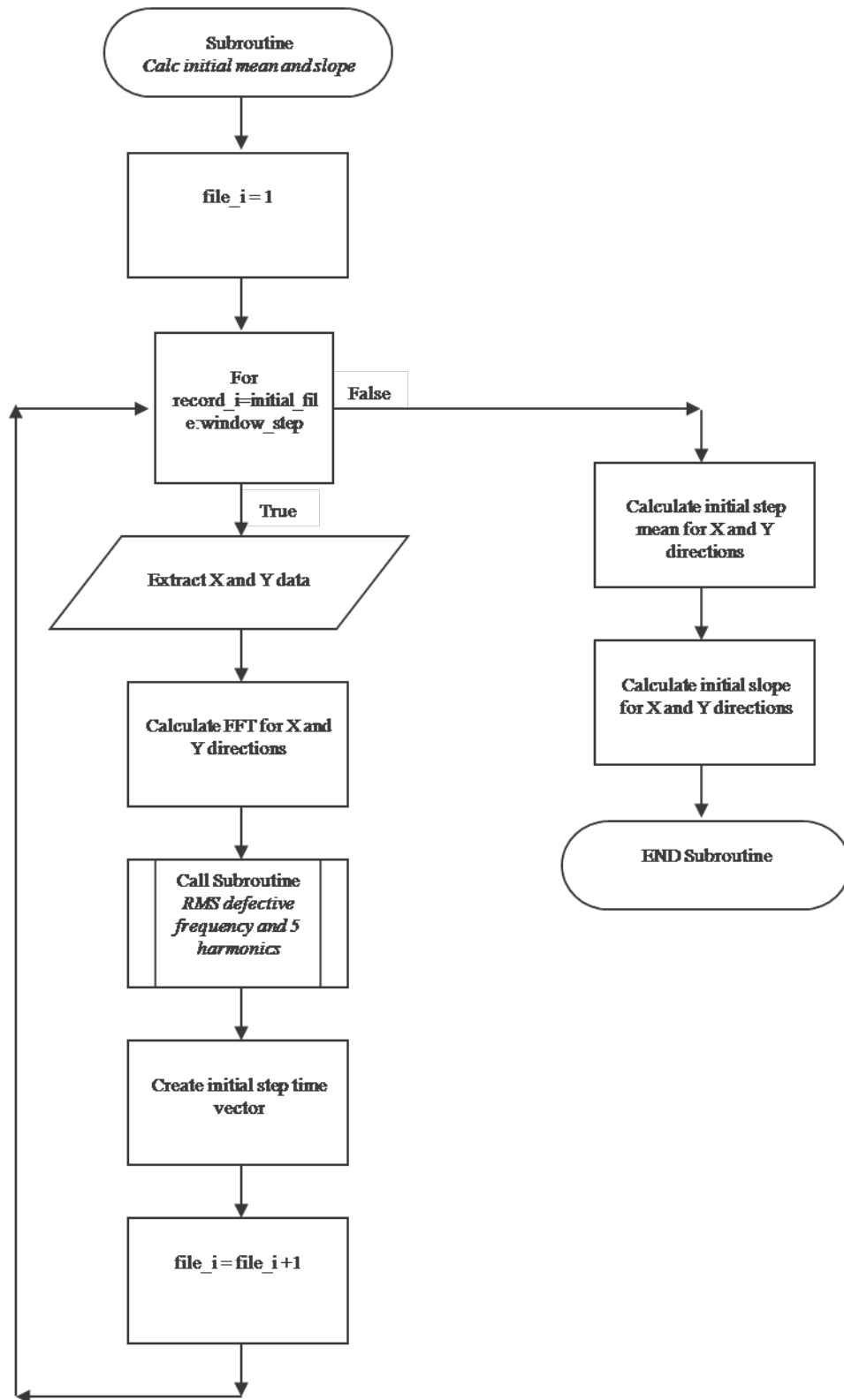


**Figure B.3:** Subroutine: Calculate initial mean and slope

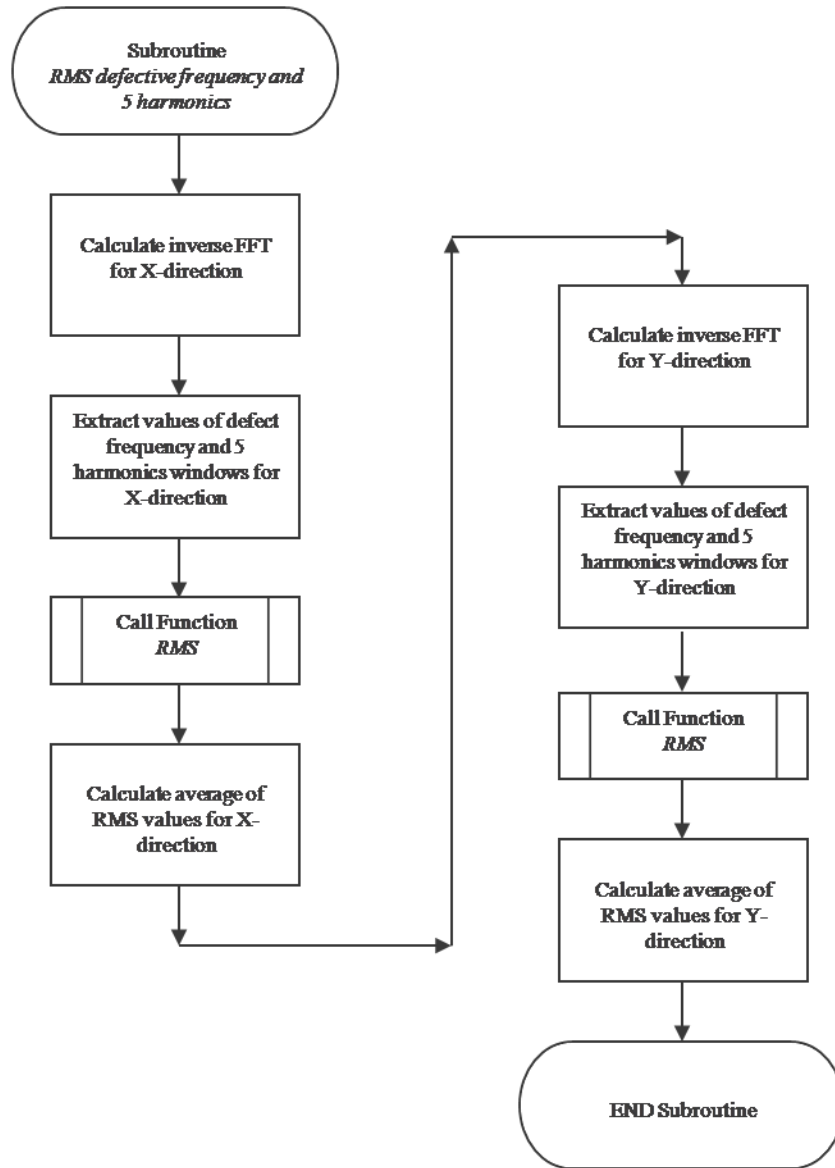


**Figure B.4:** Subroutine: RMS defective frequency and 5 harmonics

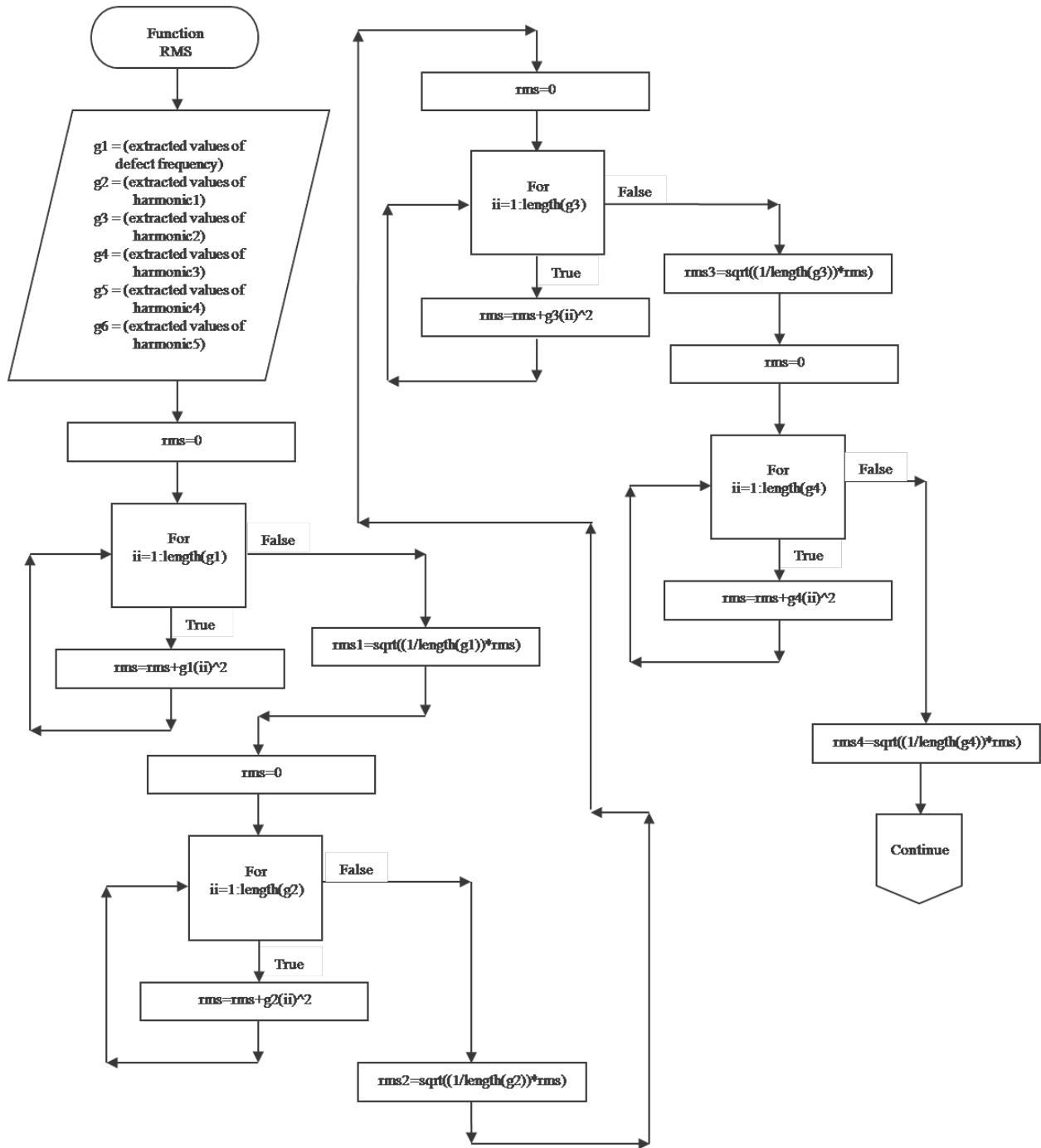
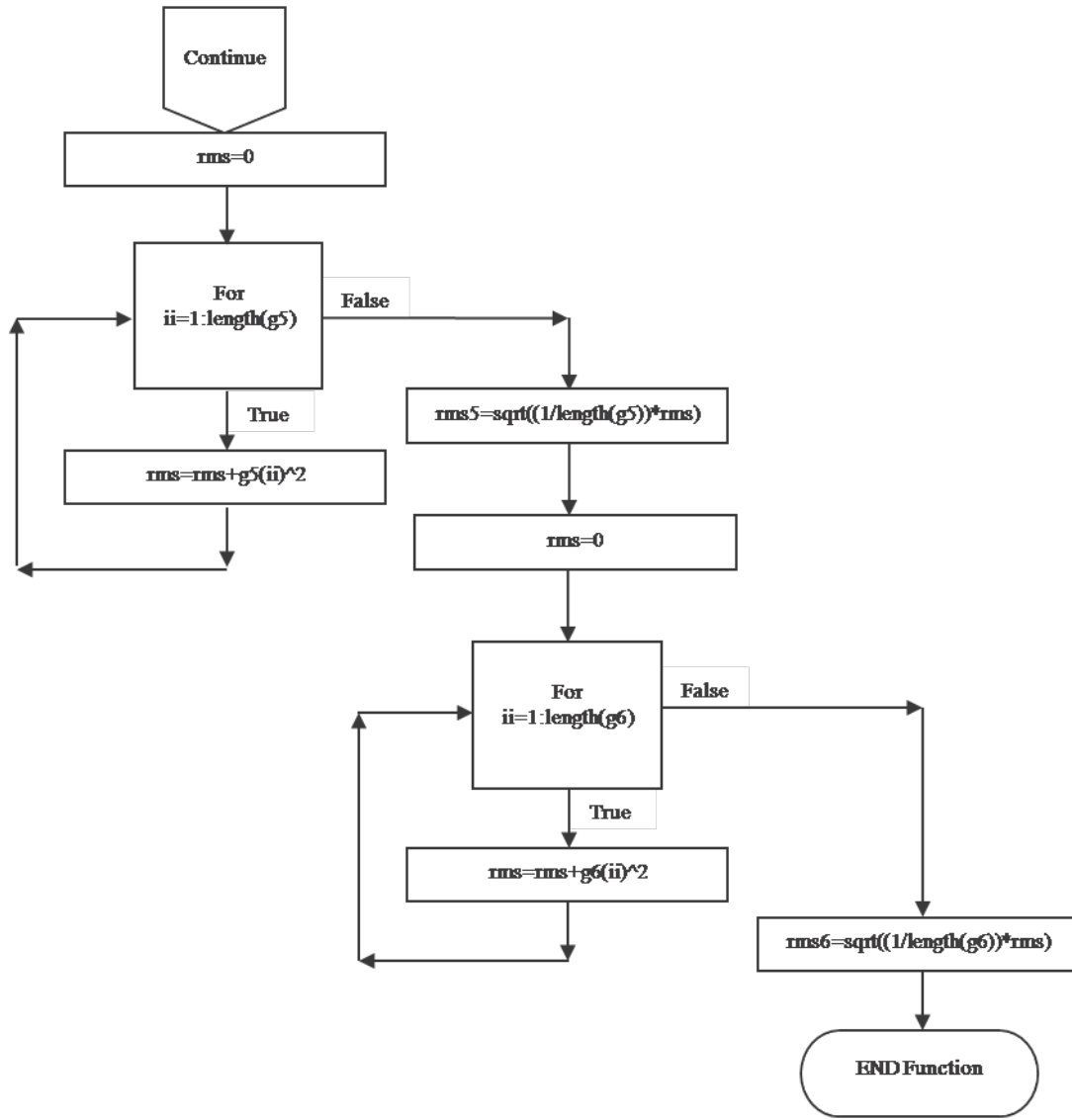


Figure B.5: Function: RMS, continued on next page



**Figure B.6:** Function: RMS, continued from previous page

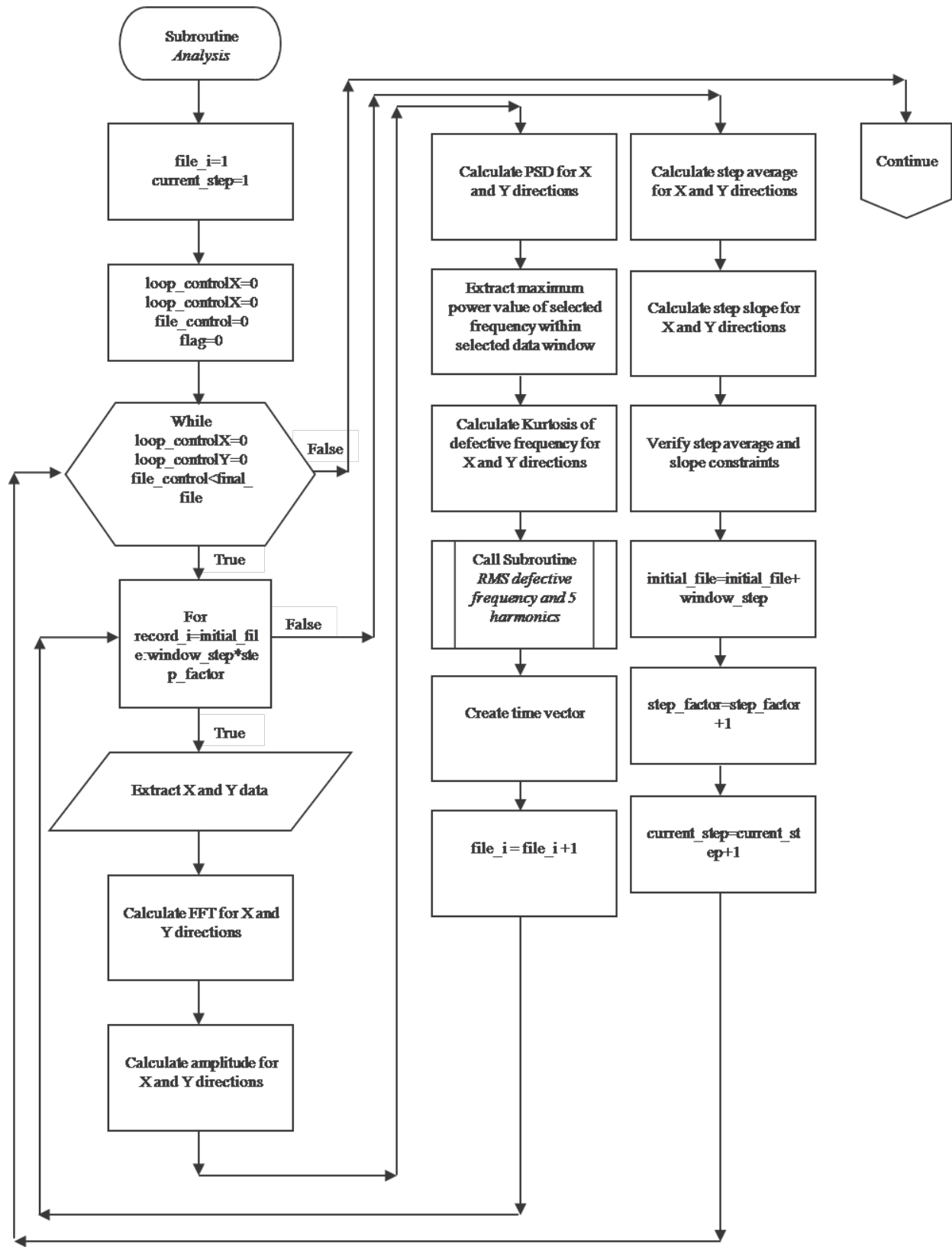
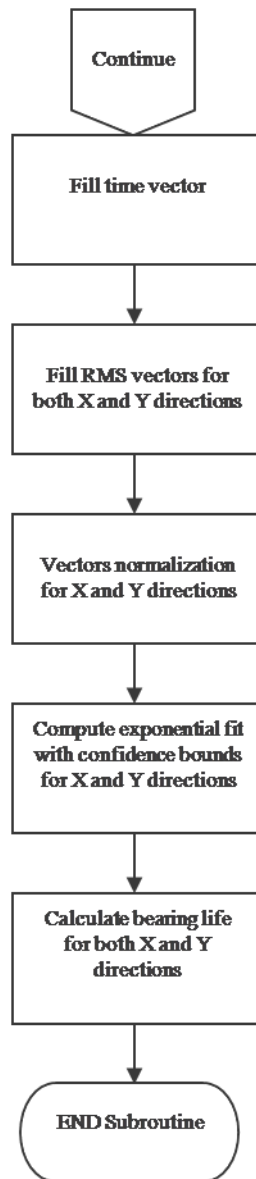


Figure B.7: Subroutine: Analysis, continued on next page



**Figure B.8:** Subroutine: Analysis, continued from previous page

## C. MATLAB BUILT-IN FUNCTIONS

---

---

### Kurtosis

In this section the kurtosis value is calculated using both the definition outlined in the theory and the MATLAB built-in function called *kurtosis*. The purpose is to confirm that the definition of kurtosis used in the analysis gives the same results as the MATLAB function. Let's consider the following data:

Data
2
3
4
6

Using the definition:

$$Kurt = \frac{N \sum_{i=1}^N (s_i - \bar{s})^4}{[\sum_{i=1}^N (s_i - \bar{s})^2]^2}$$

$$\bar{s} = 3.75 \quad N = 4$$

$s_i$	$s_i - \bar{s}$	$(s_i - \bar{s})^2$	$(s_i - \bar{s})^4$
2	-1.75	3.0625	9.379
3	-0.75	0.5625	0.316
4	0.25	0.0625	0.0039
6	2.25	5.0625	25.629
Total	0	8.75	35.3279

$$Kurt = \frac{4(35.3279)}{(8.75)^2} = 1.8457$$

Using MATLAB function:

$g = kurtosis(A)$  returns the sample kurtosis of  $A$ . For vectors,  $kurtosis(A)$  is the kurtosis of the elements in the vector  $A$ . If we define the vector  $A$  using the above data, the kurtosis can be calculated using the MATLAB built-in function. **Figure C.1** shows the result.

```
A =  
  
    2  
    3  
    4  
    6  
  
The kurtosis of vector A is  
  
kurt =  
  
    1.8457
```

**Figure C.1:** MATLAB output of Kurtosis value

## FFT

In order to compare the results of the Fast Fourier Transform using the definition explained in the theory against the MATLAB built-in function *fft*, we took 10 data points of the accelerometer data from the second test recorded on 02/12/2004. The data corresponds to bearing 1 in  $X$ -direction. **Figure C.2** shows the data vector. **Figure C.3** shows the results using both methods. We can clearly see that both methods lead to the same results.

```

x =
    -0.0490
    -0.0420
     0.0150
    -0.0510
    -0.1070
    -0.0780
    -0.0200
    -0.0460
    -0.0630
     0.0680

```

**Figure C.2:** Accelerometer data.

```

FFT using definition
fourier =

    -0.0373
     0.0168 + 0.0046i
    -0.0041 - 0.0027i
    -0.0058 + 0.0230i
    -0.0090 + 0.0092i
    -0.0075 - 0.0000i
    -0.0090 - 0.0092i
    -0.0058 - 0.0230i
    -0.0041 + 0.0027i
     0.0168 - 0.0046i

FFT using MATLAB built-in function
fourier2 =

    -0.0373
     0.0168 + 0.0046i
    -0.0041 - 0.0027i
    -0.0058 + 0.0230i
    -0.0090 + 0.0092i
    -0.0075
    -0.0090 - 0.0092i
    -0.0058 - 0.0230i
    -0.0041 + 0.0027i
     0.0168 - 0.0046i

```

**Figure C.3:** Comparison of the FFT calculation using both the definition and MATLAB built-in function.

## Find

The purpose of the MATLAB built-in function *find* is to find indices and values of nonzero elements. We can illustrate this using a simple example. Suppose that we want extract the element indices of the numbers greater than 10 of a vector *A*. shows the MATLAB results. It is clearly to see that the elements 1 and 3 contain the numbers greater than 10. **Figure C.4** shows the results.

```
A =  
  
    20  
     3  
    40  
     6  
  
c=find(A>10)  
  
c =  
  
     1  
     3
```

**Figure C.4:** MATLAB results using the function `find`